Dissertation

submitted to the
Combined Faculties for the Natural Sciences and for Mathematics
of the Ruperto-Carola University of Heidelberg, Germany

for the degree of
Doctor of Natural Sciences

presented by
Alexander Jethwa, M.Sc.
born in Göttingen, Germany

Oral examination: October 9, 2017

Identification of regulators of mutant p53 accumulation in lymphoma using RNA interference

Referees:

Prof. Dr. Philipp Beckhove

Prof. Dr. Thorsten Zenz

Summary

In over 40% of all cancers, the key tumor suppressor p53 is inactivated via mutation. Mutant (mut) p53 can gain new properties (gain-of-function, GOF), which actively contribute to tumorigenesis. In many tumors, a massive accumulation of mutp53 protein is observed and a prerequisite for the GOF activity. Therefore, tumors often depend on sustained high levels of mutp53, which suggests that interfering with mutp53 accumulation may be exploitable in cancer therapy. However, the mechanisms that control excessive mutp53 stabilization are not fully understood. To this end, the main aim of this study was to identify regulators of mutp53 accumulation in Burkitt's lymphoma (BL) as a model for a highly aggressive cancer.

Despite the presence of functional MDM2, the main negative regulator of p53, mutp53 was found to be stabilized in BL. To identify proteins regulating mutp53 levels in an unbiased fashion, a flow cytometry-based RNA interference (RNAi) screen was conducted in a mutp53 BL cell line model. The primary screen hit was TRRAP (transformation/transcription domain-associated protein), a constituent of several histone acetyltransferase (HAT) complexes. TRRAP knock-down and knock-out resulted in depletion of mutp53 protein (but not mRNA) in lymphoma and colorectal cancer cell lines with a diverse spectrum of p53 mutations. Conversely, TRRAP overexpression increased mutp53 levels. Mass spectrometric analysis of the mutp53 interactome after TRRAP knock-down indicated that TRRAP silencing caused nuclear export of mutp53 and degradation via the MDM2-proteasome axis, suggesting targeting of mutp53 to the physiological p53 degradation machinery. Gene expression profiling after TRRAP knock-down showed a suppression of cell cycle-related genes and an induction of interferon signaling, which however did not contribute to mutp53 regulation. To map functional regions of TRRAP, a CRISPR/Cas9 mutagenesis approach ("CRISPR scanning") was applied which identified a 109 amino acid region in the N-terminal HEAT repeat region crucial for mutp53 accumulation and cell survival. In wild-type p53 BL cells, TRRAP silencing attenuated p53 stabilization and activity upon genotoxic stress. Finally, to transfer the results from RNAi screening, a drug-based screening was performed and identified that inhibition of histone deacetylases (HDAC) and specifically HDAC1/2/3 decreased mutp53 levels to a surprisingly similar extent as TRRAP knock-down.

In summary, this study identifies TRRAP as a key regulator of p53 levels and links histone-modifying complexes to p53 protein accumulation. Based on the GOF properties of mutp53, this may provide a basis for therapeutic targeting of mutp53 in lymphoma and other cancers.

Zusammenfassung

Bei über 40% aller Krebsarten wird der zentrale Tumorsuppressor p53 durch Mutationen inaktiviert. Mutiertes (mut) p53 gewinnt oft neue Eigenschaften („gain-of-function“, GOF), die aktiv zur Tumorentstehung beitragen können. Des Weiteren kann in vielen Tumoren eine massive Akkumulation des mutp53-Proteins beobachtet werden. Dies ist eine Voraussetzung für die GOF-Aktivität, weswegen Tumore häufig auf ein konstitutiv hohes mutp53-Level angewiesen sind. Daher könnte dies für eine gezielte Krebstherapie von Nutzen sein; allerdings sind die Mechanismen der fehlerhaften mutp53-Akkumulation nur unzureichend bekannt. Aus diesem Grund war das Hauptziel dieser Studie, Regulatoren der mutp53-Akkumulation im Burkitt-Lymphom (BL) als Modell für hochaggressiven Krebs zu identifizieren.

Trotz Expression von funktionalem MDM2, dem zentralen negativen Regulator von p53, zeigte sich, dass mutp53 im BL akkumulierte. Um Regulatoren des mutp53-Levels zu identifizieren, wurde ein Durchflusszytometrie-basierter RNA-Interferenz (RNAi) Screen in einem mutp53 BL-Zelllinienmodell durchgeführt. Hierdurch wurde TRRAP (transformation/transcription domain-associated protein) identifiziert, welches ein Bestandteil von vielen Histonacetyltransferasekomplexen ist. In Lymphom- und Kolonkarzinom-Zelllinien mit unterschiedlichen p53-Mutationen verursachten sowohl ein TRRAP Knockdown als auch ein Knockout eine Degradierung von mutp53-Protein (aber nicht mRNA). Im Gegenzug resultierte eine TRRAP-Überexpression in einem erhöhten mutp53-Level. Um den zu Grunde liegenden molekularen Mechanismus zu entschlüsseln, wurde eine massenspektrometrische Analyse der mit mutp53-interagierenden Proteine nach TRRAP Knockdown durchgeführt. Dabei zeigte sich ein Abbau von mutp53 mittels der MDM2-abhängigen physiologischen p53-Degradationsmaschinerie, bestehend aus einem nukleären Export und gefolgt von einer proteasomalen Degradierung. Eine anschließende Genexpressionsanalyse zeigte eine Suppression von Zellzyklusgenen und eine Induktion des Interferon-Signalweges nach TRRAP Knockdown, welches allerdings nicht zur mutp53-Regulation beitrug. Um funktionale Domänen von TRRAP aufzufinden, wurde eine CRISPR/Cas9-basierte Methode („CRISPR Scanning“) angewandt. Dabei wurde eine aus 109 Aminosäuren bestehende Region in der N-terminalen HEAT repeat-Region von TRRAP identifiziert, die eine zentrale Rolle für die mutp53-Stabilisierung und für das Zellüberleben spielte. In BL-Zellen mit Wildtyp-p53 zeigte sich, dass ein TRRAP Knockdown die p53-Stabilisierung und –Aktivität nach genotoxischem Stress beeinträchtigte. Bei einem abschließenden Medikamenten-Screening wurde herausgefunden, dass eine Inhibition

von Histondeacetylasen (HDACs) und insbesondere von HDAC1/2/3 den mutp53-Level gleichermaßen beeinträchtigte wie ein TRRAP Knockdown.

Zusammenfassend identifiziert diese Studie TRRAP als einen zentralen Regulator des p53-Levels und verbindet Histon-modifizierende Komplexe mit der Proteinakkumulation von p53. Basierend auf der GOF-Aktivität von mutp53 könnte dies die Basis für eine zielgerichtete Therapie von Lymphomen und weiteren Krebsarten mit mutp53 darstellen.

Table of contents

List of figures

List of tables

1 Introduction

1.1 The tumor suppressor p53 – "guardian of the genome"

The transcription factor p53, which is encoded by the *TP53* gene, is arguably one of the most extensively studied proteins and plays a role in almost every aspect of cancer biology. Discovered nearly 40 years ago (in 1979) and initially erroneously identified as an oncogene, p53's role as the cell's most important tumor suppressor is now well established[1,2], which is why it was entitled "guardian of the genome"[3].

1.1.1 Activation and function of the p53 pathway

p53 is the master regulator of the cell's response to stress and mainly exerts its tumor suppressive functions by regulating gene expression[4]. An overview of the p53 activation pathway is shown in Figure 1. p53 is activated by a plethora of cellular stresses which may cause transformation, including – but not limited to – DNA damage, hypoxia, oncogene activation, spindle damage, and nucleotide depletion[5]. For the sensing of stress signals, p53 relies on signal mediators, which transmit the information about the type of stress to either p53 or its negative regulator MDM2 (for details about MDM2 see 1.1.3.1, p. 4) via post-translational modifications such as phosphorylation[5]. Many stresses result in a specific activation of individual mediators: for example, the protein ARF is only induced by oncogene activation but not by irradiation[4,6], while the protein ATM is highly sensitive for sensing DNA breaks[7,8]. After a stress signal, the half-life of p53 substantially increases from minutes to hours and p53 accumulates, which allows the formation of homotetramers. Additional post-translational modification finally facilitates binding of p53 to its specific response elements (REs) upstream of p53 target genes. In concert with auxiliary cofactors such as histone acetyltransferases (HATs), p53 then mediates or represses gene transcription in order to drive a transcriptional program specifically tailored to the cellular insult. Depending on the insult's severity, p53 typically induces DNA repair, cell-cycle arrest, or apoptosis, which ultimately results in tumor suppression[4,5]. While these canonical p53 responses are the mostly described ones, it is important to note that recent studies have challenged their role in tumor suppression[9]. For example, Brady *et al.*[10] have described a p53 mutant (L25Q;W26S) which is defective in induction of cell cycle arrest and apoptosis but, however, still retains its full tumor suppressive function. Therefore, it has been suggested that alternative cellular processes downstream of p53, such as autophagy or metabolic reprogramming, may play key roles in p53's tumor suppressive function (Figure 1)[9].

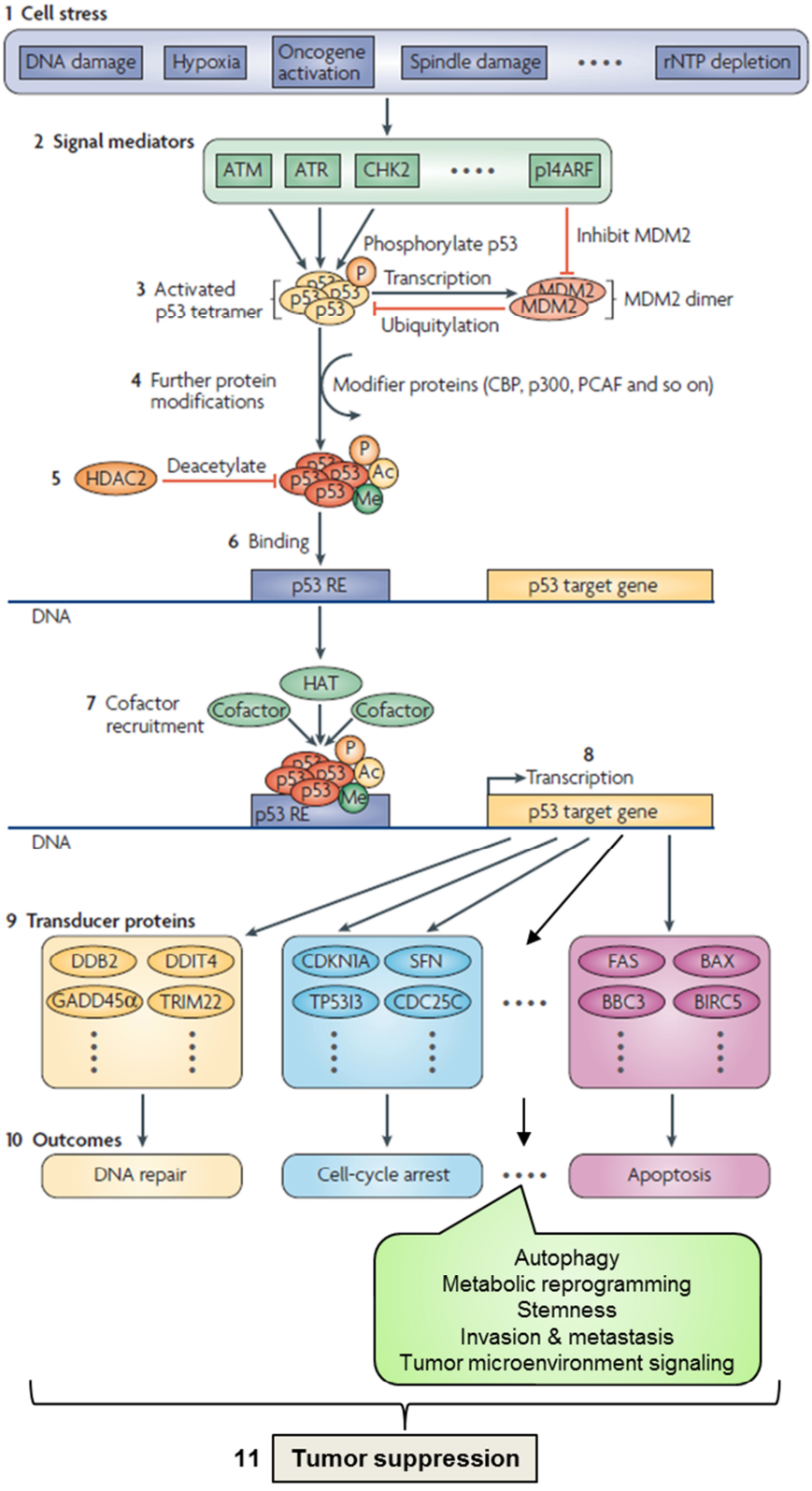

Figure 1: Activation of p53 and regulation of downstream target genes.
Cellular insults are detected by specific signal mediators, which both activate p53 and inactivate its negative regulator MDM2. With the assistance of additional modifier proteins and cofactors, p53 can bind as a tetramer to DNA response elements (REs) and mediate gene transcription. p53 target genes typically induce DNA repair, cell-cycle arrest, or apoptosis (classical p53 response). By additionally regulating cellular processes as for example autophagy or stemness, p53 activation ultimately results in tumor suppression. Adapted by permission from Macmillan Publishers Ltd: *Nat Rev Mol Cell Biol*, Riley *et al.*[5], copyright 2008, and modified based on Bieging *et al.*[9].

1.1.2 Structure of the human p53 gene and protein

The human *TP53* gene is located on chromosome 17p13.1, spans about 19 kb, and comprises eleven exons (Ensembl release 88)[11]. It is highly conserved through evolution of vertebrates[12]. Although *TP53* can give rise to ten distinct protein isoforms by different mechanisms, including alternative splicing and usage of alternative promoters, most research has been focused on its canonical and most abundant transcript (also termed TAp53α)[13], which was also the focus of this study. The canonical p53 protein consists of 393 amino acids, which can be roughly divided into three distinct functional regions (Figure 2)[14-16]: (1) the N-terminal region (amino acids 1-97), (2) the central core region (amino acids 98-292), and (3) the C-terminal region (amino acids 300-393).

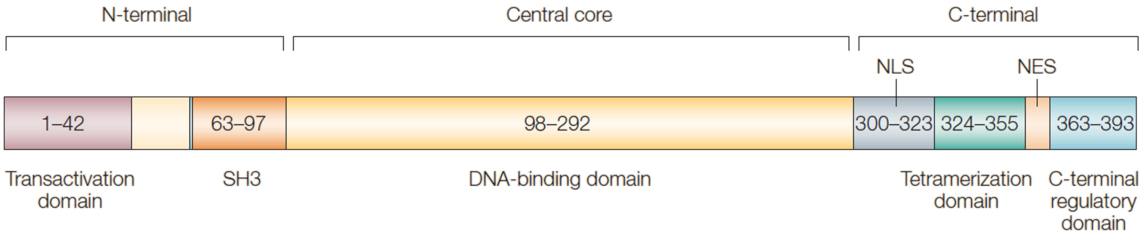

Figure 2: Domain structure of the canonical human p53 protein.
p53 consists of three major domains: (1) the N-terminal domain (including the transactivation domain and the SH3 domain), (2) the central core (DNA-binding domain), and (3) the C-terminal domain (containing the tetramerization domain, regulatory domain, NLS, and NES). Numbers indicate amino acid positions. SH3, Src homology 3-like domain. NLS, nuclear localization signal. NES, nuclear export sequence. Reprinted by permission from Macmillan Publishers Ltd: *Nat Rev Cancer*, Bode and Dong[15], copyright 2004.

The first 42 amino acids of the N-terminal region are part of the transactivation domain, which mediates the recruitment of members of the transcription machinery[17,18] and is therefore essential for p53's transactivation activity[19]. Many other interaction partners of p53 bind in this region, including p53's main negative regulator: the E3 ubiquitin ligase MDM2 (see 1.1.3.1, p. 4)[20]. The proline-rich SH3 domain (Src homology 3-like, amino acids 63-97)[15] has been shown to be important for apoptosis induction (but not growth arrest)[21] and transcriptional repression[22]. The central core of p53 comprises arguably the most important domain: the DNA-binding domain, which contains four highly conserved regions and equips p53 with the property to recognize and to bind to its specific DNA target sequences[23-26]. The C-terminus of p53 contains multiple additional important domains. The tetramerization domain (amino acids 324-355) enables tetramerization of p53 proteins[27], which is required for p53's transactivation capacity *in vivo* and for tumor suppression by growth inhibition *in vitro*[28]. The lysine-rich basic regulatory domain (amino acids 363-393) negatively regulates the binding of p53 to its target DNA sequences[14,29]. It can also facilitate binding to DNA breaks[30] and is the binding site for many p53-interacting proteins[14]. Finally, the C-terminus of p53 also contains the nuclear

localization and export signals needed for shuttling from the nucleus to the cytosol and *vice versa*[15].

1.1.3 Regulation of p53 levels and activity

Since activation of p53 has detrimental effects on proliferation, its activity is tightly controlled in physiological conditions. Therefore, p53 is negatively regulated by diverse mechanisms on multiple levels, with direct regulation of the p53 protein levels playing a central role[4].

1.1.3.1 MDM2 and the ubiquitin-proteasome pathway

The E3 ubiquitin ligase MDM2 is the "major physiological antagonist of p53"[31] and is responsible for keeping p53 levels low in unstressed conditions (Figure 3). *MDM2* is a direct target gene of p53, thereby forming a negative feedback loop: p53 induces MDM2, which in turn both degrades p53 and inhibits its transcriptional activity[32-35].

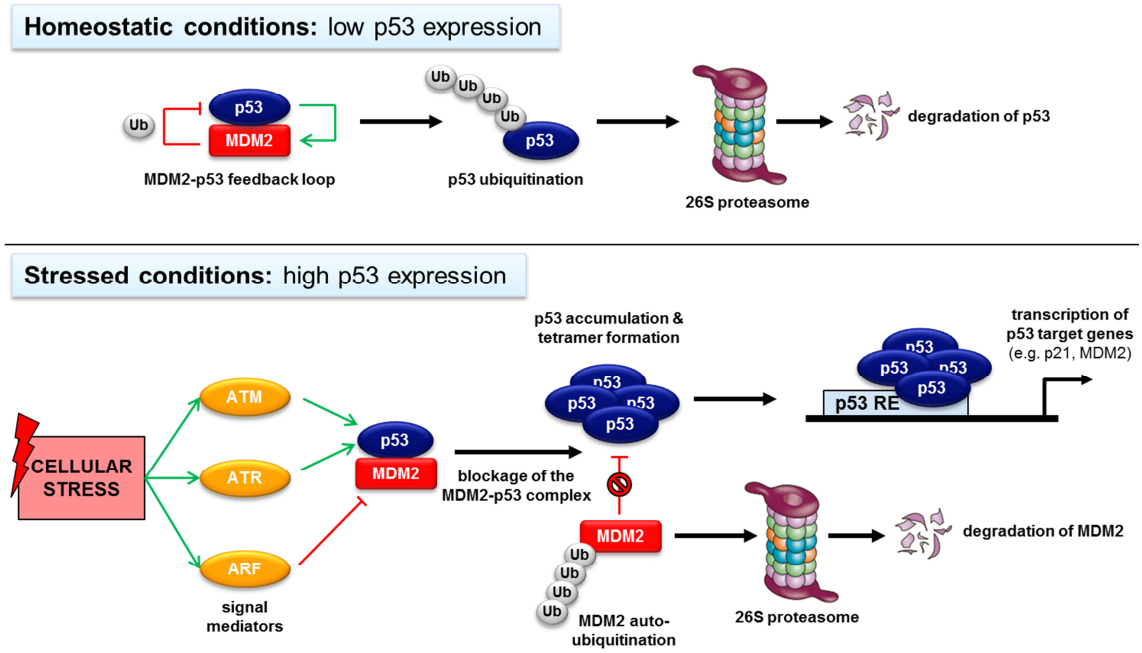

Figure 3: Regulation of p53 levels by MDM2.
In homeostatic conditions, the E3 ubiquitin ligase MDM2 (a p53 target gene) ubiquitinates p53, which is in turn degraded by the 26S proteasome. Upon stress (e.g. DNA damage), signal mediators block the formation of the MDM2-p53 complex. This allows p53 accumulation, tetramerization, and activation of its target genes after binding to response elements (REs) on the DNA. Under certain conditions, MDM2 can additionally undergo autoubiquitination and subsequent proteasomal degradation. Figure based on Metzger *et al.*[36].

The degradation of p53 by MDM2 is dependent on direct physical interaction between the N-termini of both proteins[31]. After binding, MDM2 promotes the ligation of ubiquitin via its RING finger domain to multiple lysine residues in p53's C-terminus[37], which results in proteasomal degradation of p53[38]. Upon stress signals, such as exposure to DNA-

damaging agents or ionizing radiation, the MDM2-mediated degradation of p53 is inhibited mainly by blocking of the MDM2-p53 complex formation[31]. This is, for example, achieved by phosphorylation of serine residues in the N-terminus of p53, the region where MDM2 is binding. In addition, also MDM2 can be phosphorylated, which augments its ability to promote p53 degradation[39]. Alternatively, other proteins can interfere with the binding of MDM2 to p53. The most prominent example for this is the tumor suppressor ARF, which binds to MDM2 and thereby shields p53[31]. Notably, MDM2 is also capable of self-regulation via autoubiquitination[40,41].

The cellular localization of p53 degradation is still under debate[31]. When cells are stressed, p53 accumulates in the nucleus. In contrast, p53 resides mostly in the cytosol in non-stressed conditions, where it is quickly degraded by the proteasome. Therefore, early studies suggested that MDM2 carries p53 to the cytosol[31,42]. However, the discovery that p53 harbors its own nuclear export sequence (NES) in the C-terminus[43] (Figure 2) fueled studies that led to the conclusion that ubiquitination by MDM2 changes the conformation of p53, which in turn makes the NES accessible for the cellular nuclear export machinery[31,44,45]. While these models are based on the assumption that nuclear export of p53 is a prerequisite for its degradation, other studies showed that p53 can in fact also be degraded by nuclear proteasomes[46,47].

Interestingly, MDM2 possesses additional functions for regulating p53 activity beyond ubiquitination. It can associate with subunits of the 19S proteasome in an ubiquitination-independent manner and promote the formation of a ternary complex consisting of itself, the proteasome, and p53[48]. Therefore, MDM2 may impact p53 degradation by regulating its accessibility to the proteasome machinery.

1.1.3.2 Post-translational modification of p53

p53 activation, accumulation, and the induced cellular response are fine-tuned by highly complex post-translational modifications (PTMs, Figure 4). The most important modifications include phosphorylation and acetylation[15].

Phosphorylation typically increases p53 protein stability and DNA-binding capacity[15,49]. p53 phosphorylation is reported for at least 18 different serine and threonine residues in response to stress, while many of these sites can be phosphorylated by different kinases. In addition, the same kinase may phosphorylate distinct residues in p53. Notably, the impact of dephosphorylation on p53 activity is so far not well understood[15,50].

Acetylation of p53 is induced after virtually any kind of stress exposure and may sometimes be preceded by phosphorylation[51]. p53 can be acetylated at ten different lysine residues by four major HATs: Tip60, CBP/p300, PCAF, and hMOF[50,52]. In general, acetylation of p53 is reported to have a positive effect on its stability and transcriptional activity[53], for example by shielding the acetylated residues from ubiquitination[51]. In line with this, p53 deacetylation by histone deacetylases (HDAC) usually results in ubiquitination and subsequent degradation of p53[15].

Given the high complexity and redundancy of p53 PTMs, single modifications are unlikely to have a considerable effect on p53 activity and cellular function. Instead, it is assumed that specific stresses induce different phosphorylation and acetylation patterns, which then define the appropriate cellular response[15].

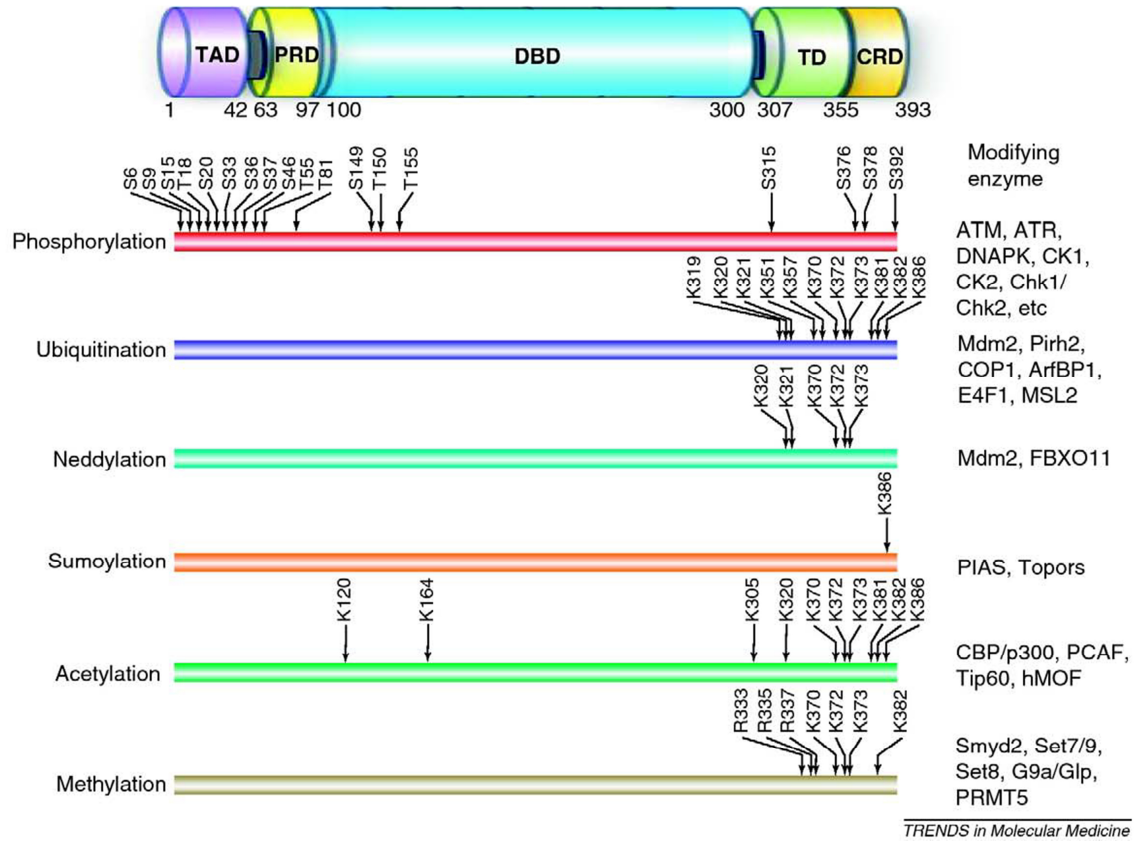

Figure 4: Post-translational modification of p53.
Summary of all reported modifications of p53, together with their modifying enzymes. TAD, transactivation domain; PRD, proline-rich domain; DBD, DNA-binding domain, TD, tetramerization domain; CRD, C-terminal regulatory domain. Numbers indicate amino acid positions of p53 protein. Reprinted from *Trends Mol Med*, Dai and Gu[52], copyright 2010, with permission from Elsevier.

1.1.4 p53 inactivation and gain-of-function in tumors

Given p53's role as the cell's most powerful tumor suppressor, it comes with no surprise that its function is compromised in the majority of human tumors. In general, p53 inactivation can arise via two distinct mechanisms: (1) by alterations in p53 activation/suppression or (2) by p53 point mutation[54].

About 50% of tumors with compromised p53 function retain wild-type p53 (wtp53) expression[54]. However, the molecular causes for p53 inactivation in these tumors are so far not well understood. Overexpression of MDM2 has been reported in some cancer cell lines and tumors[55,56]. Moreover, deletion and promoter hypermethylation of the MDM2 inhibitor ARF may cause abnormal MDM2 activation[57,58].

In the remaining tumors, p53 is inactivated via mutations in the *TP53* gene itself[54]. Overall, p53 mutations can be found in 42% of all tumors, with a highly variable frequency between different tumor types (Figure 5A). This makes p53 the most frequently mutated gene across all human cancers[59]. The majority of p53 mutations are missense mutations (74%), meaning they cause expression of a full-length protein with only a single amino acid substitution (Figure 5B)[2]. Most of these mutations cluster in the DNA-binding domain (Figure 5B)[2,60]. Mutations in codons R175, G245, R248, R249, R273, and R283 are by far the most frequent ones (so-called "hotspot mutations")[61] and were shown to be crucial for either establishing DNA contact or for stabilizing the DNA-binding surface structure (Figure 5B)[62]. In general, mutations in p53 can be divided into two categories[63]: (1) structural mutations which strongly alter the protein conformation or (2) DNA contact mutations which only impact DNA binding. Both kinds of mutations typically abrogate p53's capability to bind to its DNA response elements[64], which results in a loss of its tumor-suppressive function. This "loss of function" is further enhanced by the fact that mutant (mut) p53 has a dominant-negative effect over residual wtp53 (e.g. in case of heterozygous p53 mutation). The reason for this is that p53 protein heterotetramers, which consist of a mixture of mutp53 and wtp53 proteins, are no longer able to bind to DNA[65].

In addition to the loss of the wild-type function, mutp53 proteins often additionally acquire novel functions of their own – a phenomenon which is known as "gain of function" (GOF)[2,65]. In fact, a plethora of studies has shown that mutp53 is thus able to actively drive tumorigenesis by acting on multiple different pathways. Figure 5C and the following examples illustrate this:

- mutp53 drives genomic instability, for example by disrupting the spindle checkpoint control[66].
- mutp53 renders cells resistant towards pro-apoptotic signals[67].
- mutp53 renders cancer cells resistant towards chemotherapy[68].
- mutp53 drives cell migration and invasion[69].
- mutp53 drives the expression of chromatin regulatory genes, resulting in a global increase of histone methylation and acetylation[70].
- mutp53 drives the expression of the proteasome machinery, resulting in a degradation of tumor suppressors[71].

Based on these findings, it is not surprising that the presence of p53 mutation is associated with poor drug response, poor overall survival, and poor disease-free survival in many different cancer types, including hematopoietic cancers (Figure 5D)[2].

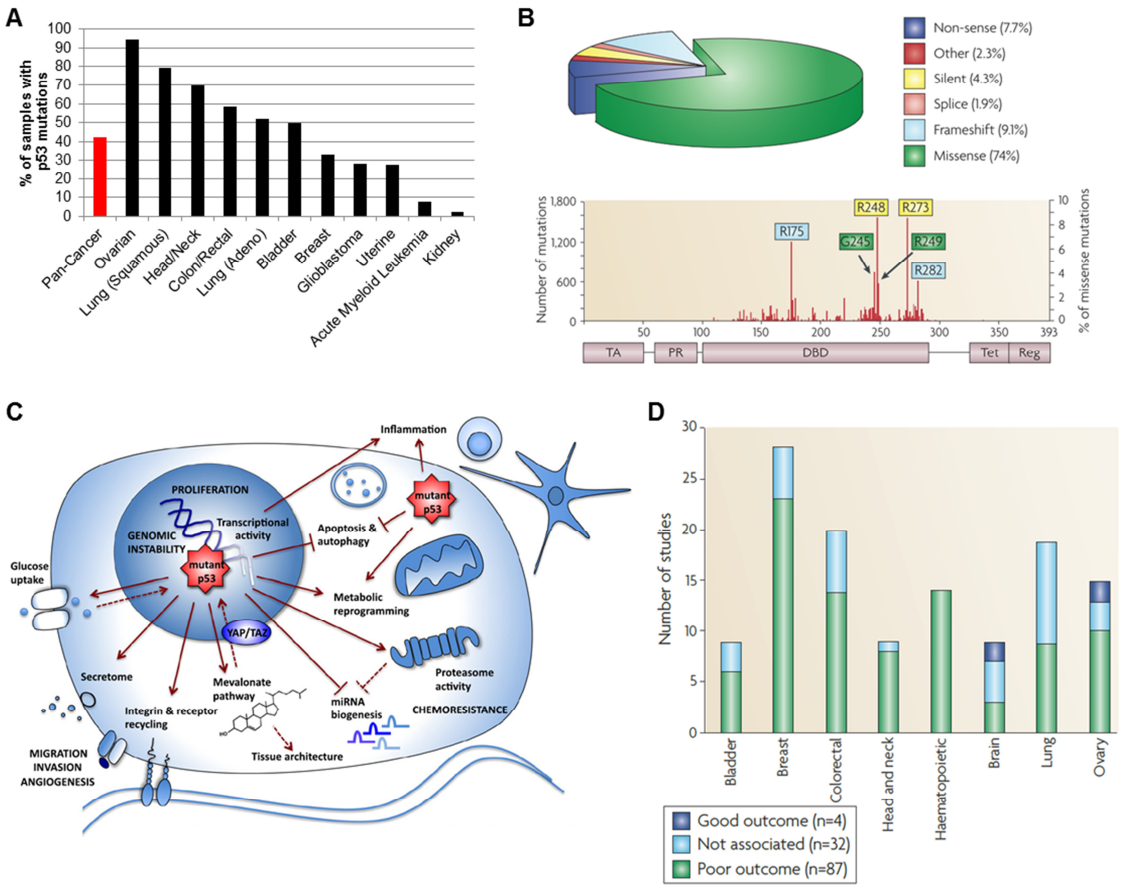

Figure 5: p53 mutations in human cancer.
(**A**) Frequency of p53 mutations in different cancer types. Based on data from Kandoth *et al.*[59]. (**B**) Distribution of p53 mutation types (top) and distribution of mutations along p53 protein (bottom) across cancer. The six hotspot mutations are highlighted. Domain annotation is similar to Figure 2. Reprinted by permission from Macmillan Publishers Ltd: *Nat Rev Cancer*, Brosh and Rotter[2], copyright 2009. (**C**) Overview of key tumorigenic functions of mutant p53. Reprinted by permission from John Wiley and Sons: *FEBS J*, Mantovani *et al.*[72], copyright 2016. (**D**) Impact of p53 mutation on patient outcome in different cancer studies. Reprinted by permission from Macmillan Publishers Ltd: *Nat Rev Cancer*, Brosh and Rotter[2], copyright 2009.

1.1.5 Mutant p53 accumulation in tumors

While the protein level of wtp53 is very low due to constant degradation by MDM2 (Figure 3), mutp53 typically undergoes massive stabilization and accumulates to extremely high levels in tumors (Figure 6)[73-75]. This observation is exploited in cancer diagnostics in a way that p53 immunohistochemistry (IHC) can serve as a surrogate for p53 sequencing: tumors with a high staining intensity typically harbor p53 missense mutations. However, the detection of p53 mutation via IHC has major drawbacks as for example tumors with frameshift or nonsense mutations do not accumulate p53 (Figure 6)[2,76].

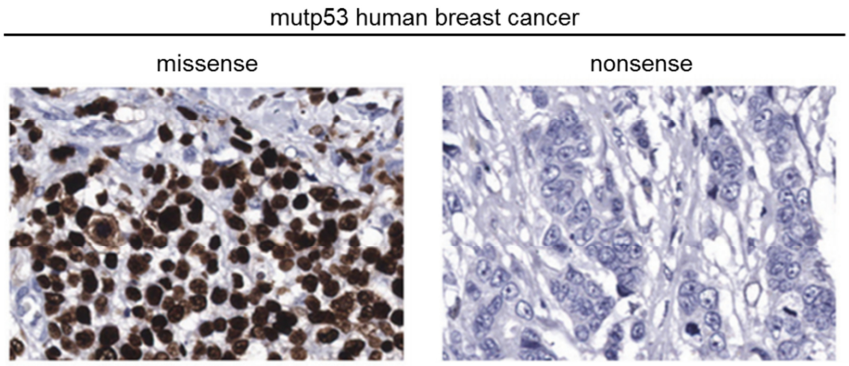

Figure 6: p53 immunohistochemistry of human breast cancer samples.
Exemplary staining of tumors with either a missense or a nonsense p53 mutation. Only the tumor with the missense mutation is characterized by strong staining. Adapted by permission from John Wiley and Sons: *J Pathol*, Bouchalova *et al.*[77], copyright 2014.

Despite the fact that mutp53 accumulation in tumors has been a very early discovery in the history of p53 research, still very little is known about its mechanistic causes. Knock-in studies revealed that mutp53 is not intrinsically stable and that it accumulates exclusively in tumors but not in normal cells[78-80]. Since mutp53 is defective in inducing MDM2 expression, it has been suggested that the disruption of the MDM2-p53 loop is responsible for mutp53 stabilization[65,81]. However, tumor cells typically show residual MDM2 expression[82,83] and more importantly, MDM2 is still capable of mutp53 binding and ubiquitination[84]. In addition, massive MDM2 overexpression is able to degrade mutp53[35]. Therefore, alternative mechanisms must contribute to the ability of mutp53 to evade degradation in cancer cells. A selection of the most relevant studies and their results is given in the following paragraphs.

Alternative splicing of MDM2 gives rise to several shorter isoforms, some of which are overexpressed in different human tumors, especially the MDM2-B isoform[85]. Recently, a study by Zheng *et al.*[86] showed that MDM2-B is able to contribute to mutp53 stabilization in tumors by inhibiting the interaction of canonical MDM2 with mutp53. In addition, the

expression of MDM2-B and accumulation of mutp53 were found to be highly correlative in human colorectal tumors.

Molecular chaperones are proteins that assist other proteins in proper folding by temporarily binding to them. Their function is especially needed in stress conditions such as cancer, which is typically characterized by expression of mutant proteins and increased proliferation, thus making it difficult to properly control proteostasis[87]. Among the chaperone proteins, heat shock protein 90 (Hsp90) plays a key role in controlling proteostasis in health and disease[87]. In fact, Hsp90 is aberrantly expressed in many human cancers and assists in folding of many mutated oncogenes, including BRAF and EGFR[88]. A study by Li *et al.*[83] showed that Hsp90 forms a stable complex with mutp53 and MDM2, thereby shielding mutp53 from degradation by MDM2 (Figure 7). Additional studies recently found that two proteins of the Bcl-2 associated athanogene (BAG) family, BAG2 and BAG5, can act as co-chaperones in a similar fashion as Hsp90 to stabilize mutp53 in tumor cells[89,90].

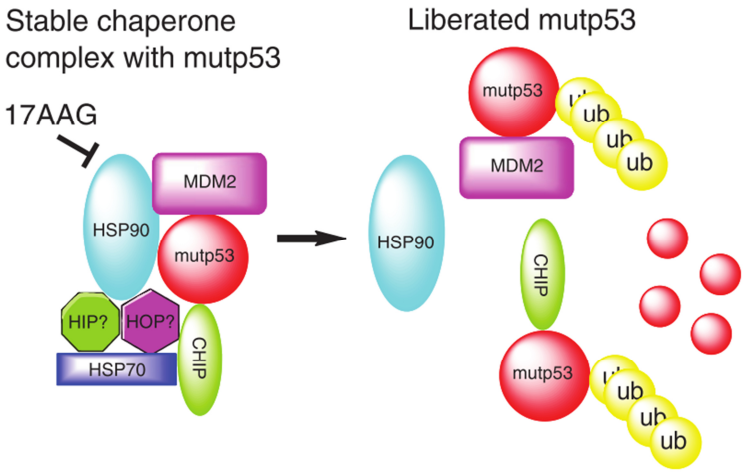

Figure 7: Chaperoning of mutant p53 by Hsp90.
Hsp90 forms a complex with mutp53, MDM2, and other chaperones and ubiquitin ligases, which protects mutp53 from degradation. Upon disruption of this complex, for example by Hsp90 inhibition, mutp53 is released and degraded via the ubiquitin-proteasome pathway. Reprinted from *Mol Cancer Res*, Li *et al.*[83], copyright 2011, with permission from AACR.

Similar to wtp53 (Figure 4), PTM of mutp53 is suggested to have an impact on its protein stability (and activity)[91]. Analysis of the pattern of p53 mutations across cancer shows that the majority of modified residues are not frequently affected by mutations. Furthermore, none of the p53 hotspot mutations (Figure 5B) undergo modification and no exclusive modifications of mutp53 have been identified. This indicates that PTM function is conserved between wtp53 and mutp53. Therefore, modifications which stabilize wtp53 can be assumed to also enhance mutp53 stability[91]. In fact, several studies showed that

stress stimuli that stabilize wtp53 (e.g. DNA damage, irradiation) also enhance mutp53 stabilization[79,92,93].

Only a limited number of studies addressed the impact of mutp53 PTM on its stability and the results are often contradictory[91]. Phosphorylation of S392 renders mutp53 sensitive to MDM2-mediated degradation and is negatively correlated with mutp53 expression[94,95]. Constitutive phosphorylation of S15 by ERK shields mutp53 from MDM2 in mouse skin tumors[96]. However, S15 phosphorylation was found to be low or absent in many different mutp53 cancer cell lines and human skin tumors[83,97].

The impact of mutp53 acetylation on its stability appears to be even more complex and remains largely elusive[91]. Minamoto *et al.*[98] and Yi *et al.*[99] have reported mutp53 hyperacetylation and subsequent degradation upon deacetylation of residues K320/K373/K382. In contrast, Perez *et al.*[100] found that mutp53 acetylation in residues K320/K373 by PCAF restored the DNA-binding ability of mutp53 and inhibited proliferation[100]. In addition, Li *et al.*[83] did not find evidence for mutp53 acetylation in basal conditions in a panel of cancer cell lines with highly stable mutp53 protein.

In summary, tumors often accumulate high levels of mutp53 protein but the mechanisms that govern this excessive accumulation are not entirely understood.

1.1.6 Targeting mutant p53 for cancer therapy

The discovery that p53 is very frequently inactivated by mutation led to the development of different mutp53-based cancer therapy approaches (Figure 8), which are discussed in detail in the following sections. One promising attempt is arguably aiming at a specific degradation of mutp53, which was also the focus of this study. In general, all approaches are based on the assumption that targeting mutp53 will have minimal side effects since it is exclusively expressed by malignant cells[101].

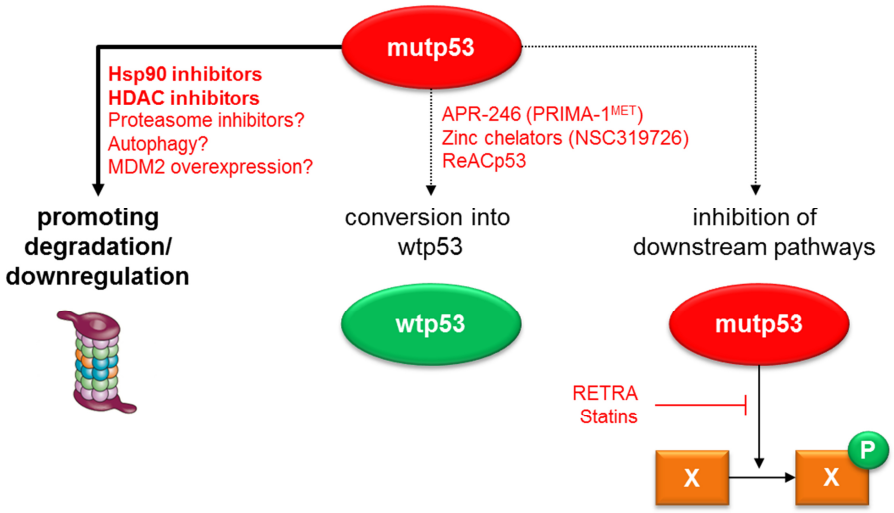

Figure 8: Overview of different strategies to target mutant p53 in cancer.
Drugs and molecular pathways/targets which are under investigation are depicted in red. Figure based on Muller and Vousden[101].

1.1.6.1 Promoting mutant p53 degradation/downregulation

Numerous studies have shown that mutp53 stabilization is a prerequisite for its GOF properties[2,65,101,102]. mutp53 silencing results in suppression of tumor growth, attenuated invasion and metastasis formation, and increased chemosensitivity in many tumor cell lines and xenografts. Recently, a landmark *in vivo* study confirmed these results using a mutp53 T-cell lymphoma mouse model expressing an inactivatable p53 hotspot mutation (R248Q)[103]. After inactivation, even advanced tumors underwent apoptosis and regression. This suggests that interfering with mutp53 accumulation may be exploitable in cancer therapy. However, as already mentioned earlier (see 1.1.5, p. 9), the mechanisms that govern erroneous accumulation are not well understood.

Since it has been shown that mutp53 can be aberrantly stabilized by Hsp90 (Figure 7), treatment of breast, prostate, and colorectal tumor cells with the Hsp90 inhibitor 17-AAG was found to result in mutp53 destabilization and thereby to impair proliferation[83]. These findings have been recently validated *in vitro* and *in vivo* by using Ganetespib, a next-generation Hsp90 inhibitor[103]. Ganetespib is currently tested (in combination with Paclitaxel) in Phase I and II studies in ovarian cancer patients (GANNET53 trial).

Treatment of mutp53 cells with HDAC inhibitors has been reported to downregulate mutp53 expression on diverse levels. While the central function of HDACs is the regulation of transcription by removing acetyl groups from histones, they can also deacetylate a plethora of non-histone proteins. The finding that HDACs are often overexpressed in cancer lead to the development of many HDAC inhibitors[104]. Blagosklonny *et al.*[105] were first in observing mutp53 destabilization and p21 induction

upon treatment of breast and prostate cancer cell lines with the pan-HDAC inhibitors FK228 and Trichostatin A. Later, it was found that HDAC1, 2, and 8 are crucial for maintaining *TP53* transcription[106,107]. However, most attention has recently been paid to HDAC6 because it is a key positive regulator of Hsp90. Inhibition of HDAC6 causes mutp53 degradation and impairs proliferation *in vitro*[82]. Combined inhibition of Hsp90 and HDACs was shown to suppress tumor growth and prolong survival of mutp53 mice[103].

Since wtp53 levels are typically kept low via proteasomal degradation, treatment of wtp53 cells with proteasome inhibitors results in p53 accumulation[108]. Surprisingly, a study by Halasi *et al.*[109] found that proteasome inhibition causes mutp53 degradation in numerous cancer cell lines, most likely via stabilization of MDM2. In fact, it has long been known that MDM2 overexpression is able to degrade mutp53[35]. Later, Choudhury *et al.*[110] reported that proteasome inhibition results in mutp53 degradation via autophagy. (Macro-)autophagy is the process by which cells degrade unwanted material contained in the cytoplasm, including whole cell organelles[111]. In line with this, Rodriguez *et al.*[112] found that autophagy induction by glucose starvation specifically depleted mutp53 but stabilized wtp53 in various cancer cell lines. In contrast, inhibition of macroautophagy with Spautin-1 surprisingly also resulted in degradation of multiple p53 mutants via the chaperone-mediated autophagy pathway[113]. In summary, these results indicate that the role of proteasome- and autophagy-mediated degradation of mutp53 levels is multi-layered and likely to be dependent on the cellular context[101].

Due to the fact that many mutp53 tumors retain MDM2 expression[82,83] and that MDM2 overexpression is able to degrade mutp53[35], another appealing therapeutic approach to target mutp53 may be to increase MDM2 levels. However, since p53 is the main positive regulator of MDM2, this may be challenging because the p53-MDM2-feedback loop is disrupted in a mutp53 context[65,81]. In fact, only a limited number of transcriptional regulators of MDM2 besides p53 have been reported so far[114]. Nevertheless, one promising candidate protein is PTEN, which has been shown to promote mutp53 GOF by inhibiting MDM2 transcription[115]. Importantly, PTEN inhibition can cause a reduction of both mutp53 levels and tumor growth *in vivo*[115]. Notably, a specific small-molecule inhibitor against PTEN (SF1670) was developed by Rosivatz *et al.*[116] but has not yet been tested in a mutp53 context.

In summary, multiple different approaches have been developed that aim at degrading mutp53 especially in solid tumors. However, a deeper understanding of the mechanisms that drive mutp53 accumulation will help in advancing them as well as in developing novel approaches.

1.1.6.2 Restoring wild-type p53 activity

Although p53 mutations can be found in virtually any residue in its DNA-binding domain (Figure 5B), they all have in common that they impair proper folding of the p53 core domain at physiological temperature[117]. Ultimately, this results in a loss of DNA binding capacity. Since mutp53 was shown to regain this capacity at low temperatures[63,117-119], this led to the hypothesis that the defect in DNA binding is reversible, meaning that mutp53 can be refolded and thereby "re-educated" to wtp53[120]. Due to the fact that tumor cells are typically flooded with mutp53 protein, its refolding into wtp53 with potent tumor suppressive function is an attractive therapeutic approach[120]. Moreover, mutp53 tumors are expected to be exquisitely sensitive towards wtp53 reactivation since the inactivation of p53 has been selected during tumor evolution[117]. Multiple pioneer studies proved that for example binding of antibodies to either the N- or C-terminus of mutp53 successfully reactivated DNA binding[117]. These findings initiated the search for small molecules and peptides able to bind to mutp53 and to restore wtp53 activity, which is now pursued by many research groups mostly by either chemical screenings or rational design[101,117,120,121].

A promising small molecule identified in a cell-based assay is APR-246 (also called PRIMA-1^{MET}), which is able to bind mutp53 and to restore its wild-type activity. It has been shown to inhibit growth of mutp53 cancer *in vitro* and *in vivo* and is now in clinical development[122]. In fact, it has already successfully passed Phase I studies in hematological tumors expressing mutp53[123,124] and is currently tested in a Phase II study in patients with high-grade serous ovarian cancer (Aprea Therapeutics).

Another promising approach is based on the fact that wtp53 depends on zinc for proper folding, while mutp53 is often impaired in zinc binding[125]. The supply of zinc to cells or mice expressing mutp53 has been shown to restore its DNA-binding capacity and to suppress tumor growth[126]. The same effect can be achieved by using small molecule zinc chelators (zinc metallochaperones) such as NSC319726 (also called ZMC1)[127].

Some p53 mutants (e.g. the hotspot mutations R175H and R248Q) have been shown to form amyloid aggregates, which not only sequester mutp53 but also residual wtp53 together with additional tumor suppressors such as p63 and p73[128]. Recently, Soragni *et al.*[129] reported a peptide (ReACp53) which inhibits mutp53 aggregate formation and rescues wtp53 function, thereby causing cancer cell death *in vitro* and tumor xenograft regression *in vivo*. However, the specificity towards mutp53 and thereby the mode of action of ReACp53 has been challenged recently by Wang and Fersht[130].

1.1.6.3 Inhibition of signaling pathways deregulated by mutant p53

Another approach to target mutp53 is to inhibit the signaling pathways downstream of mutp53 GOF (Figure 5C). This has, however, only been exploited in few studies so far[101] most likely due to the vast heterogeneity and context-dependency of mutp53 GOF. Several mutp53 proteins have been reported to inhibit the function of the tumor suppressor proteins p63 and p73 by binding to them, which contributes to tumorigenesis[101]. Kravchenko *et al.*[131] identified a small molecule named RETRA that is able to release p73 specifically in mutp53 cancer cells, which results in activation of p73 target genes and thereby inhibits cancer growth *in vitro* and *in vivo*.

In a 3D culture model of breast cancer cells, mutp53 was shown to drive the expression of the mevalonate pathway, which is mainly responsible for cholesterol synthesis. In fact, blockage of cholesterol synthesis with Simvastatin or Mevastatin resulted in growth inhibition, cell cycle arrest, and apoptosis in mutp53 breast cancer cells[132].

1.2 Non-Hodgkin lymphoma

Non-Hodgkin lymphoma (NHL) describes a heterogeneous group of lymphoproliferative diseases and can be broadly divided into two subsets which derive from either B lymphocytes or T lymphocytes, respectively. Despite equal frequencies of B cells and T cells in the human body, the vast majority (85-90%) of NHL originate from B cells (B-NHL), indicating that specific processes during B-cell development may be particularly tumorigenic[133-135].

1.2.1 Role of the germinal center reaction in lymphomagenesis

Germinal centers (GCs) play a crucial role in humoral immunity and are compartments in which B cells undergo differentiation and harsh selection[133,136-139]. In general, GCs can be roughly divided into two distinct zones (Figure 9): While the dark zone (DZ) is almost solely made up of proliferating B cells ("centroblasts") and reticular cells, the light zone (LZ) contains besides non-dividing B cells ("centrocytes") also macrophages, T cells, and follicular dendritic cells[138].

The main task of the GC reaction is the generation of specific B-cell clones able to secrete antibodies with the highest affinity (Figure 9)[138]. To achieve this, activated B cells first undergo rapid proliferation and somatic hypermutation (SHM) in the DZ[138,139]. During SHM, the enzyme activation-induced cytidine deaminase (AID) induces DNA breaks in the variable region of the immunoglobulin gene (IgV). Erroneous repair mechanisms introduce single nucleotide exchanges, which gives rise to a heterogeneous population of centroblasts with diverse antigen affinities[139]. After trafficking to the LZ and differentiation into non-dividing centrocytes, cells expressing B-cell receptors (BCRs) with the highest affinity are positively selected[138]. Subsequently, part of the centrocytes undergoes immunoglobulin (Ig) class-switch recombination (CSR), which is again mediated by AID. During CSR, the C-region of the Ig heavy chain is exchanged with that of a different Ig gene via intrachromosomal deletional recombination[133,140]. This results in antibodies with an identical antigen affinity but with a different effector function[133,139]. Finally, centrocytes differentiate into precursors of antibody-secreting plasma cells ("plasmablasts") or memory B cell precursor cells, both of which are needed for an effective protection against pathogens[133,138,139]. Notably, GC B cells often shuttle multiple times between the DZ and LZ, thus giving rise to B cells with the highest possible antigen affinities[138].

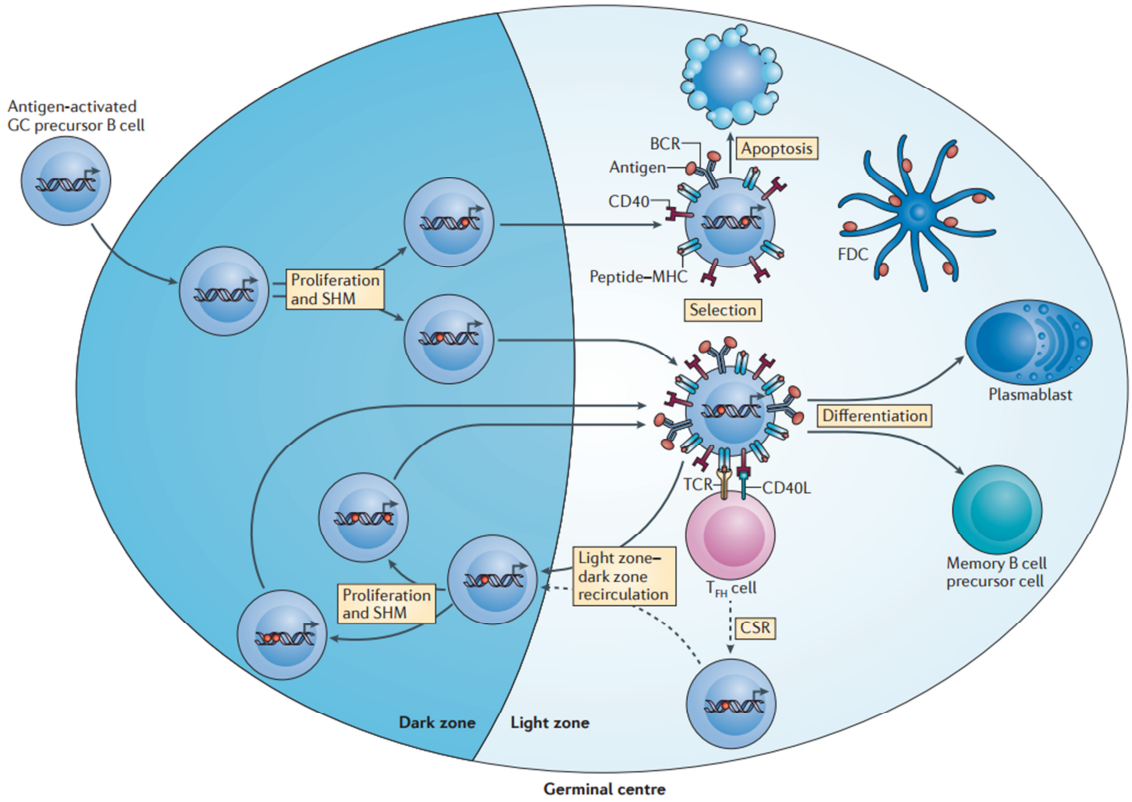

Figure 9: The germinal center (GC) reaction.
GCs are formed in peripheral lymphoid organs upon T-cell-dependent antigen exposure. Activated B cells undergo massive proliferation and somatic hypermutation (SHM) in the variable region of the immunoglobulin gene in the dark zone, resulting in a heterogeneous B-cell population with diverse antigen affinities. In the light zone, B cells with a high affinity B-cell receptor are positively selected, mainly by interacting with T cells. A subset of selected B cells circles back to the dark zone to further enhance antigen affinity, while others undergo immunoglobulin class-switch recombination (CSR) to change their antibody effector function. Eventually, GC B cells differentiate into plasmablasts or memory B cell precursor cells. Reprinted by permission from Macmillan Publishers Ltd: *Nat Rev Immunol*, De Silva and Klein[138], copyright 2015.

For several reasons, errors in the GC reaction are believed to be the major cause for most B-NHLs (Figure 10), including Burkitt's lymphoma (BL), follicular lymphoma (FL), and diffuse large B cell lymphoma (DLBCL)[141]. First, almost all B-NHLs are characterized by mutated IgV, indicating that they originate from GC B cells[142,143]. Second, the gene expression profiles of many B-NHLs are highly similar to the profiles of healthy DZ or LZ GC B cells[144]. Third, B-NHLs typically harbor two types of genetic aberrations, namely aberrant SHM (ASHM) and chromosomal translocations, both of which are part of the physiological Ig remodeling machinery activated specifically in the GC[138,139]. ASHM mostly occurs in DLBCL and typically targets non-Ig loci, thereby introducing activating mutations in proto-oncogenes such as *MYC*[145]. Chromosomal translocations are frequently caused by erroneous CSR and often merge a regulatory region of an Ig gene with an oncogene, thereby for example resulting in MYC overexpression in BL[146].

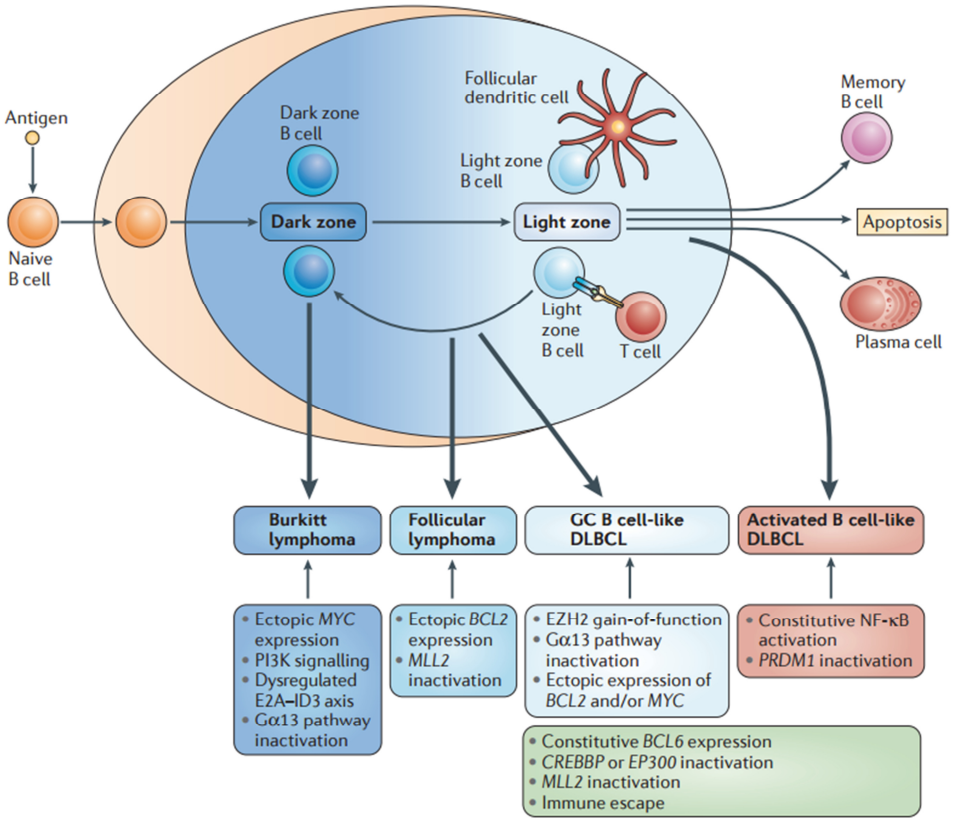

Figure 10: Cellular origin and oncogenic alterations of B-cell non-Hodgkin lymphomas derived from the germinal center (GC) reaction.
While Burkitt's lymphoma is derived from GC B cells in the dark zone and characterized by MYC overexpression, follicular lymphoma originates from B cells in the light zone and shows BCL2 overexpression. Both diffuse large B-cell lymphoma (DLBCL) subtypes also stem from light zone B cells and constitutively express BCL6. Reprinted by permission from Macmillan Publishers Ltd: *Nat Rev Immunol*, Basso and Dalla-Favera[141], copyright 2015.

1.2.2 Burkitt's lymphoma (BL)

BL is a highly aggressive NHL which is derived from DZ GC B cells (Figure 10)[141]. In 1985, Guy de Thé termed BL the "Rosetta stone of cancer"[147], indicating that the mechanisms of BL lymphomagenesis may also play a role in cancer biology in general. In fact, BL research has substantially contributed to an improved understanding of tumorigenesis due to the fact that[148]:

- BL has the highest growth rate (doubling time 24-48 h) among all human cancers[149].
- BL was the first human cancer reported to be associated with a virus (Epstein-Barr virus, EBV)[150] and the first human lymphoma shown to be associated with human immunodeficiency virus (HIV)[151].
- BL was among the first human cancers identified to show an aberrant oncogene activation (MYC) driven by chromosomal translocation[152,153].

1.2.2.1 Classification, diagnosis & treatment

Unlike many other cancers, BL is typically a disease of younger patients: approximately every second BL patient is less than 40 years old[154]. Since its discovery in 1958 by the surgeon Denis Burkitt[155], the World Health Organization (WHO) today discriminates three different BL variants with comparable morphology, genetics, and immunophenotype[148,156,157]:

1. **Endemic BL** (eBL) is strongly associated with EBV and malaria infection and describes the cases occurring only in Africa and Papua New Guinea. In these areas, eBL makes up approximately every second cancer diagnosis in children and virtually every lymphoma diagnosis[148]. eBL patients most commonly suffer from tumors in the jaw or facial bone, while tumors in the abdomen and bone marrow infiltration are rare[154].
2. **Sporadic BL** (sBL) describes tumors occurring anywhere else in the world, usually in the West, and is typically not linked to viral infection. sBL is the most common NHL in children up to 14 years (in the United States) and occurs more frequently in boys[135,148]. sBL patients most commonly suffer from tumors in the abdomen[154].
3. **Immunodeficiency-related BL** is typically seen in patients infected with HIV who develop acquired immunodeficiency syndrome (AIDS)[148].

Diagnosis of BL is often based on histopathology (Figure 11A)[148,154]. Typical of BL is its "starry sky" appearance in histology, which is caused by macrophages that are surrounded by densely packed lymphoma cells[158]. In addition, BL cells show intensive staining for Ki-67 and CD20/CD10, reflecting their very high proliferation rate and B-cell lineage[148].

BL can be treated very effectively with high-dose chemotherapy composed of Doxorubicin, Vincristine, Etoposide, and alkylators[159], which can be combined with the anti-CD20 antibody Rituximab[160]. The overall cure rate for young patients in the range of 15-40 years is excellent and around 85-90%, but treatment of adult patients remains challenging, most likely because of elevated therapy-related toxicity[148,154,159]. In addition, the risk of treatment toxicity due to tumor lysis syndrome is extremely high, especially at the beginning of the therapy. Therefore, BL patients require intensive supportive care, which is particularly difficult to sustain in low-income countries[148]. Overall, this suggests that novel therapy approaches are needed to treat both elderly BL patients and BL patients in low-income countries more efficiently and more safely.

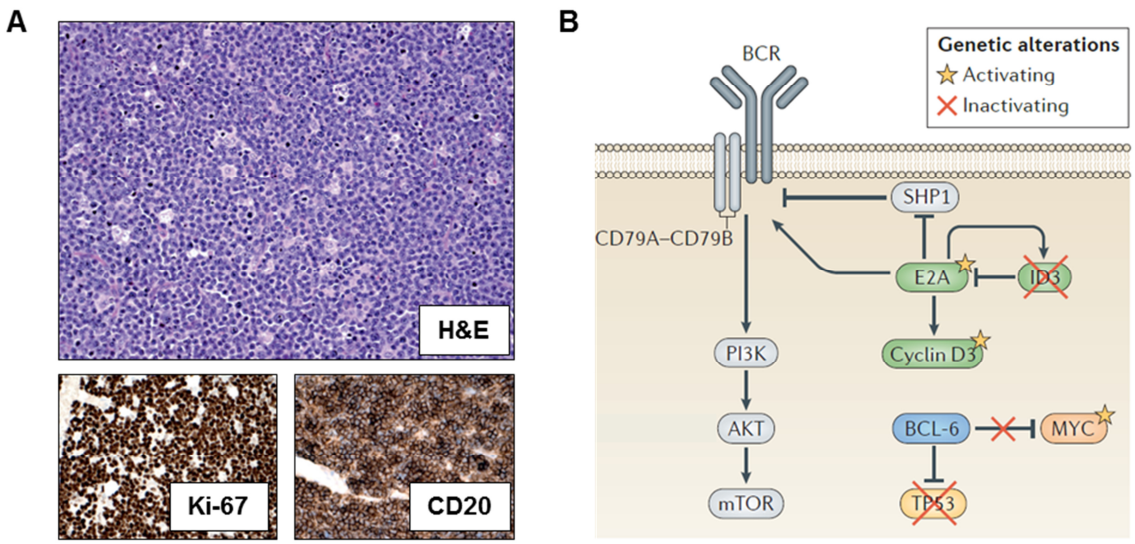

Figure 11: Histopathology and lymphomagenesis of Burkitt's lymphoma.
(**A**) Burkitt's lymphoma (BL) shows a characteristic "starry sky" pattern in hematoxylin and eosin (H&E) staining and is positive for the proliferation marker Ki-67 and the B-cell marker CD20. Adapted from *The Lancet*, Molyneux *et al.*[148], copyright 2012, with permission from Elsevier. (**B**) Overview of the key oncogenic pathways. Activation of the proto-oncogene MYC is the hallmark of BL. In addition, tonic B-cell receptor signaling via PI3K, AKT, and mTOR is active in most BLs and is further enhanced by mutations in the E2A-ID3 axis. Cyclin D3 mutations contribute to BL proliferation. In order to evade apoptosis, p53 mutation or inactivation is frequent. Adapted by permission from Macmillan Publishers Ltd: *Nat Rev Immunol*, Basso and Dalla-Favera[141], copyright 2015.

1.2.2.2 Lymphomagenesis

An overview of the oncogenic pathways in BL lymphomagenesis is given in Figure 11B. Aberrant expression of the proto-oncogene MYC caused by chromosomal translocation can be found in all BL patients and is therefore the hallmark of BL[157]. The most common translocation is t(8;14)(q24;q32) and present in 70-80% of cases[148]. All translocations put MYC under the control of an Ig enhancer region, thus resulting in constitutive MYC expression[148]. MYC is a transcription factor that plays a central role in regulating amongst others proliferation, apoptosis, DNA replication, and GC formation[141]. Although mice develop B-cell lymphomas upon ectopic MYC expression[161], MYC is assumed to require additional oncogenic events in order to induce BL[157,162]. Interestingly, MYC is also the most frequently mutated gene in BL. 70% of BL patients harbor missense mutations in MYC, which are often located in the transactivation domain and most likely introduced by ASHM (Figure 9)[163]. Selected MYC mutants have been reported to promote B-NHL lymphomagenesis more effectively than wild-type MYC[164].

MYC overexpression has been shown to sensitize cells towards apoptosis, mostly in a p53-dependent manner. Therefore, p53 inactivation is essential in MYC-driven tumors in order to escape apoptosis (Figure 11B)[165]. p53 mutations are present in ~35% of BL patients (range: 16.7-63.0%, Table 1) and in ~60-80% of BL cell lines[166-168] with a high

frequency of missense mutations, indicating that mutp53 may be associated with tumor progression. Mutations are typically heterozygous[166,169] and complete deletion of p53 is found in 10% of the patients[170,171]. The most frequent mutations affect codons 175, 213, and 248, while mutations in codon 273 are less common[166]. Besides p53 mutation, overexpression of the negative regulators MDM2 and MDM4 has been reported to inactivate the p53 pathway in BL patients with wtp53[171,172]. Only limited data is available on the impact of p53 mutation on BL patient outcome so far. Preudhomme *et al.*[169] reported a similar chemotherapy response rate in wtp53 and mutp53 BL patients and no impact of p53 mutation on survival. This could be explained by the residual wtp53 allele in mutp53 patients since this may render cells still sensitive towards apoptosis[169,173]. Therefore, mutp53 may not have a dominant-negative effect on wtp53 in BL[169].

Table 1: Summary of studies reporting frequencies of p53 mutation in Burkitt's lymphoma patients.

Study	# Burkitt's lymphoma patients	p53 mutation frequency [%]
Bhatia *et al.*[166]	27	37.0
Gaidano *et al.*[174]	27	33.3
Haberl *et al.*[175]	47	60.0
Kretzmer *et al.*[176]	13	61.5
Leventaki *et al.*[171]	28	17.9
Love *et al.*[177]	59	23.7
Preudhomme *et al.*[169]	21	28.6
Richter *et al.*[178]	4	50.0
Sanchez-Beato *et al.*[179]	16	18.8
Schmitz *et al.*[163]	28 + 13 cell lines	34.1
Wilda *et al.*[172]	24	16.7
TOTAL	**307 (incl. cell lines)**	**34.7**

Mutations in cyclin D3 (CCND3) can be found in ~40% of sBL patients but are rare in patients suffering from eBL (Figure 11B)[157,178]. Since CCND3 is important for the regulation of cell cycle progression, its mutations have been shown to increase protein stability and to confer cells with a proliferation advantage[163]. Therefore, CCND3 mutation is believed to maintain the high proliferation rate of BL[157].

In ~70% of sBL patients, mutations are present in either the transcription factor TCF3 (E2A) or its negative regulator ID3 (Figure 11B). Mutations in either of the proteins disrupt the negative feedback loop of TCF3 and ID3, resulting in aberrant constitutive activity of TCF3[163,178]. TCF3 was shown to not only upregulate CCND3 but also to increase BCR expression[163]. In fact, the majority of BL is dependent on antigen-independent (tonic) BCR signaling funneled through PI3 kinase (PI3K)[163]. Interestingly, when Sander *et al.*[162] combined overexpression of MYC with constitutively active PI3K in GC B cells in mice, they were able to phenocopy human BL to full extent.

1.3 RNA interference screens as tools to study gene function

RNA interference (RNAi) is a simple and powerful mechanism for controlling gene expression at the post-transcriptional level[180]. It was discovered in 1998 by Fire *et al.*[181], who found that injection of a double-stranded RNA (dsRNA) complementary to an endogenous gene in the roundworm *C. elegans* resulted in silencing of that particular gene. The discovery that the mechanisms of RNAi are conserved in mammals only three years later[182] has revolutionized the study of gene function in health and disease ever since.

1.3.1 RNAi pathway

RNAi is believed to be an endogenous cellular defense mechanism against RNA viruses. While long dsRNA can be easily used to silence target genes in for example plants and *C. elegans*, introduction of long dsRNA in mammalian cells causes induction of an interferon response, which unspecifically inhibits global protein synthesis[180]. Therefore, to use RNAi in mammals, so-called short interfering RNA duplexes (siRNAs) must be used, which typically consist of a 19 bp core duplex with 2 bp 3' overhangs on each strand (Figure 12A)[183].

An overview of the RNAi pathway is depicted in Figure 12B. siRNAs can be delivered directly to mammalian cells by transfection or electroporation and are subsequently loaded into an endogenous multiprotein complex named RNA-induced silencing complex (RISC). The antisense strand of the siRNA is then used to guide RISC to its target mRNA, while the sense strand is degraded[180]. Binding of RISC to mRNA can have two effects. In case the siRNA is fully complementary to the mRNA, a component of RISC (RNase argonaute 2, AGO2) cleaves the mRNA, resulting in degradation of the target mRNA. In case of only partial complementarity, translation of the mRNA is inhibited[184]. Both effects result in a "knock-down" of the target gene, i.e. a reduced protein expression.

Using siRNAs has the disadvantage that they are only transiently expressed, meaning they become diluted with every cell division and therefore only cause short-term silencing of their target genes[180]. In fact, it has been reported that the majority of siRNA duplexes are degraded within 48 h in cells[185]. To overcome this drawback, cells can be stably transduced (by using e.g. lentiviruses[186]) with small hairpin RNAs (shRNAs), the precursors of siRNAs (Figure 12B)[187]. After integration into the cell's genome, shRNAs are transcribed, exported from nucleus, and finally processed into siRNAs by an

RNase III-like enzyme named DICER[184]. shRNAs do not only cause long-term silencing but can also be of advantage when working with cells which are difficult to transfect[180].

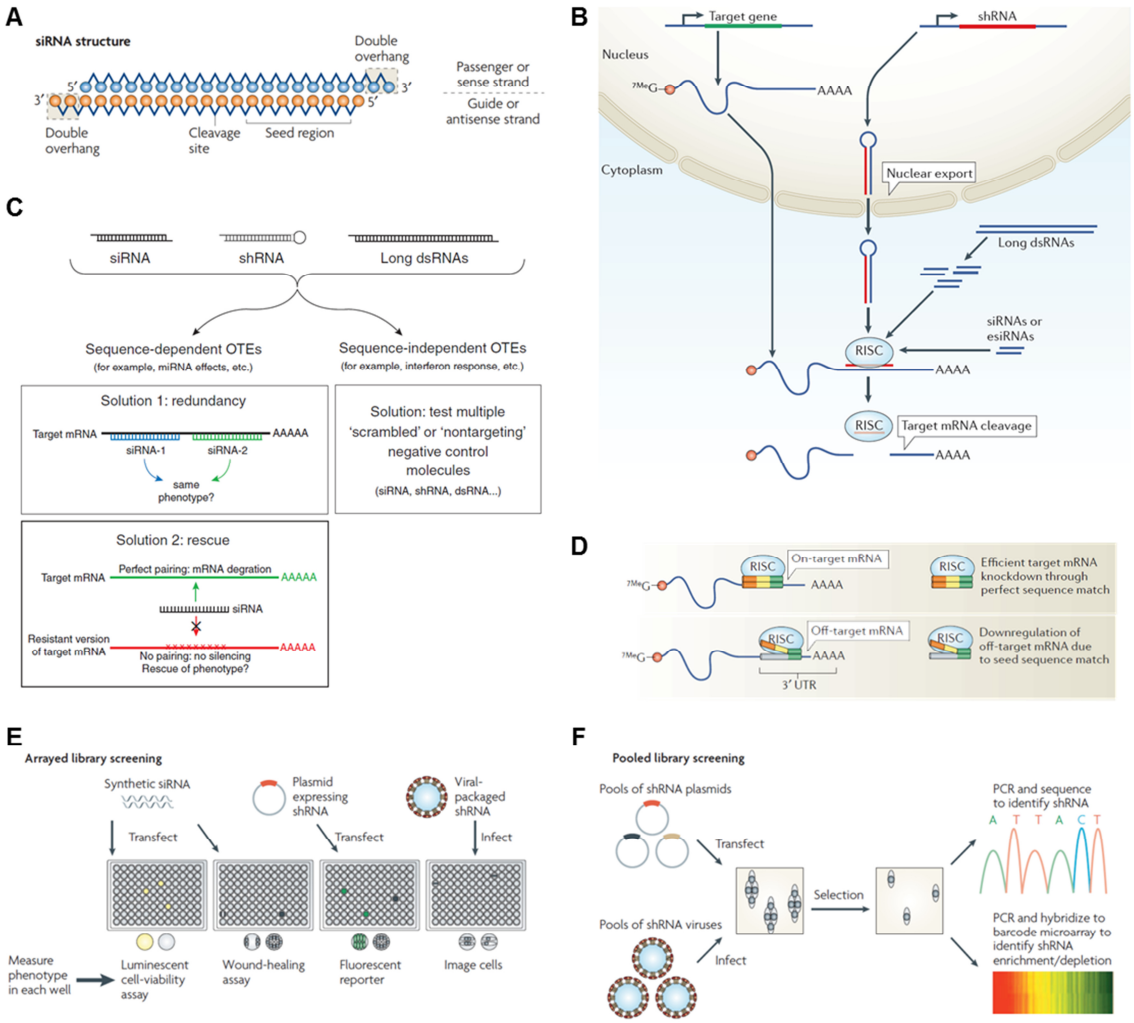

Figure 12: RNA interference (RNAi).
(**A**) Structure of a classic small interfering RNA (siRNA), which is made up of a 19 bp core duplex with 2 bp 3' overhangs on each strand. The seed region on the guide strand is indicated. Adapted by permission from Macmillan Publishers Ltd: *Nat Rev Drug Discov*, de Fougerolles *et al.*[183], copyright 2007. (**B**) Overview of the RNAi pathway. Small hairpin RNAs (shRNAs) are transcribed in the nucleus, exported, and loaded as siRNAs onto the RNA-induced silencing complex (RISC), which mediates target mRNA knock-down via mRNA binding and cleavage or translational repression (not shown). Adapted by permission from Macmillan Publishers Ltd: *Nat Rev Mol Cell Biol*, Mohr *et al.*[184], copyright 2014. (**C**) Overview of RNAi off-target effects (OTEs), which can be broadly categorized into sequence-dependent and –independent OTEs. Reprinted by permission from Macmillan Publishers Ltd: *Nat Methods*, Echeverri *et al.*[188], copyright 2006. (**D**) Comparison of the RNAi on-target and off-target effect. Adapted by permission from Macmillan Publishers Ltd: *Nat Rev Mol Cell Biol*, Mohr *et al.*[184], copyright 2014. (**E**) Arrayed RNAi screens. Cells are typically grown in multi-well plates and transfected or transduced with a single silencing trigger per well, which allows measuring more complex phenotypes. Adapted by permission from Macmillan Publishers Ltd: *Nat Rev Drug Discov*, Iorns *et al.*[180], copyright 2007. (**F**) Pooled RNAi screens. Cells are typically transduced with a pool consisting of a large number of shRNAs in a single batch and grown under selective pressure. The shRNAs contributing to the phenotype of interest are subsequently identified via PCR and sequencing or microarray (less common). Adapted by permission from Macmillan Publishers Ltd: *Nat Rev Drug Discov*, Iorns *et al.*[180], copyright 2007.

1.3.2 Off-target effects

All RNAi reagents show so-called off-target effects (OTEs), which describe all unintended interactions between the silencing triggers and cellular molecules that lead to phenotypic changes[188]. In general, OTEs can be categorized into sequence-dependent and sequence-independent effects (Figure 12C). The former are based on the fact that RNAi reagents require total complementarity between them and their target mRNAs only within the 8 bp siRNA "seed region" (Figure 12A,D), while the remaining base pairs do not necessarily have to match[188]. Several examples exist in the literature where investigators report that some of their phenotypes emerged only due to seed match effects[189]. Given that seed regions are very short, it remains an unresolved issue to either fully computationally predict OTEs or to design highly specific silencing triggers[184]. Sequence-independent OTEs describe all effects caused by mere introduction of RNAi reagents into cells[189]. Examples in the literature include alterations in microRNA (the naturally occurring counterpart of siRNA) processing and expression[190], induction of an interferon response[191], or induction of a cellular stress response[192].

Since OTEs could lead to false results, RNAi experiments require proper controls and intensive validation. Sequence-independent OTEs can be easily controlled by including "scrambled" or "non-targeting" silencing triggers[188]. In contrast, the control of sequence-dependent OTEs is more challenging and is most properly addressed by "redundancy or rescue"[188] (Figure 12C). Redundancy refers to the fact that multiple independent RNAi reagents targeting the same transcript should produce similar phenotype changes. This is based on the idea that it is extremely unlikely that silencing triggers with different seed regions will share the same OTEs and thereby give rise to the same off-target phenotypes. Rescue refers to an approach where the silencing phenotype is reversed ("rescued") by co-expression of a modified version of the targeted transcript that is resistant to silencing (e.g. by introduction of silent mutations). Since rescue experiments are often difficult to perform, most investigators aim for the redundancy approach by testing at least two independent silencing triggers in their experiments[188]. Besides redundancy or rescue, investigators are recently also encouraged to validate their RNAi findings by using an orthogonal, non-RNAi method. Mohr *et al.*[184] envision that CRISPR/Cas9-mediated knock-out may become routine for validating RNAi experiments in the future. However, it is reported that the phenotypes caused by knock-down and knock-out, i.e. by reduced transcript expression and complete loss of expression, must not always be comparable[193].

1.3.3 RNAi screens

While RNAi was initially used to investigate merely single genes of interest in separate experiments, it is now possible to use complex RNAi libraries consisting of hundreds of thousands of silencing triggers to "screen" the function of many genes in parallel in high-throughput experiments[194]. For example, the usage of genome-wide RNAi libraries allows probing of every single gene in the genome for a desired phenotype. Today, numerous different RNAi libraries are available (both commercially and free of charge) and researchers can even generate their own libraries to specifically target their genes of interest. RNAi screens are "forward genetic screens" ("phenotype-to-genotype" approach), meaning they start with lowering the expression of many genes, followed by a selection of cells with a phenotype of interest, which is then ended with the identification of the silencing triggers that caused the phenotypic changes[194,195].

RNAi screens can be performed in either arrayed or pooled format[180,195]. In an arrayed format (Figure 12E), silencing triggers (usually siRNAs) are arranged in multi-well plates with a single trigger per well. Cells are then seeded directly on top of the triggers, often together with a transfection reagent, and the phenotype of each well is determined separately. Although arrayed screens are in general more expensive and time-consuming, they allow a measurement of more complex phenotypes (e.g. cell morphology by microscopy). In addition, demultiplexing of arrayed screens is straightforward since the silencing triggers can be easily identified via their position on the plate. In contrast, in a pooled format (Figure 12F), a large number of silencing triggers (usually shRNAs) is mixed and used altogether for transduction of a mass of cells in a single batch. Importantly, the reaction conditions are optimized in a way so that on average one cell will only harbor a single RNAi reagent. Moreover, in order to maintain the library representation, every individual silencing trigger is integrated into a large number of cells (typically ~500 cells/RNAi reagent). Cells are then selected for the phenotype of interest and the silencing triggers are typically demultiplexed via next-generation sequencing or microarray. Pooled screens have the advantage of being cheaper and being easier to perform, bear however the limitation that they can only be used for studying fairly simple phenotypes (e.g. effects on cell growth). In general, pooled screens can be categorized as positive selection (e.g. expose cells to a drug, select surviving cells) or negative selection screens (e.g. depletion of cells due to a lethal knock-down).

RNAi screens have been used very successfully in the past for an identification of genes that play a role in numerous biological processes, including cancer biology with the

discovery of novel oncogenes, synthetic lethal interactions, and potential drug targets[180,184,196]. For example, Toyoshima *et al.*[197] performed an arrayed siRNA screen and identified the druggable kinase CSNK1e as a novel therapeutic target in MYC-driven cancer. One of the most comprehensive RNAi datasets has been generated by the Broad Institute of MIT and Harvard (Cambridge, USA) within the scope of the project "Achilles", in which the investigators screened 216 cancer cell lines in parallel to detect cancer-specific vulnerabilities[198].

In summary, RNAi screens are powerful and easy tools to unbiasedly probe large numbers of genes for their role in a particular phenotype of interest (e.g. regulation of protein levels in this study).

1.4 Scientific aims

Missense mutations in p53 cause expression of aberrant mutant p53 (mutp53) proteins that not only have lost their tumor suppressive function but also have often gained tumorigenic properties. Importantly, tumors depend on sustained and high levels of mutp53, suggesting that interfering with mutp53 accumulation may be exploitable in cancer treatment. Since the mechanism of mutp53 stabilization in tumors remains largely elusive, the **main aim of this study was to identify regulators of mutp53 accumulation**. The study was performed in Burkitt's lymphoma (BL) as a model for a highly aggressive cancer with a particularly high incidence of p53 mutations.

To achieve the aim, this study specifically focused on the following key points:

1. **Identification of candidate regulators of mutp53 accumulation.**
   To identify proteins involved in the control of mutp53 levels in an unbiased fashion, a large-scale RNA interference (RNAi) screen with flow cytometry-based phenotypic readout was performed.

2. **Validation of TRRAP as a novel regulator of p53 levels.**
   To confirm the role of the primary RNAi screen hit TRRAP (transformation/ transcription domain-associated protein) as a critical modulator of p53 levels, TRRAP expression was modulated and the impact on p53 accumulation was evaluated across cancer types and p53 mutations.

3. **Characterization of the functional mechanism underlying p53 regulation by TRRAP.**
   A set of experiments aimed at exploring the molecular mechanism of p53 regulation by TRRAP, including mass spectrometry of the mutp53 interactome and CRISPR scanning to identify TRRAP's functional regions.

4. **Identification of small molecules interfering with mutp53 accumulation.**
   To identify drugs modulating mutp53 levels for a potential clinical application, mutp53 cell lines were exposed to a panel of small molecules and their impact on mutp53 accumulation was evaluated.

2 Material & Methods

2.1 Material

2.1.1 Chemicals

Reagent	Supplier
10x Tris/Glycine/SDS Running Buffer	Bio-Rad
2-Mercaptoethanol	Sigma-Aldrich
4–15% Mini-PROTEAN TGX Precast Protein Gels	Bio-Rad
Adenosine 5'-Triphosphate solution (ATP)	GE Healthcare Life Sciences
Agar	Sigma-Aldrich
Agarose for DNA Electrophoresis	Serva
AgeI + NEBuffer 1.1	New England Biolabs
Ampicillin sodium salt	Sigma-Aldrich
Anti-human p53 mouse agarose beads	Santa Cruz Biotechnology
Bbs I (BpiI) + Buffer G	Thermo Scientific
Benzonase Nuclease	Merck
Blasticidin S HCl	Gibco
Bovine Serum Albumin (BSA)	GE Healthcare Life Sciences
BsmBI + NEBuffer 3.1	New England Biolabs
cOmplete EDTA-free Protease Inhibitor Cocktail	Roche
Dimethyl sulfoxide (DMSO)	Sigma-Aldrich
DNA Gel Loading Dye	Thermo Scientific
dNTP mix (Na salt)	Genaxxon
Dulbecco’s Modified Eagle Medium (DMEM)	Gibco
Dulbecco's Phosphate-Buffered Saline (PBS)	Gibco
EcoRI	New England Biolabs
Ethanol	Sigma-Aldrich
Ethidium Bromide solution 0.07 %	AppliChem
Fetal bovine serum (FBS)	PAN-Biotech
Formaldehyde solution 30 %, methanol-free	Carl Roth
GenElute Linear Polyacrylamide	Sigma-Aldrich
GeneRuler DNA Ladders 100 bp, 1 kb	Thermo Scientific
Glycine	Sigma-Aldrich
Hexadimethrine bromide (Polybrene)	Sigma-Aldrich
HiMark Pre-stained Protein Standard	Thermo Scientific
IGEPAL CA-630 (NP40 substitute)	Sigma-Aldrich
Interferon Alpha 2a, human	Pestka Biomedical Laboratories
IPA300, immobilized rProtein A agarose beads	RepliGen
Isopropyl-β-D-thiogalactopyranoside (IPTG)	Serva
Laemmli Sample Buffer, 2x Concentrate	Sigma-Aldrich
Laemmli Sample Buffer, 4x Concentrate	Bio-Rad
L-glutamine	Gibco
Lipofectamine	Invitrogen
Luria Broth Base powder	Invitrogen
Methanol	Sigma-Aldrich

Nicotinamide	Sigma-Aldrich
Normal mouse IgG control beads	Santa Cruz Biotechnology
Opti-MEM I Reduced Serum Medium	Gibco
PageRuler Prestained Protein Ladder	Thermo Scientific
Penicillin-Streptomycin	Gibco
Phosphatase Inhibitor Cocktail 2	Sigma-Aldrich
Phosphatase Inhibitor Cocktail 3	Sigma-Aldrich
PLUS Reagent	Invitrogen
Powdered milk	Carl Roth
Power SYBR Green Master Mix	Applied Biosystems
Protease Inhibitor Cocktail	Sigma-Aldrich
Protein A/G PLUS-Agarose beads	Santa Cruz Biotechnology
Puromycin Dihydrochloride	Gibco
QuickExtract DNA Extraction Solution	Epicentre
RIPA Lysis Buffer, 10X	Merck
RNase A	Qiagen
RNase Away	Ambion
RPMI Medium 1640	Gibco
S.O.C. Medium	Invitrogen
Shrimp Alkaline Phosphatase (rSAP)	New England Biolabs
Sodium acetate	Sigma-Aldrich
Sodium butyrate	Sigma-Aldrich
Sodium chloride	AppliChem
T4 DNA Ligase + buffer	New England Biolabs
T4 Polynucleotide Kinase + buffer	New England Biolabs
T7 Endonuclease I + NEBuffer 2	New England Biolabs
Taq DNA polymerase + PCR reaction buffer	Qiagen
TBE buffer (10X)	Genaxxon
Titanium Taq DNA polymerase + PCR reaction buffer	Clontech Laboratories
Trans-Blot Turbo Midi PVDF Transfer Packs	Bio-Rad
Tris powder	Bio-Rad
Trypan blue	Gibco
Trypsin-EDTA	Gibco
TWEEN 20	Sigma-Aldrich
Western Lightning Plus-ECL	PerkinElmer
XL10-Gold Ultracompetent *E. coli* Cells + β-mercaptoethanol	Agilent

2.1.2 Small molecule inhibitors

Inhibitor	**Supplier**
17-AAG	Selleck Chemicals
Bortezomib	Selleck Chemicals
Entinostat (MS-275)	Selleck Chemicals
Etoposide	Sigma-Aldrich
Hydroxychloroquine	Selleck Chemicals
Leptomycin B	Sigma-Aldrich
MG-132	Selleck Chemicals
Mocetinostat (MGCD0103)	Selleck Chemicals

Nutlin-3a	Selleck Chemicals
Panobinostat	Selleck Chemicals
PCI-34051	Selleck Chemicals
Ruxolitinib	Selleck Chemicals
Selinexor	Selleck Chemicals
Trichostatin A (TSA)	Selleck Chemicals
Tubacin	Selleck Chemicals
Tubastatin A	Selleck Chemicals
Verdinexor	Selleck Chemicals
Vorinostat	Selleck Chemicals

2.1.3 Consumables

Consumable	Supplier
AlumaSeal 96-well sealing film	Sigma-Aldrich
Breathe-Easy sealing membrane	Sigma-Aldrich
Cell culture dishes 10 cm, 15 cm	Corning
Cell culture flasks T225	Starlab
Cell culture flasks T25, T75	Nunc
Cell culture plate 384-well, white	Greiner Bio-One
Cell culture plates 6-well, 12-well, 24-well, 48-well, 96-well	Greiner Bio-One
Cell strainer 40 µm, 70 µm	BD
Conical tubes 15 mL, 50 mL	BD Falcon
Countess Cell Counting Chamber Slides	Invitrogen
Cryo vials	Nunc
FACS tubes	BD
Filter pipette tips 10 µL, 20 µL, 200 µL, 1000 µL, 5000 µL	Starlab, Eppendorf
PCR plate sealing foil	Steinbrenner
PCR reaction plate, 96-well	Greiner Bio-One
PCR strips	Biozym
Petri dishes	Corning
Pipettes 2 mL, 5 mL, 10 mL, 25 mL, 50 mL	Corning
Pipetting reservoirs	Integra Biosciences
Plastic bottles 125 mL, 250 mL	Nunc
QIAshredder columns	Qiagen
qPCR plate sealing foil	Biozym
qPCR reaction plate, 96-well	Biozym
Qubit Assay Tubes	Invitrogen
Reaction tubes 0.5 mL, 1.5 mL, 2 mL, 5 mL	Eppendorf
Round-Bottom Polypropylene Tubes 14 mL	BD Falcon

2.1.4 Kits

Kit	Supplier
DNeasy Blood & Tissue Kit	Qiagen
GeneMATRIX Plasmid Miniprep DNA Purification Kit	EURx
HiSpeed Plasmid Maxi Kit	Qiagen
jetPEI transfection reagent	Polyplus Transfection

Pierce BCA Protein Assay Kit	Thermo Scientific
Plasmid Maxi Kit	Qiagen
QIAquick Gel Purification Kit	Qiagen
QIAquick PCR Purification Kit	Qiagen
Qubit dsDNA BR Assay Kit	Invitrogen
RevertAid First Strand cDNA Synthesis Kit	Thermo Scientific
RNase-Free DNase Set	Qiagen
RNeasy Mini Kit	Qiagen
Zombie UV Fixable Viability Kit	BioLegend

2.1.5 Antibodies

2.1.5.1 Flow cytometry

Antibody	Host	Supplier	Cat. no.	Fluorophore
IgG2b Isotype Control	Mouse	BD Pharmingen	554298	FITC
IgG2b Isotype Control	Mouse	BD Pharmingen	556534	PE
p53 (DO-7)	Mouse	BD Pharmingen	554298	FITC
p53 (DO-7)	Mouse	BD Pharmingen	556534	PE

2.1.5.2 Western Blot

Antibody	Host	Supplier	Cat. no.	Dilution
Acetylated-Lysine	Rabbit	Cell Signaling	9441S	1:1,000
GAPDH-HRP	Mouse	Sigma-Aldrich	G9295	1:3,000
Goat-HRP	Rabbit	Abcam	ab6741	1:3,000-1:10,000
MDM2	Mouse	Santa Cruz Biotechnology	sc-965	1:200
MDM4	Rabbit	Merck	04-1555	1:1,000
Mouse-HRP	Rabbit	Abcam	ab6728	1:3,000-1:10,000
p21	Mouse	BD Pharmingen	556431	1:250
p53-HRP	Goat	R&D Systems	HAF1355	1:5,000
PARP	Rabbit	Cell Signaling	9542S	1:1,000
Rabbit-HRP	Goat	Abcam	ab6721	1:3,000-1:10,000
TRRAP	Rabbit	Cell Signaling	3966S	1:1,000

2.1.5.3 Immunoprecipitation

Antibody	Host	Supplier	Cat. no.
FLAG	Mouse	Sigma-Aldrich	F3165
Normal IgG control	Goat	Santa Cruz Biotechnology	sc-2028
Normal IgG control beads	Mouse	Santa Cruz Biotechnology	sc-2343
p53 (DO-1/1801/421)	Mouse	Custom-made (gift from Moshe Oren, WIS)	-
p53 beads (DO-1)	Mouse	Santa Cruz Biotechnology	sc-126 AC
SV40 T antigen (419)	Mouse	Custom-made (gift from Moshe Oren, WIS)	-
TRRAP	Goat	Santa Cruz Biotechnology	sc-5405

2.1.6 Plasmids

Plasmid	Function	Source
CbS-Flag-TRRAP	TRRAP expression	Addgene #32103, Michael Cole/Yardena Samuels
DECIPHER Pooled Lentiviral shRNA library Human Module I	shRNA library	Cellecta
lentiCas9-Blast	Cas9 expression	Addgene #52962, Feng Zhang
lentiCRISPRv2	sgRNA & Cas9 expression	Addgene #52961, Feng Zhang
lentiGuide-Puro	sgRNA expression	Addgene #52963, Feng Zhang
pcDNA3	cDNA expression	Gift from Moshe Oren, WIS
pcDNA3-dNp53	ΔN wtp53 expression	Gift from Moshe Oren, WIS
pcDNA3-p53	wtp53 expression	Gift from Moshe Oren, WIS
pCMV-p53-R175H	mutp53 R175H expression	Gift from Moshe Oren, WIS
peGFP-C1	GFP expression	Gift from Moshe Oren, WIS
pLKO1-TRC905 (pLKO_IPTG_3xLacO)	Inducible shRNA expression	Gift from Claudia Scholl, DKFZ
pLKO5.sgRNA.EFS.tRFP	sgRNA expression	Addgene #57823, Benjamin Ebert
pMD2.G	Lentiviral packaging	Addgene #12259, Didier Trono
pRSI12-U6-sh-HTS4-UbiC-TagRFP-2A-Puro	Constitutive shRNA expression	Cellecta
psPAX2	Lentiviral packaging	Addgene #12260, Didier Trono

2.1.7 Cell lines

Cell line	Entity	Source
Awia	Human Burkitt's lymphoma	A. B. Rickinson, University of Birmingham, UK
BJAB	Human Burkitt's lymphoma	DMSZ, Braunschweig, Germany
BL-2	Human Burkitt's lymphoma	DMSZ, Braunschweig, Germany
BL-7	Human Burkitt's lymphoma	G. M. Lenoir, IARC, Lyon, France
BL-28	Human Burkitt's lymphoma	G. M. Lenoir, IARC, Lyon, France
BL-41	Human Burkitt's lymphoma	DMSZ, Braunschweig, Germany
BL-60	Human Burkitt's lymphoma	G. M. Lenoir, IARC, Lyon, France
CA-46	Human Burkitt's lymphoma	DMSZ, Braunschweig, Germany
Cheptanges	Human Burkitt's lymphoma	A. B. Rickinson, University of Birmingham, UK
Colo320	Human colon adenocarcinoma	DMSZ, Braunschweig, Germany
DG-75	Human Burkitt's lymphoma	DMSZ, Braunschweig, Germany
HEK 293T/17	Human embryonic kidney	Stefan Fröhling, DKFZ, Heidelberg, Germany
LY-47	Human Burkitt's lymphoma	G. M. Lenoir, IARC, Lyon, France
Namalwa	Human Burkitt's lymphoma	DMSZ, Braunschweig, Germany
NCI-H1299	Human non-small cell lung carcinoma	ATCC, Wesel, Germany
Raji	Human Burkitt's lymphoma	DMSZ, Braunschweig, Germany
Ramos	Human Burkitt's lymphoma	DMSZ, Braunschweig, Germany
Salina	Human Burkitt's lymphoma	A. B. Rickinson, University of Birmingham, UK
Seraphine	Human Burkitt's lymphoma	A. B. Rickinson, University of Birmingham, UK
SUDHL-4	Human germinal center B-cell diffuse large B-cell lymphoma	DMSZ, Braunschweig, Germany
Yakobo	Human Burkitt's lymphoma	A. B. Rickinson, University of Birmingham, UK

The p53 mutation status of all cell lines was determined by high-throughput sequencing of *TP53* exons 4-10[199-201] and/or retrieved from the IARC TP53 Database[202].

2.1.8 Oligonucleotides

Oligonucleotides were obtained from Eurofins Genomics or Sigma-Aldrich in smallest scale with reverse-phase cartridge purification.

2.1.8.1 shRNA screen

Name	Sequence [5'→3']	Function
FwdHTS	TTCTCTGGCAAGCAAAAGACGGCATA	1st PCR forward primer
RevHTS1	TAGCCAACGCATCGCACAAGCCA	1st PCR reverse primer
FwdGex	CAAGCAGAAGACGGCATACGAGA	2nd PCR forward primer
IndA	AATGATACGGCGACCACCGAGATCTACACGCA**ATGC**GCA CAACCGCAA	2nd PCR reverse indexing primer
IndB	AATGATACGGCGACCACCGAGATCTACACGCA**GACT**GCA CAACCGCAA	2nd PCR reverse indexing primer
IndC	AATGATACGGCGACCACCGAGATCTACACGCA**TCAG**GCA CAACCGCAA	2nd PCR reverse indexing primer
IndD	AATGATACGGCGACCACCGAGATCTACACGCA**CGTA**GCA CAACCGCAA	2nd PCR reverse indexing primer
IndE	AATGATACGGCGACCACCGAGATCTACACGCA**AGCG**GCA CAACCGCAA	2nd PCR reverse indexing primer
IndF	AATGATACGGCGACCACCGAGATCTACACGCA**GATG**GCA CAACCGCAA	2nd PCR reverse indexing primer
GexSeqS	AGAGGTTCAGAGTTCTACAGTCCGAA	HT sequencing read primer
GexSeqIND	ACGACCACCGAGATCTACACGCA	HT indexing read primer

2.1.8.2 qRT-PCR

Name	Sequence [5'→3']	Source
qPCR_GAPDH_F	ACCCAGAAGACTGTGGATGG	Self-designed
qPCR_GAPDH_R	TCTAGACGGCAGGTCAGGTC	Self-designed
qPCR_IFNa1_F	CCCTCTCTTTATCAACAAACTTGC	Madar *et al.*[203]
qPCR_IFNa1_R	TTGTTTTCATGTTGGACCAGA	Madar *et al.*[203]
qPCR_ISG15_F	CGAACTCATCTTTGCCAGTACA	Roulois *et al.*[204]
qPCR_ISG15_R	GCCTTCAGCTCTGACACC	Roulois *et al.*[204]
qPCR_MDM2_F	GGCAGGGGAGAGTGATACAGA	PrimerBank[205]
qPCR_MDM2_R	GAAGCCAATTCTCACGAAGGG	PrimerBank[205]
qPCR_MX1_F	GTTTCCGAAGTGGACATCGCA	Madar *et al.*[203]
qPCR_MX1_R	CCATTCAGTAATAGAGGGTGGGA	Madar *et al.*[203]
qPCR_TP53_F	GGAGCACTAAGCGAGCACTG	Self-designed
qPCR_TP53_R	CACCGGATCTGAAGGGTGAAA	Self-designed
qPCR_TRRAP_F	CAGGCCACCGATCACACAA	PrimerBank[205]
qPCR_TRRAP_R	CGCTCCGGGTTGACTTTCA	PrimerBank[205]

2.1.8.3 PCR

Name	Sequence [5'→3']	Function
T7E1_MDM2_e2_F1	GTCCTGACTTGTCTCCAGCT	T7E1 assay
T7E1_MDM2_e2_R1	AGTTACGCCAGAGGTAGCAC	T7E1 assay

2.1.8.4 shRNA sequences

Name	mRNA target sequence [5'→3']	Cellecta ID
shNT	CAACAAGATGAAGAGCACCAA	-
shTP53_85	CGGCGCACAGAGGAAGAGAAT	CLL-H-025985
shTP53_86	TCAGACCTATGGAAACTACTT	CLL-H-025986
shTRRAP_233	GCCCTGTTCTTTCGCTTTGTA	CLL-H-026233
shTRRAP_234	CGCTACTTTGAGAACCCTCAA	CLL-H-026234
shTRRAP_235	CGAGAGCAAATCGAGGAAATA	CLL-H-026235

Unless stated otherwise, shTRRAP_233 was used for TRRAP knock-down experiments.

2.1.8.5 sgRNA sequences

Name	mRNA target sequence [5'→3']	Source
sgeGFP	GGGCGAGGAGCTGTTCACCG	Self-designed
sgKPNB1_HGLibA_25375	GCTAGCTTCACATTATTACT	Human CRISPR Knockout Pooled Library (GeCKO v2)[206]
sgKPNB1_HGLibB_25338	CAGAGATCCCAGTAAACCAG	Human CRISPR Knockout Pooled Library (GeCKO v2)[206]
sgmCherry	CGCCCTCGATCTCGAACTCG	Self-designed
sgMDM2	GTGGTTACAGCACCATCAGT	Human CRISPR Knockout Pooled Library (GeCKO v2)[206]
sgRPA3_MK	GATGAATTGAGCTAGCATGC	M. Kühn, Mainz University, Germany
sgSF3B4_HGLibB_43659	TCTATAGGCATGCCTCCTCC	Human CRISPR Knockout Pooled Library (GeCKO v2)[206]
sgSF3B4_HGLibB_43660	AGGTTAGTGAACCGCTGCTG	Human CRISPR Knockout Pooled Library (GeCKO v2)[206]
sgTP53	CCATTGTTCAATATCGTCCG	Human CRISPR Knockout Pooled Library (Brunello)[207]
sgTRRAP_Bru8295_2	CCACTGGGGATCGTTCAGTG	Human CRISPR Knockout Pooled Library (Brunello)[207]
sgTRRAP_Bru8295_3	CTTGATCCGCCACTATACGA	Human CRISPR Knockout Pooled Library (Brunello)[207]

The TRRAP sgRNA sequences used for CRISPR scanning are listed in the Appendix (see 6.1, p. 103).

2.1.9 Software

Software	Supplier	Function
Barcode Deconvoluter	Cellecta	shRNA bar-code quantification
FACSDiva v.8	BD	FACS analysis
FlowJo v.10	FlowJo	FACS analysis
Image Lab Software Version 5.2.1	Bio-Rad	Western Blot analysis

Lasergene	DNASTAR	*in silico* cloning, Sanger sequencing analysis
LightCycler 480 Software Version 1.5	Roche	qRT-PCR analysis
R version 3.4.0	R Foundation	Statistical analysis
RStudio Desktop 1.0.143	RStudio	Statistical analysis

2.1.10 Equipment / Instruments

Instrument	Supplier
Agarose gel electrophoresis chambers	VWR Peqlab
Agarose gel electrophoresis power supply	Elchrom Scientific
Analytical balance	Sartorius
Bacteria incubator	Sanyo
Bacteria shaker	Infors
Benchtop centrifuges	Eppendorf
Benchtop centrifuges, cooled	Heraeus
Bioanalyzer	Agilent
Cell culture centrifuge	Thermo Scientific
Cell culture hood	Thermo Scientific
Cell culture incubator	Heraeus
Cell sorter FACSAria II	BD Biosciences
ChemiDoc XRS Imaging System	Bio-Rad
cobas z 480	Roche
Cooling racks	neoLab
Countess™ II FL Automated Cell Counter	Thermo Scientific
Flow cytometers LSRII, LSRFortessa	BD Biosciences
Freezer -20°C	Liebherr
Freezer -80°C	New Brunswick
Fridge 4°C	Liebherr
Fume hood	WALDNER Laboreinrichtungen
Gel documentation station	VWR Peqlab
Hotplate stirrer	VWR
Ice machine	Hoshizaki
Liquid nitrogen tank	German-Cryo
Microscope Axiovert 40C	Zeiss
Microwave	Bartscher
Mr. Frosty freezing containers	Thermo Scientific
NanoDrop Spectrophotometer ND-1000	Thermo Scientific
PAGE running chambers	Bio-Rad
pH meter	Mettler Toledo
Pipetboy	Integra Biosciences
Pipettes	Eppendorf
Plate reader Infinite M1000 Pro	Tecan
Qubit 2.0 Fluorometer	Invitrogen
SDS-PAGE power supply	Bio-Rad
TapeStation	Agilent
Thermocycler peqSTAR	VWR Peqlab

Thermomixer	Eppendorf
Trans-Blot Turbo Transfer System	Bio-Rad
Tube rotator (rotating wheel)	Bibby Scientific
Vacuum pump	VACUUBRAND
Vortexer	IKA
Water bath	LAUDA
Water purification system (for ddH_2O)	Thermo Scientific

2.2 Cell culture methods

2.2.1 Cell cultivation

All cell lines were cultured in RPMI (293T cells: DMEM) supplemented with 10% heat-inactivated FBS, 2 mM L-glutamine, 100 U/mL penicillin, and 100 µg/mL streptomycin at 37°C in a humidified, 5% CO_2 atmosphere. Lymphoma cells were maintained at 3-5x10^5 cells/mL and were passaged twice per week. Adherent cells were detached with Trypsin if necessary. The identity of all cell lines was validated using Multiplex Cell Authentication (Multiplexion)[208]. The SNP profiles matched known profiles or were unique. The purity of cell lines was validated using the Multiplex Cell Contamination Test (Multiplexion)[209]. No Mycoplasma, SMRV or interspecies contamination was detected.

2.2.2 Cell freezing & thawing

For freezing, cells were collected by centrifugation (400 x g, 5 min), washed once with PBS, and resuspended in cell freezing medium (90% FBS, 10% DMSO) at a concentration of 3x10^6 cells/mL. 1 mL cell suspension was transferred into cryotubes and stored overnight in a Mr. Frosty container at -80°C before transfer into liquid nitrogen (LN_2) for long-term storage.

For thawing, cryotubes were quickly thawed in a 37°C water bath. The thawed cells were transferred to 9 mL pre-warmed cell culture medium, collected by centrifugation (400 x g, 5 min), resuspended in 10 mL pre-warmed cell culture medium, and seeded into appropriate cell culture flasks.

2.2.3 Lentiviral packaging

One day before transfection, 293T cells were seeded into 6-well plates (400,000 cells/well). The next day, for each packaging reaction, the appropriate target plasmid (e.g. shRNA or sgRNA expression vector) was mixed with the packaging vector psPAX2, the envelope vector pMD2.G, and PLUS reagent as indicated in Table 2 and incubated for 15 min at room temperature. After incubation, the Lipofectamine mix was

prepared as shown in Table 3, mixed gently, and added to the previously prepared mix to generate the final transfection mix. After another incubation of 15 min at room temperature, the transfection mix was gently added to the plated cells and mixed by gentle swirling. The medium of the cells was replaced with fresh DMEM 12-18 h after transfection. 48 h post-transfection, the transfection efficiency was evaluated via fluorescence microscopy if possible and the virus-containing medium was collected and centrifuged (1,000 x g, 5 min) to pellet cell debris and dead cells. The supernatant was then either used directly for transduction or stored in small aliquots at -80°C.

Table 2: Packaging-PLUS mix for transfection of 293T cells for lentiviral packaging.

	per well in 6-well plate [µL]
Target plasmid (50 ng/µL)	5
psPAX2:pMD2.G 2:1 mix (500 ng/µL)	2.5
OPTI-MEM	190
PLUS reagent	2.5
TOTAL	**200**

Table 3: Lipofectamine mix for transfection of 293T cells for lentiviral packaging.

	per well in 6-well plate [µL]
OPTI-MEM	196
Lipofectamine	4
TOTAL	**200**

2.2.4 Lentiviral transduction

Lymphoma cell lines were seeded at a density of $5x10^5$ cells/mL and the appropriate amount of lentiviral supernatant was added, typically 1/5-1/10 of the seeding volume. Cells were splitted 1:2 one day after transduction. If necessary, transduced cells were enriched with 0.5-1.0 µg/mL puromycin for 48-72 h. Puromycin selection was repeated multiple times whenever needed. For generation of Cas9-expressing cells, transduced cells were selected with 10 µg/mL blasticidin for four days. Transduced cells were maintained at a concentration of $5x10^5$ cells/mL.

2.2.5 Flow cytometry (FACS)

2.2.5.1 Monitoring of fluorescence signals (e.g. GFP, RFP)

250 µL of a dense cell culture (~$5x10^5$ cells) were collected by centrifugation in a 96-well PCR plate (400 x g, 5 min), washed once with 100 µL 2% FBS/PBS, resuspended in 100-200 µL 2% FBS/PBS, and transferred to FACS tubes. Tubes were kept on ice in the dark until analysis using an LSRFortessa or LSRII. Gating on living cells was performed

using forward/sideward scatter, cell doublet discrimination was done using area and height of the forward and sideward scatter. Data was analyzed using FlowJo v.10.

2.2.5.2 Intracellular p53 staining using paraformaldehyde for fixation

Using paraformaldehyde (PFA) for fixation preserves fluorescence signals but damages DNA. This protocol was used when cells were expressing fluorescent proteins (e.g. after shRNA transduction) and the DNA was not needed for further experiments.

250 µL of a dense cell culture (~5x10^5 cells) were collected by centrifugation in a 96-well PCR plate (400 x g, 5 min) and washed once with 100 µL PBS. To allow for live/dead cell discrimination after fixation, cells were stained with 40 µL Zombie staining solution (1:100-diluted Zombie UV dye in PBS) and incubated for 15-30 min at room temperature in the dark. After incubation, 100 µL PBS was added to the wells and the plate was centrifuged (400 x g, 5 min). The supernatant was removed and the cells were washed with 100 µL 1% BSA/PBS. Cells were fixed with 100 µL freshly prepared 2% PFA/PBS and incubated for 30 min at 4°C. After incubation, cells were pelleted (400 x g, 5 min) and washed twice with 100 µL 1% BSA/PBS. Cells were permeabilized with 100 µL ice-cold 80% EtOH/PBS at -20°C for 30 min (or stored to continue with the staining at a later time). Next, cells were pelleted (400 x g, 5 min) and washed twice with 100 µL 1% BSA/PBS. Fixed cells were stained for p53 levels with 40 µL staining solution (1:10-1:25-diluted antibody in 1% BSA/PBS) containing anti-p53 clone DO-7 coupled to FITC or PE and incubated for 1 h at 4°C in the dark. After incubation, 100 µL 1% BSA/PBS were added and cells were pelleted (400 x g, 5 min). The supernatant was removed, cells were resuspended in 100-200 µL 1% BSA/PBS, and transferred to FACS tubes. Tubes were kept on ice in the dark until analysis as indicated above.

2.2.5.3 Intracellular p53 staining using methanol for fixation and permeabilization

Using methanol (MeOH) for fixation and permeabilization quenches fluorescence signals but preserves DNA. This protocol was used when cells were not expressing any fluorescent proteins and/or when the DNA was needed for further experiments.

Cells were collected, washed, and stained for viability using Zombie UV as described above (see 2.2.5.2). Cells were fixed and permeabilized with 100 µL ice-cold MeOH and incubated at -20°C for 30 min (or stored to continue with the staining at a later time). After incubation, cells were pelleted (400 x g) and the supernatant was removed. Cells were resuspended in 100 µL PBS and incubated for at least 30 min at 4°C. Next, cells

were pelleted (400 x g, 5 min), the supernatant was removed, and cells were stained for p53 levels and analyzed as indicated above.

2.2.6 Transfection of adherent cells

For transfection of Colo320 cells, 500,000 cells/well were seeded in 6-well plates. The next day, for each well, 2.5 µg plasmid DNA were mixed with 2.5 µL PLUS reagent and 125 µL OPTI-MEM. In parallel, 12.5 µL Lipofectamine were added to 125 µL OPTI-MEM. Next, both solutions were combined and added gently to the wells after 5 min incubation at room temperature. Cells were harvested 48-72 h after transfection.

For transfection of H1299 cells, 675,000 cells were seeded in 10 cm dishes. The next day, 3 µg plasmid DNA were diluted in 150 mM NaCl in a total volume of 150 µL for each plate. In parallel, 14 µL PEI were added to 136 µL 150 mM NaCl. Next, both solutions were combined and added gently to the plates after 15-30 min incubation at room temperature. Cells were harvested 24-72 h after transfection.

2.2.7 shRNA rescue experiment

Colo320 cells were detached with Trypsin, transduced with shRNA lentiviruses in suspension as described above (see 2.2.4) in the presence of 8 µg/mL polybrene, and seeded into 6-well plates (500,000 cells/well). The next day, cells were transfected with FLAG-TRRAP as described above (see 2.2.6). Cells were harvested 48 h after transfection (= 72 h after transduction).

2.2.8 Inducible shRNAs

Namalwa cells were transduced with IPTG-inducible shRNA lentiviruses as described above (see 2.2.4) and enriched by multiple rounds of puromycin selection. For induction, cells were treated with 2 mM IPTG, which was renewed every two days.

2.3 Molecular biology methods

2.3.1 DNA extraction

Genomic DNA was extracted from ~1x10^6 washed cells using the DNeasy Blood & Tissue Kit according to the manufacturer's guidelines. In brief, cells were lysed using buffer AL and the DNA was precipitated with EtOH. Next, the DNA was bound to spin columns and washed with buffers AW1 and AW2. Finally, DNA was eluted in 100 µL

ddH_2O, quantified using a NanoDrop ND-1000 Spectrophotometer or a Qubit 2.0 Fluorometer (dsDNA BR assay kit), and stored at -20°C.

2.3.2 Plasmid cloning

2.3.2.1 Constitutive shRNAs

All shRNA sequences were extracted from the DECIPHER Pooled Lentiviral shRNA library Human Module I and cloned into the shRNA expression vector pRSI12-U6-sh-HTS4-UbiC-TagRFP-2A-Puro according to the guidelines provided by Cellecta (user manual "Cloning of shRNA Templates into shRNA Expression Vector", 1/2011). Forward and reverse oligonucleotides were designed according to the following scheme:

F: 5′-ACCG-G-NNNNNNNNNNNNNNNNNNNN-GTTAATATTCATAGC-NNNNNNNNNNNNNNNNNNNN-TTTT-3′
R: 3′-C-NNNNNNNNNNNNNNNNNNNN-CAATTATAAGTATCG-NNNNNNNNNNNNNNNNNNNN-AAAA-AAGC-5′

sticky end, constant region, sense target sequence, shRNA loop, antisense target sequence

For linearization of the expression vector pRSI12, 5 µg plasmid DNA were digested with 50 U BbsI in 1x buffer G for 2 h at 37°C. After the reaction was heat inactivated by incubation at 65°C for 20 min, the linearized vector was purified from a 0.5% preparative agarose gel using a QIAquick Gel Extraction Kit according to the manufacturer's guidelines.

For phosphorylation and annealing of shRNA oligonucleotides, 10 pmol of each forward and reverse oligo were mixed with 5 nmol ATP and 5 U T4 polynucleotide kinase (PNK) in 1x T4 PNK buffer in a total volume of 10 µL. The reaction mix was incubated for 30 min at 37°C, followed by 2 min at 95°C and gradual cooling to 25°C at a rate of -0.1°C/s. As a negative control, the oligos were replaced with ddH_2O. The reaction mix was diluted 1:5 with 1x T4 PNK buffer and was either used directly or stored at -20°C.

For ligation, 10 ng linearized pRSI12 were mixed with 0.5 µL oligo mix and 40 U T4 DNA ligase in 1x T4 ligase buffer in a total volume of 10 µL. The reaction mix was incubated for 2 h at 16°C. As a negative control, the oligo mix was replaced with the negative control from the previous step.

For transformation, XL10-Gold ultracompetent *E. coli* cells were thawed on ice, mixed with 4 µL β–mercaptoethanol, and incubated for 10 min on ice. After incubation, 1 µL cells was added to the ligation mix and incubated for 30 min on ice. As a negative control, the negative control from the previous step was used. After incubation, cells were heat-shocked by incubation at 42°C for 30 s, followed by incubation on ice for at least 2 min. Next, 30 µL pre-warmed S.O.C. medium were added and cells were

incubated at 37°C for 1 h while shaking. Finally, transformed cells were plated on LB agar supplemented with 100 µg/mL ampicillin and incubated overnight at 37°C.

The next day, colonies were picked from each transformation and used for inoculation of 5 mL ampicillin-containing LB medium to expand cells overnight at 37°C while shaking. Plasmids were purified using a GeneMATRIX Plasmid Miniprep DNA Purification Kit according to the manufacturer's instructions and quantified using a NanoDrop ND-1000 Spectrophotometer. Finally, the sequence of all plasmids was validated via Sanger sequencing (GATC Biotech) using a primer which specifically amplified the shRNA inserts.

2.3.2.2 Inducible shRNAs

shRNA sequences were similar to the ones described above (see 2.3.2.1) and were cloned into the IPTG-inducible shRNA expression vector pLKO1-TRC905 (pLKO_IPTG_3xLacO). Forward and reverse oligonucleotides were designed according to the following scheme:

F: 5'-CCGG-NNNNNNNNNNNNNNNNNNNNN-CTCGAG-NNNNNNNNNNNNNNNNNNNNN-TTTTTG-3'
R: 3'-NNNNNNNNNNNNNNNNNNNNN-GAGCTC-NNNNNNNNNNNNNNNNNNNNN-AAAAACTTAA-5'

sticky end, sense target sequence, shRNA loop, constant region, antisense target sequence

For linearization of the expression vector, 2 µg plasmid DNA were digested with 5 U AgeI and 20 U EcoRI in 1x NEBuffer 1.1 for 2 h at 37°C. The linearized vector was purified from a 0.8% preparative agarose gel using a QIAquick Gel Extraction Kit according to the manufacturer's guidelines.

Phosphorylation and annealing of the shRNA oligos was performed similarly as described above (see 2.3.2.1).

For ligation, 20 ng linearized vector were mixed with 0.5 µL oligo mix and 40 U T4 DNA ligase in 1x T4 ligase buffer in a total volume of 10 µL. The reaction mix was incubated for 2 h at 16°C.

Transformation, plasmid purification, and validation were performed similarly as described above (see 2.3.2.1).

2.3.2.3 sgRNAs

sgRNA sequences were obtained either from the Human Brunello CRISPR knockout pooled library (D. Root and J. Doench, Addgene #73178)[207] or were designed based on rules defined by Doench *et al.*[207]. They were cloned into the sgRNA expression vectors

lentiGuide-Puro, lentiCRISPRv2, or pLKO5.sgRNA.EFS.tRFP based on published protocols[206,210,211] or protocols provided on Addgene. Forward and reverse oligonucleotides were designed according to the following scheme:

```
F: 5'-CACCG-NNNNNNNNNNNNNNNNNNN-3'
R:     3'-C-NNNNNNNNNNNNNNNNNNN-CAAA-5'

sticky end, sgRNA sequence
```

For linearization of the expression vector, 5 µg plasmid DNA were digested with 20 U BsmBI in 1x NEBuffer 3.1 for 1.5 h at 55°C. After incubation, the linearized vector was dephosphorylated by addition of 2.5 µL rSAP and incubation at 37°C for 1 h, followed by heat inactivation at 65°C for 5 min. Next, the linearized vector was purified from a 0.5% preparative agarose gel using a QIAquick Gel Extraction Kit according to the manufacturer's guidelines.

Phosphorylation and annealing of the sgRNA oligos was performed similarly as described above for shRNAs (see 2.3.2.1).

For ligation, 50 ng linearized vector were mixed with 0.5 µL oligo mix and 40 U T4 DNA ligase in 1x T4 ligase buffer in a total volume of 10 µL. The reaction mix was incubated for 1 h at room temperature.

Transformation, plasmid purification, and validation were performed similarly as described above for shRNAs (see 2.3.2.1).

2.3.3 RNA extraction

RNA was extracted from ~1x10^6 washed cells using the RNeasy Mini Kit according to the manufacturer's guidelines. In brief, cells were disrupted in buffer RLT and homogenized using QIAshredder spin columns. Lysates were loaded onto spin columns, followed by an on-column DNase digestion. Next, the RNA was washed using buffers RW1 and RPE. Finally, the RNA was eluted in 30 µL RNase-free H_2O and quantified using a NanoDrop ND-1000 Spectrophotometer. Before storage at -80°C, the RNA integrity was checked on a 1% agarose gel. Only samples showing sharp, clear 28S and 18S rRNA bands were used for further experiments.

2.3.4 cDNA synthesis

cDNA synthesis was performed using the RevertAid First Strand cDNA Synthesis Kit according to the manufacturer's instructions. In brief, RNA samples were thawed on ice and checked for integrity as described above. 500 ng RNA were mixed with 1 µL random

hexamer primers, incubated at 65°C for 5 min, and briefly chilled on ice. Next, reaction buffer, RNase inhibitor, dNTPs, and reverse transcriptase were added and the reaction was incubated for 5 min at 25°C, followed by 1 h at 42°C and 5 min at 70°C. “No reverse transcriptase” controls were included for all samples. The cDNA was diluted 1:10 with ddH_2O and stored at -20°C.

2.3.5 qRT-PCR

qRT-PCR was performed using the Power SYBR Green Master Mix according to the manufacturer’s guidelines. In brief, for every gene of interest, a master mix was prepared consisting of 10 µL Power SYBR Green Master Mix, 2 µL primer mix (forward + reverse, 5 µM each), and 8 µL of diluted cDNA. Primers for qRT-PCR were self-designed, taken from the literature, or obtained from PrimerBank[205]. For every sample, the “no reverse transcriptase” control was included. For every primer, a “no template” control was included (cDNA replaced with ddH_2O) to check for potential primer dimer formation. Reactions were performed in triplicates in white 96-well PCR plates and run on a cobas z 480 Analyzer. The following PCR program was used: 10 min at 95°C, 40 cycles of 15 s at 95°C and 1 min at 60°C, followed by a thermal dissociation protocol for SYBR green detection for recording of the melting curves. Data were analyzed using LightCycler 480 Software Version 1.5. Gene expression was quantified using the $\Delta\Delta C_t$ method and GAPDH expression was used as a reference for normalization.

2.3.6 Gene expression profiling by microarray

For gene expression profiling by microarray, 1 µg total RNA was submitted to the DKFZ Genomics & Proteomics Core Facility for analysis on a Illumina HumanHT-12 v4 BeadChip, containing >47,000 probes mapping to >31,000 annotates genes. The core facility performed quality control, reverse transcription, labeling, and chip hybridization and provided normalized relative expression values and adjusted p values. Differentially expressed probes were defined as adj. $p < 0.05$ and $|\log2 \text{ fold change}| > 1$. Data was further processed and analyzed using R version 3.4.0. Gene set enrichment analysis was done using the R package “piano”[212] (method “PAGE”[213], MSigDB[214] gene set collections “hallmark”[215] and “c2cgp”) or using Enrichr[216,217] (data set “GO Biological Process 2017”). Gene expression data of MDA-MB-231 cells 48 h after treatment with 3.17 µM Mocetinostat was downloaded from NCBI GEO (GSE65495)[218].

2.3.7 Western Blot

For Western Blotting, ~1x10^6 cells were washed with PBS and snap frozen as pellets on dry ice or with LN_2. Pellets were resuspended in freshly prepared 1x RIPA Lysis buffer supplemented with protease inhibitors and 125 U/mL benzonase and incubated for 30 min on ice with occasional vortexing. After incubation, lysates were cleared by centrifugation (10,000 x g, 15 min, 4°C). If necessary, protein concentration was quantified with a Pierce BCA Protein Assay Kit according to the manufacturer's instructions. Samples were mixed with 2x or 4x Laemmli buffer before ~20 µg were loaded onto 4-15% gradient polyacrylamide protein gels together with an appropriate protein standard. Separation was performed at 90-120 V in 1x Tris/Glycine/SDS running buffer for ~1.5 h. Proteins were blotted onto PVDF membranes for 10 min at 2.5 A using a Trans-Blot Turbo Blotting System. After blotting, membranes were blocked in 5% milk/TBST (20 mM Tris, 150 mM NaCl, 0.1% Tween 20, 5% milk powder, pH 7.6) for 1 h at room temperature or overnight at 4°C while shaking. Primary antibodies were diluted according to the manufacturer's datasheets in 5% milk/TBST or 5% BSA/TBST and incubated with the membranes overnight at 4°C while shaking. The next day, blots were washed three times with TBST for 5 min at room temperature while shaking and incubated with diluted secondary antibodies (1:3,000-1:10,000 in 5% milk/TBST) for 1 h at room temperature while shaking. Subsequently, blots were washed again three times with TBST for 5 min at room temperature while shaking. Finally, protein expression was detected using freshly prepared ECL solution and a ChemiDoc XRS System. Image acquisition and analysis was done using Image Lab Software Version 5.2.1.

2.3.8 Immunoprecipitation

2.3.8.1 Exogenous (H1299 cells)

For exogenous immunoprecipitation (IP), protein A agarose beads were first coupled to the appropriate antibodies. To this end, for each IP reaction, 50 µL 50% bead slurry were pelleted (200 x g, 1 min, 4°C) and washed three times with 800 µL NP40 buffer (50 mM Tris pH 8, 150 mM NaCl, 1.0% NP40) supplemented with protease and phosphatase inhibitors. Next, 2 µg antibody in 1 mL NP40 buffer were added to the beads, followed by incubation at 4°C while rotating for at least 30 min. Meanwhile, for each IP reaction, one confluent 10 cm dish of H1299 cells was harvested (~1x10^7 cells), washed once with PBS, resuspended in 800 µL NP40 buffer, and incubated for 30 min at 4°C while rotating for lysis. In the meantime, the antibody-coupled beads were washed three times with 800 µL NP40 buffer and finally resuspended in 100 µL NP40 buffer. A small aliquot of the diluted beads was kept as a "beads only" control. After incubation, the cell lysate was

cleared by centrifugation (10,000 x g, 10 min, 4°C) and 50 µL were kept and supplemented with Laemmli buffer as an “input” control. The remaining lysate was added to the readily diluted beads and incubated for 3-5 h at 4°C while rotating. Subsequently, beads were washed three times with 800 µL NP40 buffer for 3 min at 4°C while rotating. After the final wash, proteins were eluted from the beads by resuspension in 60 µL 2x Laemmli buffer and incubation at 85°C for 10 min. The eluent was stored at -20°C until analysis by Western Blot as described above (see 2.3.7).

2.3.8.2 Endogenous (BL cell lines)

For endogenous IP, protein A/G agarose beads were first coupled to the appropriate antibodies (this step was skipped when precoupled beads were used). To this end, for each IP reaction, 20 µL 50% bead slurry were pelleted (1,000 x g, 2 min, 4°C) and washed three times with 800 µL NP40 buffer (50 mM Tris pH 8, 150 mM NaCl, 1.0% NP40) supplemented with protease, phosphatase, histone deacetylase inhibitors (sodium butyrate + nicotinamide), and benzonase. Next, 2 µg antibody in 1 mL NP40 buffer were added to the beads, followed by incubation at 4°C while rotating for at least 30 min. Meanwhile, for each IP reaction, $4x10^7$ cells were harvested, washed twice with PBS, resuspended in 800 µL NP40 buffer, and incubated for 30 min at 4°C while rotating for lysis. In the meantime, the antibody-coupled beads were washed three times with 800 µL NP40 buffer and finally resuspended in 100 µL NP40 buffer. A small aliquot of the diluted beads was kept as a “beads only” control. After incubation, 20 µL bead slurry were added to the cell lysate, followed by incubation for 1 h at 4°C while rotating for pre-clearing. Next, the lysate was cleared by centrifugation (17,000 x g, 10 min, 4°C) and the supernatant was pre-cleared again. After the second pre-clearing, 50 µL of the lysate were kept and supplemented with Laemmli buffer as an “input” control. The remaining lysate was added to the readily diluted beads and incubated for 4 h at 4°C while rotating. Subsequently, beads were washed five times with 800 µL NP40 buffer for 5 min at 4°C while rotating. After the final wash, proteins were eluted from the beads by resuspension in 40 µL 0.1 M glycine (pH 2.5) and incubation for 5 min at room temperature. Finally, the beads were pelleted and the supernatant was neutralized by addition of 4 µL 1.5 M Tris-HCl (pH 8.8), supplemented with Laemmli buffer, cooked for 3 min at 95°C, and stored at -20°C until analysis by Western Blot as described above (see 2.3.7) or mass spectrometry as described below (see 2.3.9).

2.3.9 Mass spectrometry

Namalwa cells with IPTG-inducible TRRAP or control knock-down were induced for 48 h or 96 h, respectively, before they were harvested directly or subjected to p53 immunoprecipitation as stated above (see 2.3.8.2). Mass spectrometry experiments were performed by Mandy Rettel and data analysis was performed by Frank Stein (both EMBL Proteomics Core Facility, Heidelberg, Germany). The following three sections (2.3.9.1, 2.3.9.2, and 2.3.9.3) were written jointly by them:

2.3.9.1 Sample preparation

"All reagents were prepared in 50 mM HEPES (pH 8.5). Cysteines were reduced using dithiothreitol (56°C, 30 min, 10 mM). Samples were cooled to 24°C and alkylated with iodacetamide (room temperature, in the dark, 30 min, 10 mM). Subsequently, the samples were prepared for LC-MS/MS using the SP3 protocol[219], digested with trypsin (enzyme to protein ratio, 1:50) at 37°C overnight. TMT 10-plex isobaric label reagents (ThermoFisher) were added to the samples following the manufacturer's instructions. Clean up of labeled peptides was performed using OASIS HLB µElution Plate (Waters). Offline high pH reverse phase fractionation was performed using an Agilent 1200 Infinity high-performance liquid chromatography (HPLC) system, equipped with a Gemini C18 column (3 µm, 110 Å, 100 x 1.0 mm, Phenomenex). The solvent system consisted of 20 mM ammonium formate (pH 10.0) as mobile phase (A) and 100% acetonitrile as mobile phase (B). In total, 15 fractions for total proteome experiments and 5 fractions for IP experiments were obtained and analyzed."

2.3.9.2 Liquid chromatography-mass spectrometry/mass-spectrometry (LC-MS/MS)

"Peptides were separated using the UltiMate 3000 RSLC nano LC system (Dionex) fitted with a trapping cartridge (µ-Precolumn C18 PepMap 100, 5µm, 300 µm i.d. x 5 mm, 100 Å) and an analytical column (Acclaim PepMap 100 75 µm x 50 cm C18, 3 µm, 100 Å). The outlet of the analytical column was coupled directly to a QExactive plus (Thermo) using the proxeon nanoflow source in positive ion mode. Solvent A was water, 0.1% formic acid and solvent B was acetonitrile, 0.1% formic acid. Trapping time was 6 min with a constant flow of solvent A at 30 µL/min onto the trapping column. Peptides were eluted via the analytical column a constant flow of 0.3 µL/min. During the elution step, the percentage of solvent B increased in a linear fashion from 2% to 4% B in 4 min, from 4% to 8% in 2 min, then 8% to 28% for a further 96 min, and finally from 28% to 40% in another 10 min. Column cleaning at 80% B followed, lasting 3 min, before returning to initial conditions for the re-equilibration, lasting 10 min.

The peptides were introduced into the mass spectrometer (QExactive plus, ThermoFisher) via a Pico-Tip Emitter 360 µm OD x 20 µm ID; 10 µm tip (New Objective) and a spray voltage of 2.3 kV was applied. The capillary temperature was set at 320°C. Full scan MS spectra with mass range 350-1400 m/z were acquired in profile mode in the FT with resolution of 70,000. The filling time was set at maximum of 100 ms with a limitation of $3x10^6$ ions. DDA was performed with the resolution of the Orbitrap set to 35,000, with a fill time of 120 ms and a limitation of $2x10^5$ ions. Normalized collision energy of 32 was used. A loop count of 10 with count 1 was used and a minimum AGC trigger of $2e^2$ was set. Dynamic exclusion time of 30 s was applied. The peptide match algorithm was set to 'preferred' and charge exclusion 'unassigned', charge states 1, 5 - 8 were excluded. Isolation window was set to 1.0 m/z and 100 m/z set as the fixed first mass. MS/MS data was acquired in profile mode."

2.3.9.3 Data analysis

"Raw mass spectrometry data was processed with IsobarQuant[220] and peptide and protein identification was performed with the Masot 2.4 (Matrix Science) search engine. R was used to analyze the raw output data from IsobarQuant. First, the output files of IsobarQuant were loaded into R and merged. Only proteins that were quantified with using at least two unique peptide matches were kept for the downstream analysis. Only proteins which were identified in all three replicates were used for the statistical analysis. The raw data was then saved in an ExpressionSet R object. Subsequently, potential batch effects were removed using limma[221] and data was normalized using variance stabilization, vsn strategy[222]. To identify proteins that were significantly different between the various conditions, limma was again used. Proteins annotated as hit if either a false discovery rate below 5% or a p-value smaller then 0.01 was obtained."

2.3.10 T7 endonuclease I (T7E1) assay

The T7E1 assay was performed for monitoring of CRISPR/Cas9-mediated modification of the appropriate genomic loci. For DNA extraction, 250 µL of a dense cell culture (~$5x10^5$ cells) were collected by centrifugation (400 x g, 5 min), resuspended in 20 µL QuickExtract solution, and vortexed for 15 s. The mixture was incubated for 6 min at 65°C, vortexed for 15 s, and incubated for 2 min at 98°C. The DNA-containing lysate was then used as a template together with PCR primers specific for the targeted locus in the PCR reaction indicated in Table 4 below.

Two 8.5 µL aliquots were taken from the PCR reaction, mixed with 1 µL NEBuffer 2, and denatured and slowly reannealed using the following thermocycler program: 95°C for

10 min, ramp to 85°C at a rate of -2°C/s, ramp to 25°C at a rate of -0.1°C/s, store at 4°C. After incubation, 0.5 µL (5 U) T7E1 were added to every second aliquot and incubated for 20 min at 37°C. Finally, the reaction products were resolved on a 2% agarose gel by electrophoresis.

Table 4: Master mix and PCR reaction for T7 endonuclease I (T7E1) assay.

Reaction mix	per rnx [µL]	PCR program	
10x PCR reaction buffer	5	**1.** 94°C, 3 min	
dNTPs (10 mM each)	1	**2.** 94°C, 30 s	
Primer forward (10 µM)	1	**3.** 58°C, 30 s	
Primer reverse (10 µM)	1	**4.** 72°C, 30 s	→ go to 2. for 35x
DNA	5	**5.** 72°C, 10 min	
ddH_2O	36.5	**6.** 8°C, forever	
Taq polymerase	0.5		
TOTAL	**50**		

2.3.11 CRISPR scanning

CRISPR scanning was performed according to the original publication by Shi *et al.*[223]. sgRNAs targeting TRRAP were designed based on rules defined by Doench *et al.*[207], aiming for comparable on-target scores (median: 70.0, see 6.1). sgRNAs were cloned into pLKO5.sgRNA.EFS.tRFP and packaged into lentiviral particles as described above (see 2.3.2.3 and 2.2.3). Namalwa-Cas9 cells were transduced at a transduction efficiency of ~25% (see 2.2.4) and tagRFP657 expression (= APC channel in FACS) and p53 levels were monitored by flow cytometry over time (see 2.2.5). CRISPR scanning was kindly performed by Marius Jentzsch.

2.4 Patient data

Lymphoma patient data was generated by the ICGC MMML (Molecular Mechanisms of Malignant Lymphoma)-Seq consortium and approved by the ethics commission of the University of Göttingen, Germany. Patients were classified into lymphoma subtypes based on their gene expression profiles[224]. p53 mutations were determined by Sanger sequencing of exons 4-10. Tissue microarray (TMA) data were provided and analyzed by Wolfram Klapper (University of Kiel, Germany). TMA scores were assigned based on the percentage of p53-positive cells as given in Table 5 below. Parts of the data have been published previously[201,224-226].

Table 5: Definition of the tissue microarray scores for quantification of p53 protein levels in lymphoma patient samples.

p53-positive cells in tumor [%]	Tissue microarray (TMA) score
0	0
1-25	1
26-50	2
51-75	3
>75	4

2.5 shRNA screen

The shRNA library packaging and screening procedure was performed based on the manufacturer's instructions ("Cellecta Pooled Bar-Coded Lentiviral shRNA Libraries User Manual") and previous publications[227,228] with modifications.

2.5.1 shRNA library

For the shRNA screen, the DECIPHER Pooled Lentiviral shRNA Library Human Module I consisting of 27,500 shRNAs targeting 5,043 genes was used. In this library, each shRNA was labeled with a unique bar-code sequence. The plasmid backbone of the library (pRSI12) contained a TagRFP gene and a puromycin resistance gene for labeling and selection purposes.

2.5.2 Lentiviral packaging of the shRNA library

One day before transfection, $1.2x10^7$ 293T cells were seeded per plate in a total of ten 15-cm cell culture plates. The next day, the shRNA library plasmids were mixed with the packaging vector psPAX2, the envelope vector pMD2.G, and PLUS reagent as indicated in Table 6 and incubated for 15 min at room temperature. After incubation, the Lipofectamine mix was prepared as shown in Table 7, mixed gently, and added to the previously prepared mix to generate the final transfection mix. After another incubation of 15 min at room temperature, the transfection mix was gently added to the plated cells and mixed by gentle swirling. The medium of the cells was replaced with fresh DMEM 24 h after transfection. 48 h post-transfection, the transfection efficiency was evaluated via fluorescence microscopy and the virus-containing supernatant was collected and filtered using a 0.45 µm filter. The supernatant was stored in small aliquots at -80°C. The packaging was kindly performed by Mikołaj Słabicki (DKFZ/NCT).

Table 6: Packaging-PLUS mix for transfection of 293T cells for lentiviral packaging of the shRNA library.

	per 10 cm dish [µL]
pRSI12 shRNA library (500 ng/µL)	12
psPAX2:pMD2.G 2:1 mix (500 ng/µL)	60
OPTI-MEM	1168
PLUS reagent	60
TOTAL	**1300**

Table 7: Lipofectamine mix for transfection of 293T cells for lentiviral packaging of the shRNA library.

	per 10 cm dish [µL]
OPTI-MEM	1310
Lipofectamine	90
TOTAL	**1400**

2.5.3 shRNA library titration

To determine the amount of lentiviral supernatant needed for achieving the appropriate transduction efficiency, Raji cells were seeded in a 24-well plate at a concentration of $5x10^5$ cells/mL and transduced with increasing amounts of lentiviral supernatant. 24 h post-transduction, cells were splitted 1:2. Three days post-transduction, the transduction efficiency was quantified by measurement of the RFP+ population by flow cytometry (see 2.2.5.1).

2.5.4 Cell transduction, culturing & sorting

In order to achieve an infection rate of 400 cells/shRNA, $2.75x10^7$ Raji cells (at a concentration of $5x10^5$ cells/mL) were transduced with the appropriate amount of lentiviral supernatant to reach a transduction efficiency of ~50% (MOI 0.7). One day after transduction, cells were splitted 1:2 by addition of fresh medium. The next day, the transduction efficiency was determined via flow cytometry (see 2.2.5.1) and cells were selected with 0.8 µg/mL puromycin for 48 h. After puromycin selection, cells were splitted into two separate flasks and handled separately as technical duplicates. Cells were maintained at a concentration of ~$5x10^5$ cells/mL during the screen. On day eight after transduction, cells were collected and washed once with PBS. One quarter of the cells (~$1x10^8$) were pelleted, snap frozen on dry ice, and stored at -20°C (input control). The remaining cells were fixed with ice-cold MeOH and stained for intracellular p53 levels as described previously (see 2.2.5.3). Stained cells were filtered with a 40 µm cell strainer and subjected to flow cytometry sorting using a FACSAria II, collecting p53-low and p53-high cells, each representing ~15% of the original population. Efficient sorting was

ensured by reanalysis of the sorted populations. Finally, sorted cells were counted, pelleted, snap frozen on dry ice, and stored at -20°C.

2.5.5 Genomic DNA extraction & precipitation

Genomic DNA was extracted using the DNeasy Blood & Tissue Kit according to the manufacturer's instructions as described above (see 2.3.1). Max. $4x10^6$ cells were used per spin column and an additional RNase digestion step was performed. DNA was eluted using 100 µL buffer AE and the eluent was reused for a second elution.

In order to increase the DNA concentration and to remove the buffer AE, the genomic DNA was precipitated after purification. In brief, 0.1 volumes 3 M NaOAc (pH 5.2), 1 µL linear polyacrylamide, and 2 volumes 95% EtOH were added to the genomic DNA, followed by 0.5-1 h incubation at -80°C. After incubation, the solution was centrifuged (17,000 x g, 15 min) and the supernatant was decanted. The DNA was washed with 1 mL 70% EtOH, incubated for 5 min at room temperature, and centrifuged. The supernatant was decanted and the DNA pellet was air-dried for a few minutes at room temperature. Finally, the pellet was dissolved in 50-100 µL ddH_2O and quantified by Qubit.

2.5.6 shRNA bar-code amplification, purification & quantification

The shRNA bar-code sequences were amplified by nested PCR in order to decrease contamination with genomic DNA and to attach adapter sequences for high-throughput sequencing.

For the 1st PCR, ~160-180 µg DNA from the input samples and the entire DNA from the sorted samples (~10-30 µg) were used as a template in the PCR reactions denoted below in Table 8, each containing maximal 25-30 µg DNA. As a positive control, 10 ng of the shRNA plasmid library were used. As a negative control, DNA was replaced with ddH_2O.

Table 8: Master mix and PCR program for the 1st PCR for shRNA bar-code amplification.

Reaction mix	per rnx [µL]	PCR program	
10x PCR reaction buffer	5	**1.** 94°C, 3 min	
dNTPs (10 mM each)	1	**2.** 94°C, 30 s	
Primer FwdHTS (10 µM)	1.5	**3.** 65°C, 10 s	
Primer RevHTS1 (10 µM)	1.5	**4.** 72°C, 20 s	→ go to 2. for 16x
DNA (max. 25-30 µg)	40.5	**5.** 68°C, 2 min	
Titanium Taq polymerase	0.5	**6.** 8°C, forever	
TOTAL	**50**		

After the PCR reaction was finished, all reactions from the same sample were pooled and used directly (unpurified) as a template in the 2nd PCR reaction as indicated below in Table 9. For each sample, four separate reactions were performed using an optimized number of cycles to obtain equal bar-code amplification for all samples and to avoid the generation of PCR fusion products.

Table 9: Master mix and PCR program for the 2nd PCR for shRNA bar-code amplification.

Reaction mix	per rnx [µL]	PCR program	
10x PCR reaction buffer	5	**1.** 94°C, 3 min	
dNTPs (10 mM each)	1	**2.** 94°C, 30 s	
Primer FwdGex (10 µM)	2.5	**3.** 65°C, 10 s	
Indexing primer IndA-F (unique for each sample, 10 µM)	2.5	**4.** 72°C, 10 s	→ go to 2. for 14-18x
1st PCR reaction product	2	**5.** 68°C, 2 min	
ddH_2O	36.5	**6.** 8°C, forever	
Titanium Taq polymerase	0.5		
TOTAL	**50**		

After the PCR reaction was finished, all reactions from the same sample were pooled and purified using a QIAquick PCR Purification Kit according to the manufacturer's guidelines. Briefly, PCR products were mixed with buffer PB, bound to a spin column, washed with buffer PE, and eluted in 30 µL ddH_2O. Purified PCR products were quantified by Qubit and stored at -20°C.

2.5.7 High-throughput sequencing

For high-throughput sequencing of shRNA bar-codes, purified PCR products were adjusted to a concentration of 10 nM, pooled equimolarly, and submitted to the DKFZ Genomics & Proteomics Core Facility for 50 bp single read Illumina HiSeq 2000 sequencing. Before sequencing, the core facility performed quality control, quantification, and mixed the samples with 40% PhiX Control. Sequencing was done using 10 pmol per sample for cluster generation, 500 nM of the custom sequencing primer GexSeqS, and 500 nM of the custom indexing primer GexSeqIND. The core facility provided demultiplexed FASTQ files for further analysis.

2.5.8 Data analysis

Data analysis was performed based on Slabicki *et al.*[228]. Raw sequencing reads were unzipped and trimmed to 18 bp in order to contain only the shRNA bar-codes using R. Bar-codes were quantified using the "Barcode Deconvoluter" software provided by Cellecta with a tolerance of one error and correction of N symbols. Details are given below in Table 10.

Table 10: Cell yield, DNA yield, and high-throughput sequencing statistics of shRNA screen samples.

Replicate	Sample	# cells [x10^6]	DNA [µg]	# mapped reads	# shRNAs detected	reads/ shRNA
1	Input	100	186.6	10,011,029	27,470	364
1	p53 low	6.8	25.6	9,248,424	27,312	339
1	p53 high	7.0	25.3	12,558,639	26,467	475
2	Input	100	163.3	9,841,530	27,473	358
2	p53 low	6.9	28.4	10,097,383	27,344	369
2	p53 high	9.5	10.0	9,604,804	24,186	397

shRNA bar-code counts were processed with R for further analysis. First, ten reads were added to all shRNAs to minimize the number of false positives in the low-abundance tail of the shRNA distribution[229]. Next, control shRNAs targeting luciferase or nine essential genes and shRNAs with a low abundance in the input samples (< 0.25 normalized reads and < 6 cpm) were deleted. After each sample was normalized, the dispersion was calculated and a negative binomial generalized log-linear model was fitted to the read counts using the R package "edgeR"[230,231]. For each shRNA, the fold change was calculated and used to determine robust z-scores ($z_{robust} = \frac{x-\tilde{x}}{MAD}$). P values were calculated with a likelihood ratio test, comparing p53-low or p53-high samples against the input samples, and adjusted for multiple testing by employing the Benjamini-Hochberg method. To collapse all k shRNAs targeting the same gene g into a single score, weighted z-scores were calculated with the weighted z-transformation method[232]:

$$z_{weighted}(g) = \frac{\sum_{i=1}^{k} w_i * z_i}{\sqrt{\sum_{i=1}^{k} {w_i}^2}}, \text{ with } w_i = (1 - p_i)$$

3 Results

3.1 Characterization of p53 mutations and levels in Burkitt's lymphoma

To characterize the frequency of p53 mutation and the impact of mutations on protein accumulation in aggressive B-cell lymphoma, sequencing and protein expression data from the ICGC MMML-Seq consortium were analyzed (Figure 13A). 43% (n=29/67) of patients diagnosed with Burkitt's lymphoma (BL) carried at least one mutation in p53. All mutations except one were found to be missense mutations located in the DNA-binding domain, including the typical hot spot mutations (i.e. R248, R273). Malignant lymphoma patient samples ($p<0.0001$) as well as BL patient samples ($p<0.05$) with p53 mutation showed higher p53 levels and therefore aberrant p53 stabilization compared to wild-type p53 patient samples (Figure 13B).

To identify representative disease models, p53 levels were characterized in a panel of BL cell lines with either wild-type p53 (wtp53) or mutant p53 (mutp53) by intracellular flow cytometry. This allowed quantification of the protein accumulation and identification of populations with heterogeneous expression levels (Figure 13C). While cell lines retaining wtp53 showed a low basal p53 protein level, p53 levels were higher but also more variable in mutp53 cell lines, which is in line with the findings from BL patients (Figure 13B). In a subset of mutp53 cell lines (BL-41, BL-60, Yakobo), a heterogeneous pattern of p53 protein expression was observed, i.e. the population was a mixture of p53-low and p53-high cells. Since all cell lines carried homozygous *TP53* mutations, this heterogeneity was not caused by retention of a wild-type allele, but was rather suggestive of differences in the degradation of mutp53.

To test whether p53 accumulation in BL cell lines with mutp53 was caused by *TP53* mRNA overexpression, qRT-PCR was performed which indicated no correlation of p53 mRNA expression with protein expression (Figure 13D). All mutp53 BL cell lines except CA-46 were found to have low mRNA expression, suggesting a translational or post-translational mechanism of mutp53 stabilization.

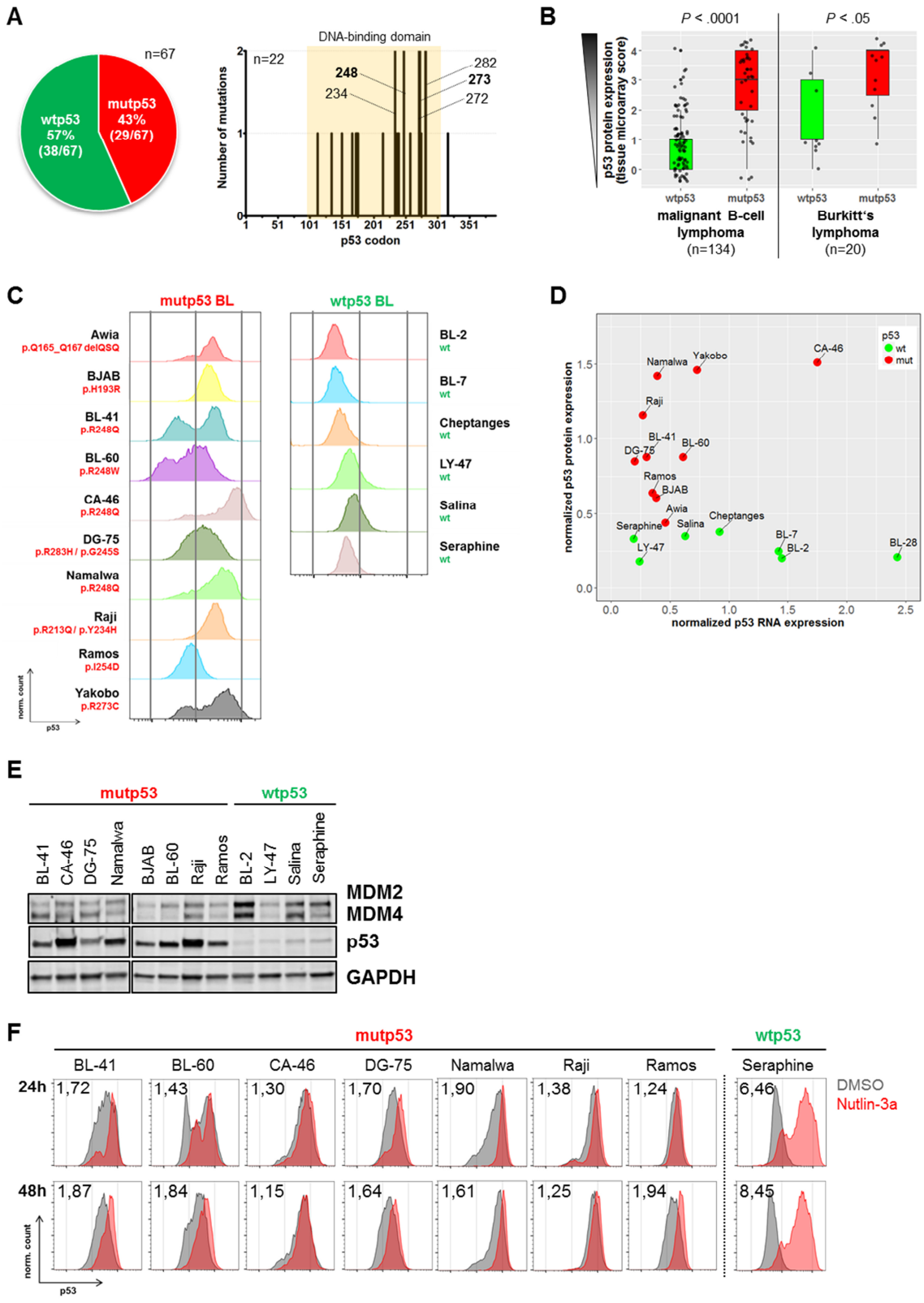

Figure 13: Characterization of p53 mutations and levels in Burkitt's lymphoma (BL).
(**A**) Frequency and distribution of p53 mutations in BL patients (n=67 or n=22, respectively). The DNA-binding domain of p53 is highlighted. Data from the ICGC MMML-Seq consortium. (**B**) p53 protein expression (determined by tissue microarray) in malignant B-cell lymphoma (n=134) and BL (n=20) samples stratified by p53 mutation status. The score indicates the percentage of p53-positive cells (Table 5, p. 50). P values were determined by Student's t-test. Data from the ICGC MMML-Seq consortium. (**C**) Basal p53 protein expression in wtp53 and mutp53 BL cell lines determined by intracellular flow cytometry. The p53

mutations are specified. (**D**) Comparison of p53 mRNA (qRT-PCR) and protein (flow cytometry) expression in wtp53 and mutp53 BL cell lines. (**E**) Protein level of p53, MDM2, and MDM4 in BL cell lines stratified by p53 mutation status. Expression was determined by Western Blot. GAPDH, loading control. Experiment performed by Jennifer Hüllein and reprinted with permission from Hüllein[201]. (**F**) p53 flow cytometry of BL cell lines after treatment with 0.1% DMSO (grey) or 10 µM of the MDM2 inhibitor Nutlin-3a (red) for 24 h or 48 h. Values denote the ratio of the p53 median fluorescence intensity (MFI) between treated and control cells. Experiment performed jointly with Sophie Rabe.

Since mutp53 stabilization in tumors may be caused by loss of expression of the E3 ubiquitin ligase MDM2[65,81], the major negative regulator of p53, basal MDM2 protein expression was assessed (Figure 13E). MDM2 expression was confirmed in both wtp53 and mutp53 cell lines, which suggests that mutp53 is stabilized despite the presence of MDM2. To evaluate whether mutp53 stabilization was caused by a functional defect in MDM2, BL cell lines were exposed to the MDM2 inhibitor Nutlin-3a and p53 levels were quantified by flow cytometry (Figure 13F). As expected, a ~6-8-fold increase in p53 was observed in the wtp53 cell line Seraphine upon Nutlin-3a exposure. In mutp53 cell lines, Nutlin-3a treatment also resulted in mild p53 stabilization (1.15-1.94-fold), albeit to variable extent.

In summary, although part of the mutp53 population may still be subject to MDM2-mediated degradation, the overall ability of endogenous MDM2 to promote mutp53 degradation in BL appears to be markedly compromised.

3.2 shRNA screen for regulators of mutant p53 protein accumulation

To identify proteins involved in the control of mutp53 accumulation in an unbiased fashion, a positive selection RNA interference (RNAi) screen with flow cytometry-based phenotype readout was performed in a mutp53 BL cell line model (Raji). The screening strategy is depicted in Figure 14 below.

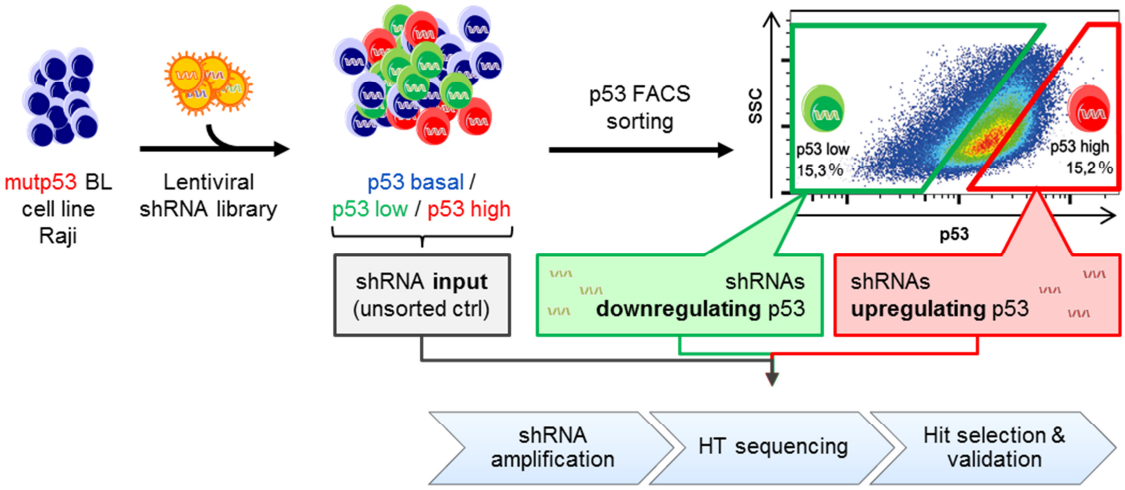

Figure 14: shRNA screening strategy for identification of regulators of mutant p53 protein accumulation.
The mutp53 Burkitt's lymphoma (BL) cell line Raji was transduced with a lentiviral shRNA library targeting ~5,000 genes with 5-6 shRNAs each. After selection of transduced cells with puromycin and in total 8 d in culture, part of the cells was harvested as input control ("unsorted", grey). The remaining cells were stained for their intracellular p53 levels and subjected to flow cytometry-based sorting in order to collect two distinct populations: p53-low (green) and p53-high cells (red), each representing ~15% of the total population. After sorting, the genomic DNA was extracted and the shRNA bar-codes were amplified and subjected to high-throughput (HT) sequencing. Finally, hits were identified by using the weighted z-score method. The experiment was performed in technical duplicates.

In brief, cells were transduced with a complex lentiviral shRNA library targeting ~5,000 genes with 5-6 shRNAs per gene. Cells were infected with an efficiency of ~50% (MOI 0.7) in order to assure delivery of a single silencing trigger per cell in the majority of cells (Figure 15A). After eight days in culture, part of the cells was collected as input control. The remaining cells were stained for their intracellular p53 levels and subjected to flow cytometry-based sorting to collect two distinct populations: p53-low and p53-high cells, each representing ~15% of the bulk population. Reanalysis of the sorted populations indicated efficient sorting based on p53 levels without introduction of a size bias, i.e. p53-low cells were not smaller than p53-high cells as indicated by comparable forward/sideward scatter (FSC/SSC) properties (Figure 15B). After sorting, the genomic DNA was extracted from all populations and the bar-codes that uniquely correspond to every shRNA were amplified using nested PCR (Figure 15C,D). PCR products were then

subjected to high-throughput sequencing in order to determine and quantify the shRNAs contributing to the phenotype of both sorted populations.

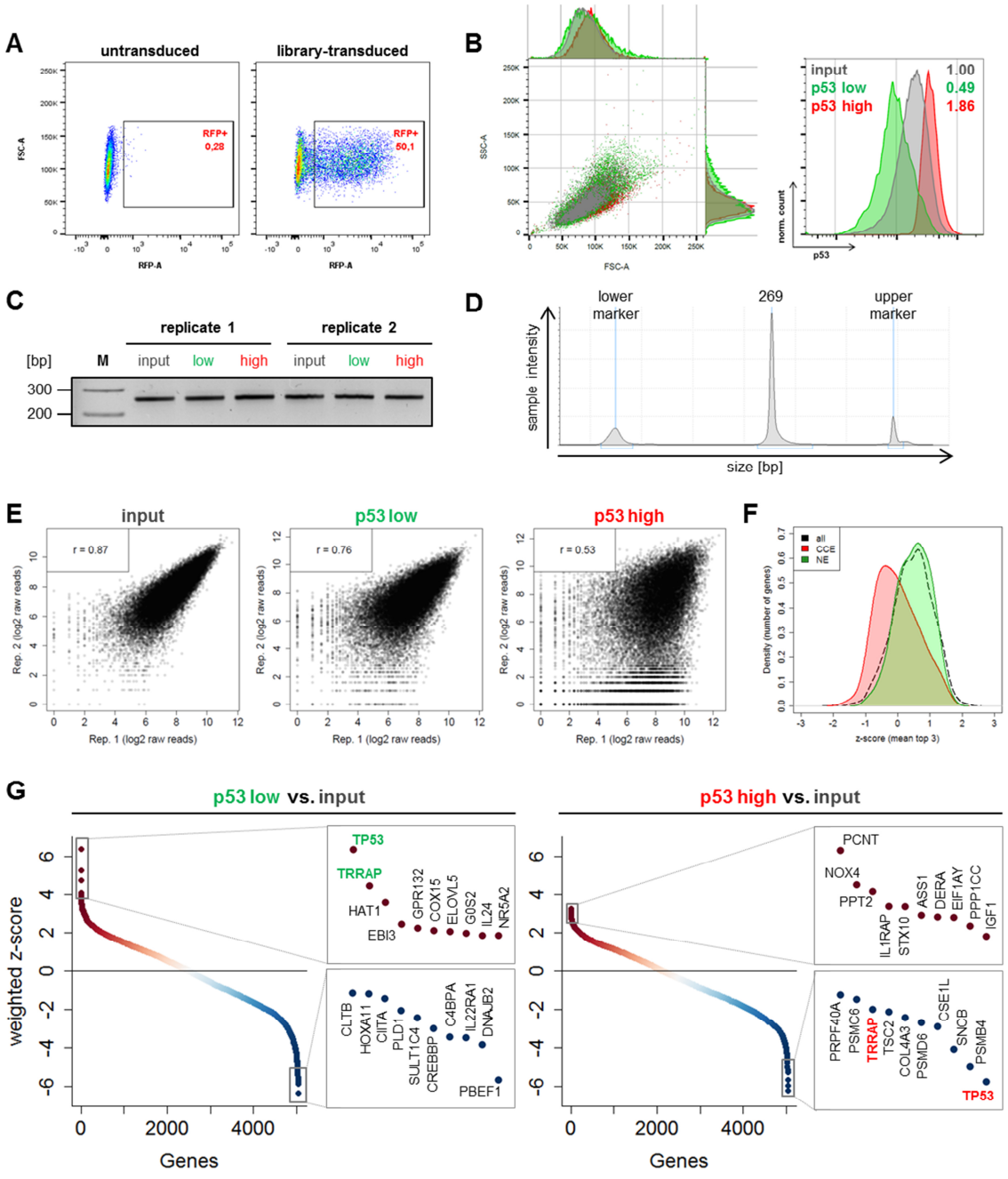

Figure 15: Performance and results of the shRNA screen.
(**A**) Transduction efficiency (%RFP+ cells) of shRNA library-transduced cells 3 d post-transduction as determined by flow cytometry. (**B**) Reanalysis of cell size/granularity (FSC/SSC) and p53 levels of sorted populations by flow cytometry. Values denote the p53 median fluorescence intensity (MFI) normalized to input. (**C**) Agarose gel electrophoresis of PCR-amplified shRNA bar-codes. (**D**) Quality control (TapeStation) of the high-throughput sequencing library of shRNA bar-codes before sequencing. (**E**) Reproducibility of technical replicates. For each sample pair, raw read counts were log2-transformed and plotted against each other. The Pearson correlation coefficient (r) is indicated. (**F**) Distribution of the gene level z-score (top three shRNAs) for all genes targeted in the screen (black) and for genes classified as "constitutive core essentials" (CCE, red) or non-essential (NE, green) based on Hart *et al.*[233]. (**G**) Distribution of weighted z-scores for all genes targeted in the screen, comparing the p53-low population or the p53-high population with the input. Boxes highlight the top ten or bottom ten genes, respectively.

To assess the initial quality of the screen data, the shRNA bar-code counts in technical replicates of all samples were correlated, which showed that measurements were reproducible (Pearson correlation r=0.53-0.87, Figure 15E). As expected, essential genes (as defined by Hart *et al.*[233]) were depleted in the input samples compared to the initial plasmid library (Figure 15F). Notably, cyclin-dependent kinase 6 (CDK6) was the second most depleted gene (data not shown) and has been reported previously to be essential in BL[163].

To identify screen hits, the weighted z-score method was used, which combined all shRNAs targeting the same gene into a single score. Using this method, only genes targeted by multiple enriched shRNAs were assigned a high score, while genes targeted by a single enriched shRNA got a low score. Weighted z-scores (wZ) were calculated for both populations, p53-low and p53-high cells, by comparing them against the input sample in separate analyses (Figure 15G). Importantly, *TP53* was the top scoring hit (rank 1/5033, wZ = 6.38) in the p53-low population and the most depleted gene in the p53-high population (rank 5033/5033, wZ = -6.21), validating the feasibility of the experimental approach. The focus was put on genes behaving in a similar fashion as p53 (enriched in one population while depleted in the other population). Among the top ten genes in both populations, TRRAP (transformation/transcription domain-associated protein) was the only candidate meeting these very stringent criteria (Figure 15G), of both strong enrichment in the p53-low population (rank 2/5033, wZ = 5.24) and depletion in the p53-high population (rank 5026/5033, wZ = -4.97). Therefore, TRRAP was chosen for further validation and investigation.

3.3 TRRAP regulates mutant p53 levels across entities and p53 mutations

TRRAP (transformation/transcription domain-associated protein) is a member of the phosphatidylinositol 3-kinase-related kinase (PIKK) family[234-236], which includes well-characterized p53 regulators such as ATM, ATR, and DNA-PKcs. As a common component of multiple histone acetyltransferase (HAT) complexes, TRRAP's main function is the recruitment of HATs to chromatin during transcription and DNA repair[237].

To confirm the impact of TRRAP silencing on mutp53 levels, the two top scoring shRNAs from the RNAi screen were studied. shRNAs were packaged into lentiviral particles and transduced into a mutp53 BL cell line (Namalwa). Both silencing triggers caused strong downregulation of TRRAP on both mRNA and protein level (Figure 16A,B). While a depletion of mutp53 protein to 20-50% of the basal level was observed upon TRRAP knock-down (Figure 16B), no changes of *TP53* mRNA levels were found (Figure 16A), suggesting that TRRAP regulates mutp53 on a translational or post-translational level.

To validate these findings, TRRAP was knocked-down in additional mutp53 BL cell lines with different p53 mutations and p53 levels were quantified by flow cytometry. TRRAP silencing resulted in mutp53 depletion in all seven tested BL cell lines, regardless of their kind of p53 mutation (Figure 16C, red). However, the extent of downregulation was variable. For example, an almost complete loss of mutp53 was observed in Namalwa cells after TRRAP knock-down, while only a subpopulation of cells lost mutp53 in CA-46. Next, it was tested whether silencing of TRRAP would also impair mutp53 accumulation in diffuse large B-cell lymphoma (DLBCL). TRRAP knock-down caused mutp53 downregulation to 32-36% of the basal level in SU-DHL4 (Figure 16C, green). To study whether TRRAP's role in mutp53 regulation would be limited to lymphoma, TRRAP was silenced in the colorectal cancer (CRC) cell line Colo320, which caused a phenotype comparable to BL and DLBCL, i.e. mutp53 downregulation to 41-78% of the basal level (Figure 16C, blue). These data suggest that TRRAP regulates mutp53 levels across a diverse set of cancers. To confirm the RNAi effects with an independent technique, TRRAP was knocked out in Namalwa-Cas9 BL cells via CRISPR/Cas9 genome editing (Figure 16D). In agreement with the previous results, TRRAP knock-out resulted in depletion of mutp53 to 51-67% of the basal level.

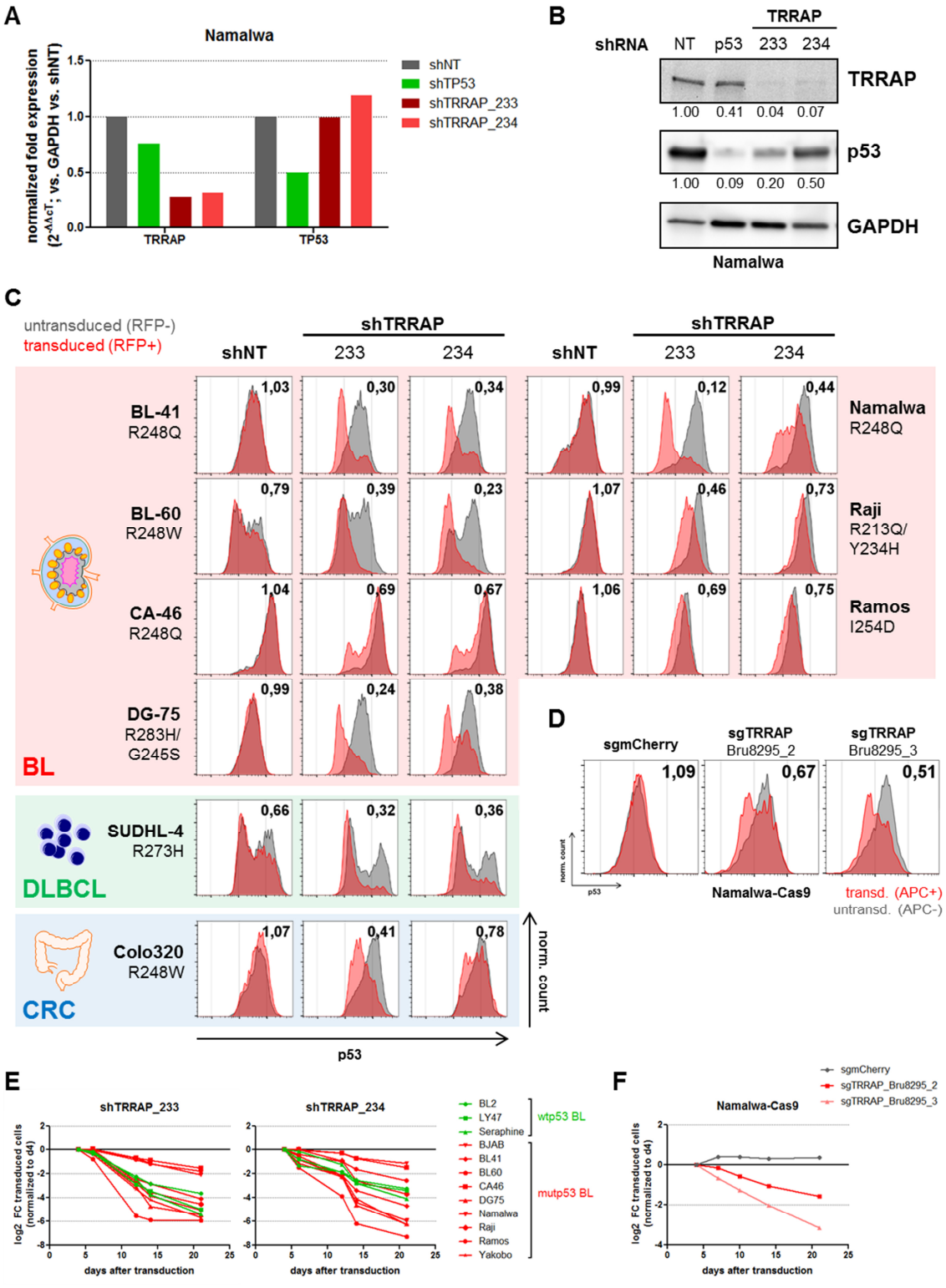

Figure 16: TRRAP silencing depletes mutant p53 across entities and p53 mutations.
(**A**) mRNA level of *TRRAP* and *TP53* in Namalwa cells transduced with shRNAs against TRRAP and p53. Cells were selected with puromycin for 48 h and harvested 3 d post-transduction. Expression values were determined by qRT-PCR and normalized to GAPDH and to cells transduced with a non-targeting shRNA (NT). (**B**) Protein level of TRRAP and p53 in Namalwa cells transduced with shRNAs against TRRAP and p53. Cells were selected with puromycin for 48 h and harvested 7 d post-transduction. Expression was determined by Western Blot and normalized to GAPDH and to cells transduced with a non-targeting shRNA (NT). (**C**) p53 flow cytometry 7 d or 8 d after shRNA-mediated knock-down of TRRAP in different mutp53 cancer cell lines: Burkitt's lymphoma (BL), diffuse large B-cell lymphoma (DLBCL), and colorectal cancer

(CRC). For each cell line, the p53 mutation is specified. Values denote the ratio of the p53 median fluorescence intensity (MFI) between transduced (red) and untransduced cells (grey). shNT, non-targeting shRNA. (**D**) p53 flow cytometry 7 d after sgRNA-mediated knock-out of TRRAP in Namalwa-Cas9 cells. Values denote the ratio of the p53 median fluorescence intensity (MFI) between transduced (red) and untransduced cells (grey). sgmCherry, negative control. Experiment performed by Marius Jentzsch. (**E**) Depletion of TRRAP-silenced BL cells over time. BL cells were transduced with two independent shRNAs against TRRAP and the proportion of transduced cells (RFP+) was followed over time by flow cytometry. Depletion of transduced cells is shown as log2 fold change (FC) normalized to d 4 after transduction. Red, mutp53 BL; green, wtp53 BL. (**F**) Depletion of TRRAP knock-out Namalwa-Cas9 mutp53 BL cells over time. Cells were transduced with two independent sgRNAs against TRRAP and the proportion of transduced cells (APC+) was followed over time by flow cytometry. Depletion of transduced cells is shown as log2 fold change (FC) normalized to d 4 after transduction. sgmCherry, negative control. Experiment performed by Marius Jentzsch.

To investigate whether interfering with TRRAP expression would impact cell proliferation and to test a potential p53 dependency, cell growth competition assays were performed. BL cell lines were transduced at an efficiency of ~50% with fluorescently-labeled shRNAs (Figure 16E) or sgRNAs (Figure 16F) against TRRAP and the proportion of transduced cells was followed over time by flow cytometry. In all cases, the transduced cells were outgrown by their untransduced counterparts, indicating that interfering with TRRAP expression impaired cell growth. Notably, TRRAP silencing equally affected cell growth in mutp53 and wtp53 BL cells.

In summary, these results suggest that TRRAP is a regulator of mutp53 levels independent of cancer entity and p53 mutation. In addition, TRRAP appears to be crucial for cell growth in both mutp53 and wtp53 cells.

3.4 TRRAP overexpression increases mutant p53 levels

To further understand the role of TRRAP in regulating mutp53 levels, the impact of TRRAP overexpression on mutp53 accumulation was tested. These experiments were performed in the CRC cell line Colo320 since the TRRAP overexpression construct was too large for lentiviral packaging (17 kb) and satisfactory transfection efficiencies could not be achieved in the BL cell lines. Transfection of FLAG-TRRAP resulted in upregulation of TRRAP but not *TP53* mRNA (Figure 17A), which translated into mild upregulation of TRRAP protein compared to untransfected cells (Figure 17B). Importantly, p53 flow cytometry showed that TRRAP overexpression resulted in an increased level of mutp53 (Figure 17C). Finally, in order to prove the on-target effect of a previously used shRNA against TRRAP (shTRRAP_233, Figure 16), TRRAP silencing was performed in the context of TRRAP overexpression, which resulted in a rescue of the p53 phenotype to basal levels (Figure 17D). In summary, these findings are in strong support of the silencing and knock-out experiments (Figure 16) and thus provide further evidence that TRRAP regulates mutp53 levels.

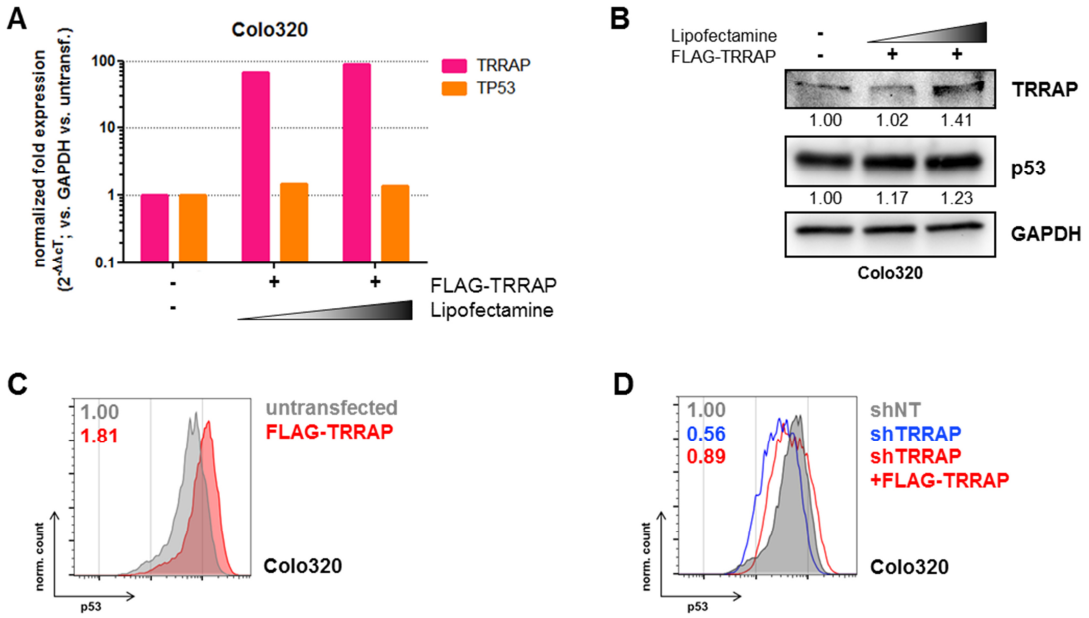

Figure 17: TRRAP overexpression increases mutant p53 levels.
(**A**) mRNA level of *TRRAP* and *TP53* in Colo320 cells 48 h post-transfection with FLAG-TRRAP using different amounts of transfection reagent (Lipofectamine). Expression values were determined by qRT-PCR and normalized to GAPDH and to untransfected cells. (**B**) Protein level of TRRAP and p53 in Colo320 cells 48 h post-transfection with FLAG-TRRAP using different amounts of transfection reagent (Lipofectamine). Expression was determined by Western Blot and normalized to GAPDH and to untransfected cells. (**C**) p53 flow cytometry 72 h post-transfection with FLAG-TRRAP in Colo320 cells. Values denote the ratio of the p53 median fluorescence intensity (MFI) between transfected (red) and untransfected cells (grey). (**D**) Molecular rescue of the TRRAP knock-down phenotype by FLAG-TRRAP overexpression in Colo320 cells. Cells were transduced with either a non-targeting shRNA (shNT, grey) or with an shRNA against TRRAP (blue). 24 h after transduction, part of the TRRAP-silenced cells was transfected with FLAG-TRRAP (red). Cells were analyzed by p53 flow cytometry 4 d after transduction. Values denote p53 median fluorescence intensities (MFI) normalized to cells transduced with the NT.

3.5 Investigation of the physical interaction of TRRAP and mutant p53

Previous studies showed that mutp53 can be stabilized by the binding of chaperones such as Hsp90[83]. Since TRRAP has been reported to bind to wtp53[238], it was explored whether TRRAP stabilized mutp53 via physical interaction. To this end, the p53-null cell line H1299 was used and both FLAG-tagged TRRAP (Figure 17) and mutp53 (mutation R175H) were introduced by transfection (Figure 18A). Immunoprecipitation (IP) of both FLAG-TRRAP and mutp53 resulted in co-IP of mutp53 or TRRAP, respectively, indicating binding of TRRAP to mutp53.

To address whether TRRAP bound preferentially to mutp53 compared to wtp53, FLAG-TRRAP was transfected together with either mutp53 or wtp53 in H1299 cells (Figure 18B). FLAG-TRRAP IP resulted in stronger co-IP of mutp53 than wtp53, suggesting enhanced binding of TRRAP to mutp53. Notably, TRRAP also bound to a truncated form of wtp53, which lacked the 40 N-terminal amino acids (ΔN in Figure 18B), suggesting that TRRAP binds p53 outside of its N-terminus.

To confirm these results in an endogenous setting, the experiment was repeated in mutp53 BL cells (Figure 18C). However, in contrast to the previous results in the exogenous system, neither IP of p53 nor IP of TRRAP resulted in co-IP of the respective other protein. Notably, mutp53 co-immunoprecipitated with MDM2.

In summary, this suggests that TRRAP may not bind to mutp53 in BL, indicating that mutp53 is unlikely to be stabilized by physical interaction with TRRAP.

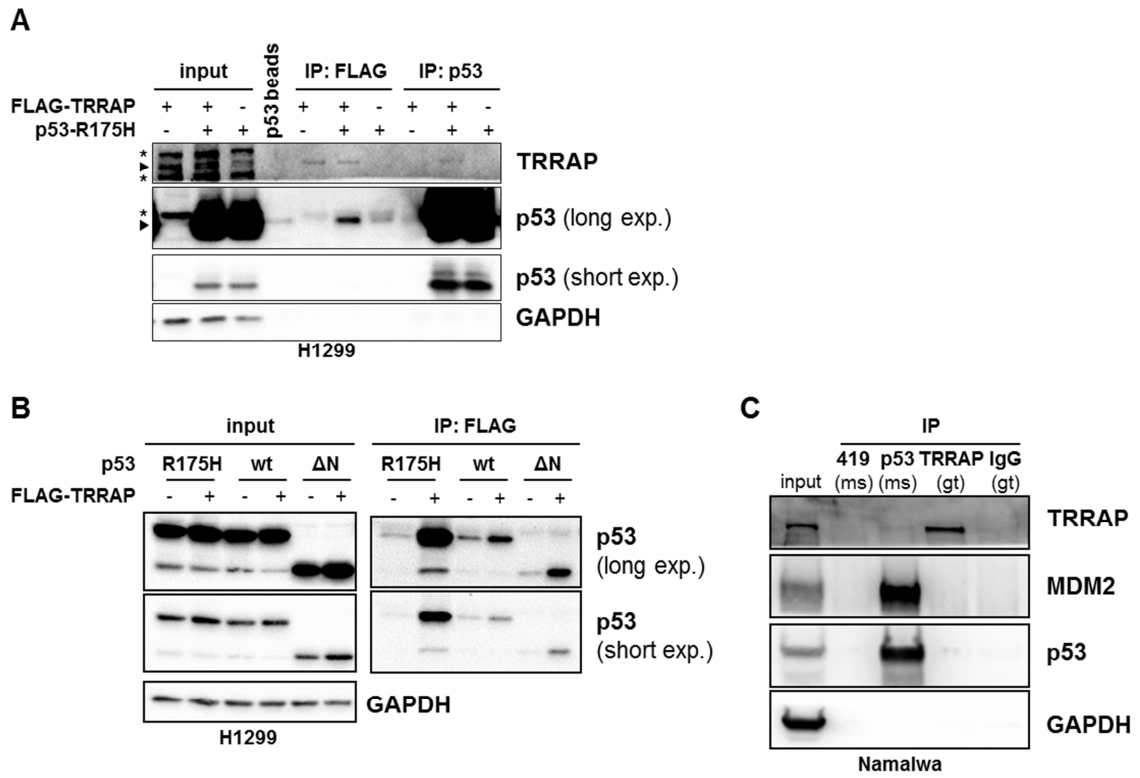

Figure 18: Investigation of the binding of TRRAP to mutant p53 and MDM2 by immunoprecipitation. (**A**) Western Blot after immunoprecipitation of FLAG and p53 48 h after transfection of p53-null H1299 cells with FLAG-TRRAP and mutp53 (R175H). *, unspecific band; ►, specific band; GAPDH, loading control. (**B**) Western Blot after FLAG immunoprecipitation 24 h after transfection of p53-null H1299 cells with FLAG-TRRAP and different p53 constructs: mutp53 (R175H), wtp53, and ΔNp53 lacking the first 40 amino acids. GAPDH, loading control. (**C**) Western Blot after immunoprecipitation of mutp53 and TRRAP in Namalwa mutp53 BL cells. 419, anti-SV40 T-antigen mouse (negative control for IP p53); IgG, normal goat IgG (negative control for IP TRRAP); exp., exposure time; GAPDH, loading control.

3.6 TRRAP silencing exports mutant p53 from the nucleus to the cytosol

To obtain a global view on the alterations in protein expression and mutp53-interacting proteins upon TRRAP silencing, total proteome and mutp53 immunoprecipitates (IPs) were quantified by mass spectrometry after TRRAP or control knock-down in mutp53 BL cells (Figure 19A). Flow cytometry indicated that mutp53 protein was depleted in a time-dependent manner upon TRRAP silencing (Figure 19B). Accordingly, mass spectrometry of the total proteome samples showed that both TRRAP and mutp53 protein were depleted upon TRRAP silencing (Figure 19C). In total, TRRAP knock-down significantly altered the expression of 44 proteins (23 down-, 21 upregulated, adj. $p<0.05$ & $|log2FC|>0.5$; Figure 19D), suggesting that the TRRAP-dependent mutp53 degradation was relatively specific. Gene set enrichment analysis showed that TRRAP silencing suppressed mTOR signaling and MYC targets, while it induced interferon signaling (Figure 19E).

To identify mutp53 binding partners in each condition (control or TRRAP knock-down, Figure 19A), the focus was set on proteins significantly enriched in p53 IPs compared to IgG control IPs. Overall, 37 proteins binding to mutp53 were found across all samples (Figure 19F), which were significantly enriched for previously reported p53 interactors[239] (Figure 19G, 8/37, 21.6%, p=0.0002, hypergeometric test). For example, the protein methyltransferase CARM1 has been shown to physically interact with p53 and to regulate p53-dependent transcription via histone methylation[240].

To quantify changes upon TRRAP knock-down, mutp53-bound proteins in TRRAP-silenced samples were compared to proteins in control knock-down samples (Figure 19G). TRRAP silencing induced major alterations in mutp53-binding proteins, which could be categorized into 2 classes: (1) 18 mutp53 interactors lost upon TRRAP knock-down and (2) 19 interactors gained upon TRRAP silencing. To gain insights into the molecular function of the proteins in both categories, gene set enrichment analysis was performed (Figure 19H). Proteins recruited to mutp53 upon TRRAP silencing were significantly enriched for functions related to translational initiation. Accordingly, seven of the thirteen subunits of the eukaryotic translation initiation factor 3 (eIF3) were found in this group (EIF3E,F,G,H,I,L,M). In contrast, proteins lost upon TRRAP knock-down mainly participated in mRNA biogenesis. In fact, six members of the spliceosome were detected in this group (SF3A1, SF3B1, SF3B2, HNRNPA0, HNRNPC, HNRNPDL).

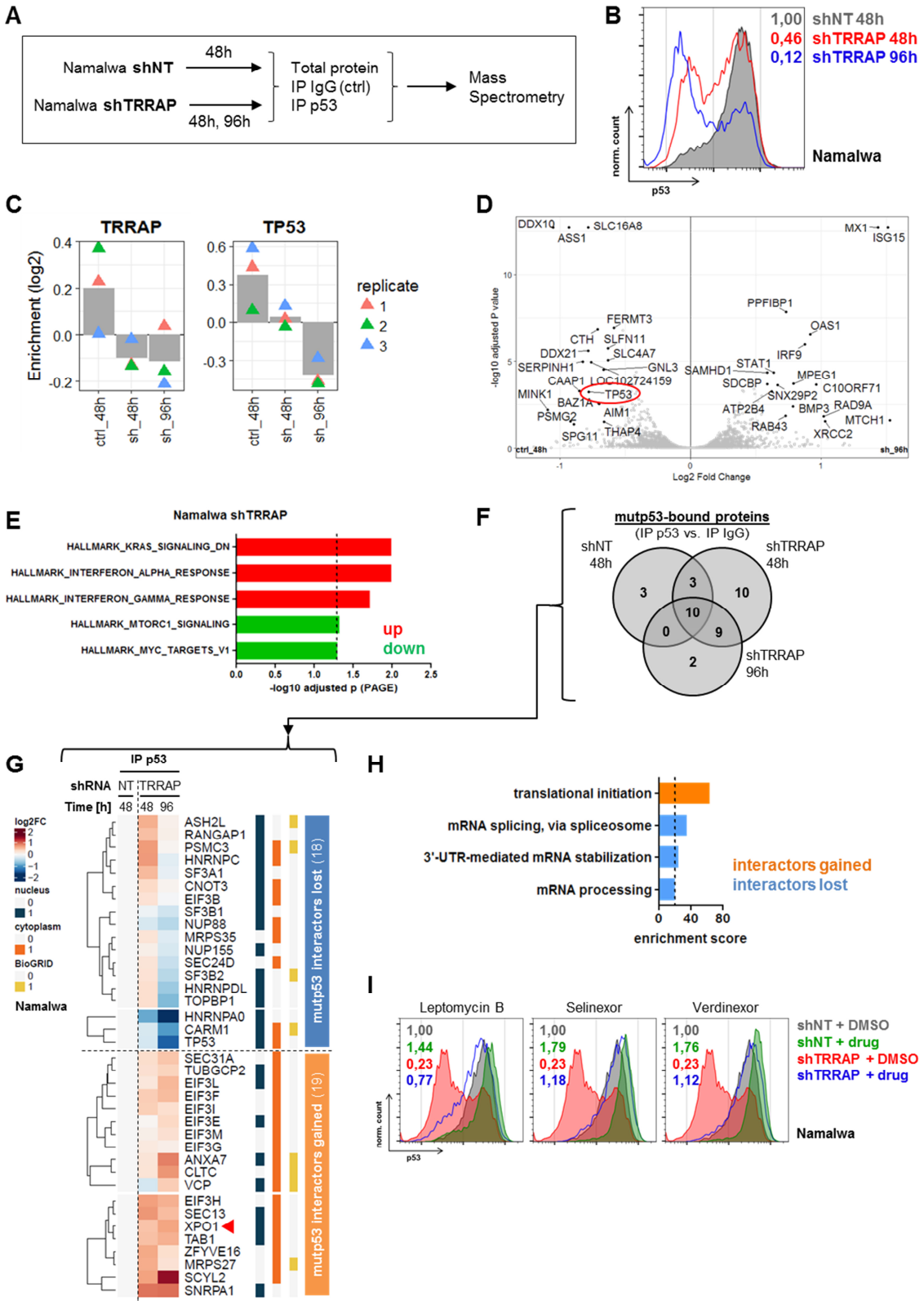

Figure 19: TRRAP silencing exports mutant p53 from the nucleus to the cytosol.
(**A**) Experimental design. Namalwa mutp53 BL cells were transduced with an IPTG-inducible shRNA against TRRAP or a non-targeting control (NT). 48 h or 96 h after induction, cells were lysed and either collected immediately (total protein) or subjected to immunoprecipitation with antibodies against p53 or IgG (negative control) before mass spectrometry. The experiment was performed in biological triplicates. (**B**) p53 flow cytometry of Namalwa cells 48 h or 96 h after IPTG induction of an shRNA against TRRAP or non-targeting control (NT). Values denote p53 median fluorescence intensities (MFI) normalized to cells transduced with

the NT. (**C**) Normalized enrichment of p53 and TRRAP protein in mass spectrometry samples. Grey bars indicate mean intensity values. Analysis performed by Arne Smits. (**D**) Volcano plots for differential total protein expression 96 h (right) after TRRAP knock-down in Namalwa cells, normalized to a non-targeting control (NT). Proteins denoted in black were significantly differentially expressed (adj. $p < 0.05$, $|log2FC| > 0.5$). p53 is highlighted in red. P values were calculated using moderated t-statistic (R package "limma"[221]) and adjusted for multiple testing using the Benjamini-Hochberg procedure. Analysis performed by Arne Smits. (**E**) Gene set enrichment analysis of significantly differentially expressed genes from panel D. Upregulated gene sets are denoted in red, downregulated in green. Analysis was performed using Parametric Analysis of Gene Set Enrichment (PAGE)[213] with the MSigDB[214] gene set collection "Hallmark"[215]. Only significantly altered gene sets are shown (adj. $p < 0.05$). (**F**) Venn diagram showing the overlap of mutp53-bound proteins (proteins significantly enriched in p53 IPs compared to IgG control IPs) after control or TRRAP knock-down. Analysis performed by Frank Stein. (**G**) Heatmap of all mutp53-bound proteins from panel F. Values denote hierarchically clustered log2 fold changes of protein abundances in TRRAP-silenced samples compared to control knock-down samples. The cellular localization[241] and known p53 interactions[239] are indicated, XPO1 is highlighted with an arrow (◄). Analysis performed by Frank Stein. (**H**) Gene set enrichment analysis of proteins contained within each cluster from panel G. Gene sets from interactors gained are denoted in orange, gene sets from interactors lost in blue, respectively. Analysis was performed using Enrichr[198,199] with "GO Biological Process 2017" data set. Values indicate enrichment scores. Only annotations with an enrichment score >20 are shown. (**I**) Rescue of the TRRAP silencing-mediated mutp53 depletion by treatment with nuclear export inhibitors. Namalwa cells were transduced with an IPTG-inducible shRNA against TRRAP or a non-targeting control (NT). 48 h after induction, cells were treated with DMSO (0.005%), Leptomycin B (20 nM), Selinexor (500 nM), or Verdinexor (500 nM) for 14 h before they were subjected to p53 flow cytometry. Values denote p53 median fluorescence intensities (MFI) normalized to DMSO-treated cells transduced with the NT.

Since mRNA splicing takes place in the nucleus and translation in the cytoplasm, the cellular localization of all mutp53-interacting proteins lost and gained upon TRRAP knock-down was annotated[241] (Figure 19G). While the vast majority of the former proteins were annotated to be localized in the nucleus (16/18, 88.9%), the latter proteins were mainly reported to be in the cytosol (18/19, 94.7%). Importantly, exportin 1 (XPO1/CRM1), the key protein for facilitating protein export from the nucleus to the cytosol, was among the proteins recruited to mutp53 after TRRAP knock-down (red in Figure 19G). Therefore, it was hypothesized that mutp53 was exported from the nucleus to the cytosol upon TRRAP knock-down and that the export was a prerequisite for mutp53 degradation. To test this, TRRAP was silenced in the context of the nuclear export inhibitors Leptomycin B, Selinexor, and Verdinexor (all targeting XPO1/CRM1) and mutp53 levels were quantified by flow cytometry (Figure 19I). Treatment with the inhibitors resulted in mild mutp53 upregulation (1.44-1.79-fold) in control knock-down samples. TRRAP silencing resulted in a mutp53 downregulation to 23% of the basal level, which was rescued to full extent by co-treatment with all nuclear export inhibitors.

In summary, this suggests that nuclear export is required to mediate TRRAP effects on mutp53 levels. Thus, TRRAP may stabilize mutp53 by retaining it in the nucleus.

3.7 TRRAP silencing destabilizes mutant p53 via the MDM2-proteasome axis

The nuclear export and cytosolic degradation of mutp53 observed upon TRRAP silencing (Figure 19) were evocative of the final steps of physiological wtp53 degradation, where these steps are mediated by MDM2 and the proteasome[31,37,38]. Therefore, the involvement of the MDM2-proteasome axis in the degradation of mutp53 after TRRAP knock-down was tested. To this end, TRRAP was silenced in the context of the MDM2 inhibitor Nutlin-3a and p53 levels were quantified by flow cytometry (Figure 20A). While TRRAP knock-down alone reduced the mutp53 level to 17% of the basal level, co-treatment with Nutlin-3a was able to fully rescue the phenotype.

To confirm these findings with an independent technique, MDM2 knock-out cells were generated by transducing Namalwa-Cas9 cells with sgRNAs targeting either MDM2 or GFP (negative control) (Figure 20B). Efficient cutting of the correct genomic locus was confirmed by T7E1 assay, which indicated indel formation in *MDM2* exon 2 in case of sgMDM2-transduced cells. Notably, a minor subpopulation still retained the uncut wild-type *MDM2* allele. In support of the previous findings, mutp53 depletion upon TRRAP silencing was almost completely rescued in cells harboring MDM2 knock-out but not in control cells. The small subpopulation of MDM2 knock-out cells which still showed mutp53 downregulation most likely retained MDM2 expression as already indicated by the T7E1 assay.

Although mutp53 was stabilized despite the presence of MDM2 (Figure 13E), it has been reported that MDM2 overexpression can cause degradation of mutp53[35]. Therefore, MDM2 expression was investigated after TRRAP knock-down (Figure 20C,D). While TRRAP silencing caused mild upregulation (1.54-1.66-fold) of MDM2 protein in wtp53 cells, MDM2 mRNA and protein expression were slightly reduced (0.76-0.82-fold) after TRRAP knock-down in mutp53 cells. This suggests that mutp53 destabilization upon TRRAP silencing is not caused by increased MDM2 expression.

Given the fact that MDM2 typically drives proteasomal degradation of p53, the role of the proteasome in TRRAP-driven mutp53 degradation was investigated. To this end, TRRAP was silenced in the context of the proteasome inhibitor Bortezomib and p53 levels were quantified by flow cytometry (Figure 20E). Bortezomib treatment resulted in mild mutp53 upregulation (1.20-fold) in control knock-down samples. TRRAP silencing resulted in a reduction of mutp53 expression to 59% of the basal level, which was rescued to full extent by proteasome inhibition.

In summary, these results suggest that TRRAP silencing targets mutp53 to the physiological MDM2-dependent wtp53 degradation machinery, including nuclear export followed by proteasomal degradation.

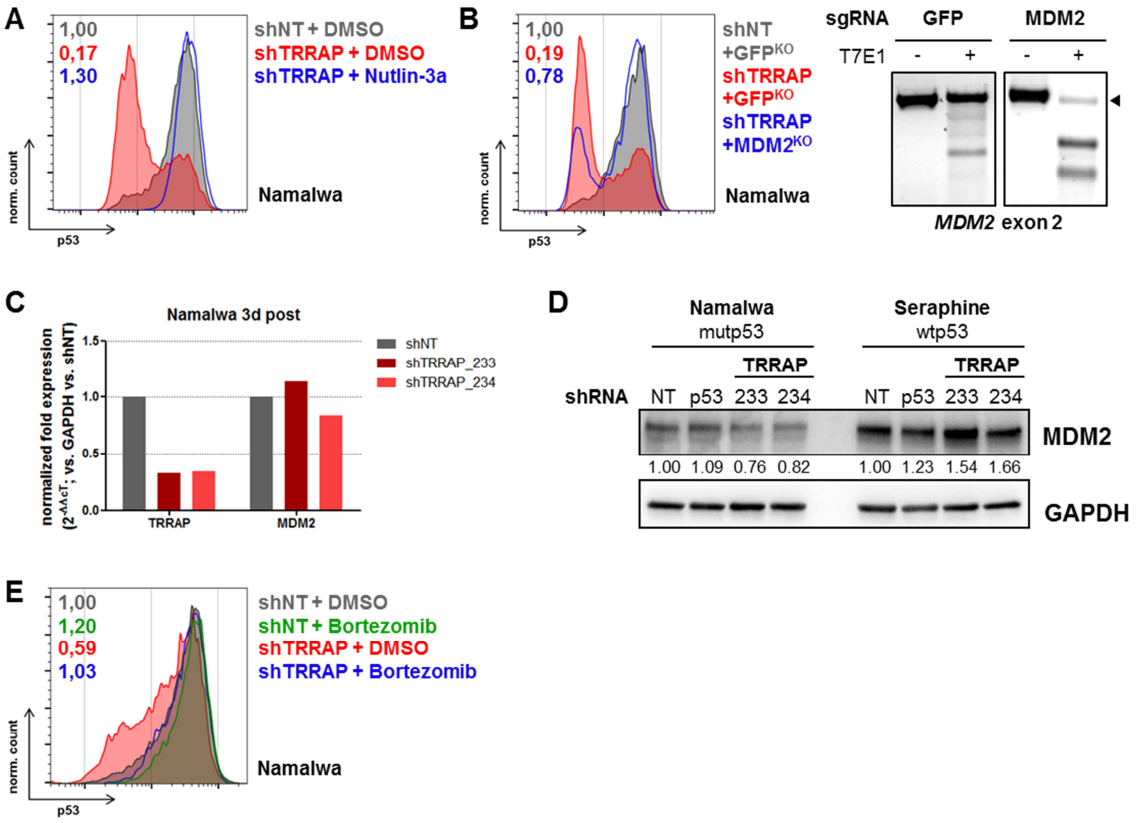

Figure 20: TRRAP silencing destabilizes mutant p53 via the MDM2-proteasome axis.
(**A**) Rescue of the TRRAP silencing-mediated mutp53 degradation by treatment with the MDM2 inhibitor Nutlin-3a. Namalwa cells were transduced with an shRNA against TRRAP or a non-targeting control (NT). 4 d after transduction, cells were treated with DMSO (0.1%) or Nutlin-3a (10 µM) for 48 h before they were subjected to p53 flow cytometry. Values denote p53 median fluorescence intensities (MFI) normalized to DMSO-treated cells transduced with the NT. (**B**) Rescue of the TRRAP silencing-mediated mutp53 degradation by CRISPR/Cas9-mediated knock-out of MDM2. Knock-out cells were transduced with an shRNA against TRRAP or a non-targeting control (NT) and subjected to p53 flow cytometry 4 d after transduction (left). Values denote p53 median fluorescence intensities (MFI) normalized to GFP knock-out cells transduced with the NT. In order to generate knock-outs, Namalwa cells were transduced with constructs harboring both Cas9 and sgRNAs against MDM2 or GFP (negative control). After selection with multiple rounds of puromycin, targeting of the appropriate *MDM2* locus (exon 2) was monitored by T7E1 assay (right). The wild-type allele is indicated with an arrow (◄). (**C**) mRNA level of *TRRAP* and *MDM2* in Namalwa cells transduced with shRNAs against TRRAP or a non-targeting control (NT). Cells were selected with puromycin for 48 h and harvested 3 d post-transduction. Expression values were determined by qRT-PCR and normalized to GAPDH and to cells transduced with the NT. (**D**) Protein level of MDM2 in Namalwa (mutp53) and Seraphine (wtp53) cells transduced with shRNAs against TRRAP, p53, and a non-targeting control (NT). Cells were selected with puromycin for 48 h and harvested 6 d post-transduction. Expression was determined by Western Blot and normalized to GAPDH and to cells transduced with the NT. (**E**) Rescue of the TRRAP silencing-mediated mutp53 degradation by treatment with the proteasome inhibitor Bortezomib. Namalwa cells were transduced with an IPTG-inducible shRNA against TRRAP or a non-targeting control (NT). 24 h after induction, cells were treated with DMSO (0.1%) or Bortezomib (100 nM) for 14 h before they were subjected to p53 flow cytometry. Values denote p53 median fluorescence intensities (MFI) normalized to DMSO-treated cells transduced with the NT.

3.8 TRRAP silencing induces interferon signaling and suppresses cell cycle-related genes

To investigate TRRAP-mediated transcriptome changes on a global scale and a potential p53-dependence, microarray-based gene expression profiling after TRRAP silencing was performed in BL cell lines with mutp53, wtp53, or p53 knock-out (Figure 21A). While the number of significantly deregulated genes was comparable between the mutp53 and wtp53 cell line (614 vs. 680), less genes were altered in the $p53^{KO}$ line (495). When the overlap of differentially expressed genes between cell lines was calculated (Figure 21B), it was found that a small subset of genes (89/1224, 7.3%) was shared among all cell lines. To investigate this further and to reveal expression patterns, hierarchical clustering was performed, which showed that genes clustered in two different groups (Figure 21C): (1) 43 genes (48.3%) upregulated and (2) 46 genes (51.7%) downregulated in all cell lines. The expression pattern of these clusters was similar in all cell lines, indicating that TRRAP-dependent expression of these genes was not affected by p53 status.

To gain insights into the molecular function, gene set enrichment analyses was performed for the genes within the two major clusters (Figure 21D). Genes downregulated upon TRRAP knock-down were enriched for functions related to the cell cycle and included for example *CDC20*, *CCNA2*, and *CCNB2* (Figure 21C). Genes upregulated upon TRRAP silencing mainly participated in interferon signaling and included for example *ISG15*, *IRF9*, and *STAT1* (Figure 21C,D), which is in line with the results from mass spectrometry (Figure 19E). Since interferon (IFN) beta can regulate mutp53 levels[203], the role of IFN signaling in TRRAP-mediated mutp53 degradation was investigated. First, qRT-PCR of two IFN signaling pathway members (*ISG15* and *MX1*) was performed in the context of TRRAP silencing to validate the transcriptome data (Figure 21E). The expression of both genes was increased ~2-4-fold upon TRRAP knock-down, which was suppressed in the presence of the JAK/STAT inhibitor Ruxolitinib given that JAK/STAT is the main node of the IFN signaling pathway[242]. Next, the impact of IFN alpha treatment on mutp53 levels was quantified by flow cytometry (Figure 21F), which showed a mild depletion of mutp53 to 83% of the basal levels that was salvaged by co-treatment with Ruxolitinib. Finally, to address whether IFN signaling contributed to TRRAP-driven mutp53 degradation, TRRAP was silenced in the context of Ruxolitinib and mutp53 levels were quantified by flow cytometry (Figure 21G). Ruxolitinib treatment did not rescue mutp53 depletion upon TRRAP knock-down, indicating that mutp53 regulation by TRRAP is not mediated via IFN signaling.

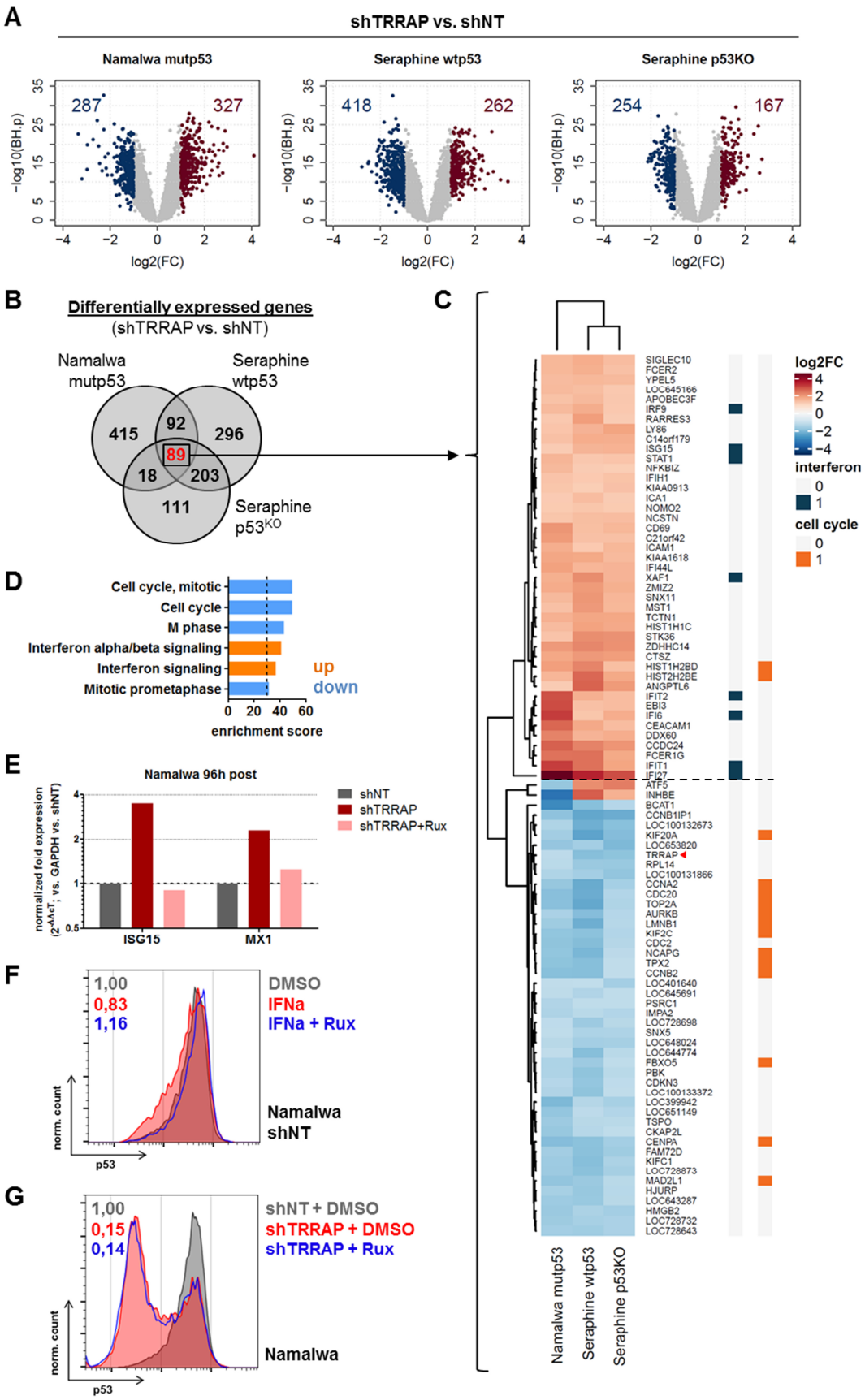

Figure 21: TRRAP silencing induces interferon signaling and suppresses cell cycle-related genes. (**A**) Volcano plots for differential gene expression 8 d after TRRAP knock-down in Namalwa (mutp53), Seraphine (wtp53), and Seraphine p53^{KO} cells, normalized to a non-targeting control (NT). Numbers denoted

in blue or red indicate the number of genes significantly down- or upregulated, respectively (adj. $p < 0.05$, $|log2FC| > 1$). (**B**) Venn diagram showing the overlap of significantly differentially expressed genes after TRRAP knock-down from panel A. (**C**) Heatmap of the 89 significantly differentially expressed genes upon TRRAP knock-down shared between all cell lines from panel B. log2 fold changes were subjected to hierarchical clustering. Genes part of interferon signaling (R-HSA-909733) or cell cycle (R-HSA-69278) are indicated (Reactome)[243] and TRRAP is highlighted with an arrow (◄). (**D**) Gene set enrichment analysis of genes within the two major clusters from panel C. Upregulated gene sets are denoted in orange, downregulated in blue, respectively. Analysis was performed using Enrichr[216,217] with the "GO Biological Process 2017" data set. Values indicate enrichment scores. Only annotations with an enrichment score >30 are shown. (**E**) mRNA level of type I interferon signaling pathway members in Namalwa cells 96 h after IPTG induction of an shRNA against TRRAP. Part of the cells was treated for 24 h with the JAK/STAT inhibitor Ruxolitinib (Rux, 2 µM). Expression values were determined by qRT-PCR and normalized to GAPDH and to cells transduced with a non-targeting shRNA (NT). (**F**) p53 flow cytometry of Namalwa cells (non-targeting control (NT) transduced) after treatment for 24 h with interferon alpha alone (IFNa, 1,000 U/mL) or IFNa together with the JAK/STAT inhibitor Ruxolitinib (Rux, 2 µM). Values denote p53 median fluorescence intensities (MFI) normalized to DMSO-treated cells (0.1%). (**G**) No rescue of the TRRAP silencing-mediated mutp53 degradation by treatment with the JAK/STAT inhibitor Ruxolitinib (Rux). Namalwa cells were transduced with an IPTG-inducible shRNA against TRRAP or a non-targeting control (NT). 72 h after induction, cells were treated with DMSO (0.1%) or Ruxolitinib (2 µM) for 24h before they were subjected to p53 flow cytometry. Values denote p53 median fluorescence intensities (MFI) normalized to DMSO-treated cells transduced with the NT.

In summary, this suggests TRRAP silencing induces an IFN response, which is unrelated to its effect on mutp53 levels. In basal conditions, TRRAP maintains a cell cycle-related transcriptional program independent of p53 status.

3.9 Identification of TRRAP's domain crucial for mutant p53 stabilization and cell survival

To identify functional regions of TRRAP important for mutp53 stabilization and to assess whether TRRAP's role for cell survival (Figure 16E,F) was mediated by independent domains, a recently developed CRISPR/Cas9 mutagenesis approach ("CRISPR scanning") was used, which was designed to identify functionally relevant protein domains[223]. CRISPR/Cas9 induces DNA double-strand breaks at its target locus, which is specified by the small guide RNA (sgRNA)[195,244]. When targeted to protein-coding genes, error-prone repair mechanisms can cause both frameshift mutations (i.e. deletion of 1,2,4,... bp) and single amino acid deletions (i.e. deletion of 3,6,9,... bp)[195,245]. CRISPR scanning is based on the fact that while in domains irrelevant for the protein function only frameshift mutations will be detrimental, in domains crucial for the protein function both mutations causing frameshifts and single amino acid deletions will be harmful. Therefore, cells transduced with sgRNAs targeting functionally important protein domains will be more quickly outcompeted by untransduced cells than cells infected with sgRNAs targeting irrelevant protein domains[223].

For CRISPR scanning, Namalwa-Cas9 cells were transduced with an efficiency of ~25% with fluorescently-tagged sgRNAs spanning the entire TRRAP protein, including all annotated domains and the N-terminal HEAT repeat region. The proportion of transduced cells and mutp53 levels were monitored over time by flow cytometry (Figure 22A). As expected for an essential protein and in agreement with previous results (Figure 16E,F), cells transduced with any sgRNA targeting TRRAP were outcompeted by their untransduced counterparts. Targeting of a 109 aa region (residues 1050-1158) within TRRAP's HEAT repeat region (HEAT repeats 21/22)[246] resulted in significantly stronger depletion of transduced cells (mean: 15.9-fold vs. 3.5-fold, $p<0.05$) and p53 protein (3.7-fold vs. 1.5-fold, $p<0.05$) than targeting of any other domain of TRRAP (yellow in Figure 22A,B). Notably, targeting of a region in TRRAP previously reported to be important for wtp53 binding[238] was neither severely toxic nor caused strong mutp53 depletion. Interestingly, a strong linear correlation between cell depletion and mutp53 depletion was observed (Pearson correlation coefficient $r=0.73$, Figure 22C), indicating that TRRAP's ability to support cell survival and to regulate mutp53 levels are tightly linked and potentially mediated by the same region. Finally, to validate the cell survival function of the newly identified TRRAP domain, it was targeted with two sgRNAs in five additional BL cell lines, which again caused a strong depletion of transduced cells over time compared to controls (Figure 22D).

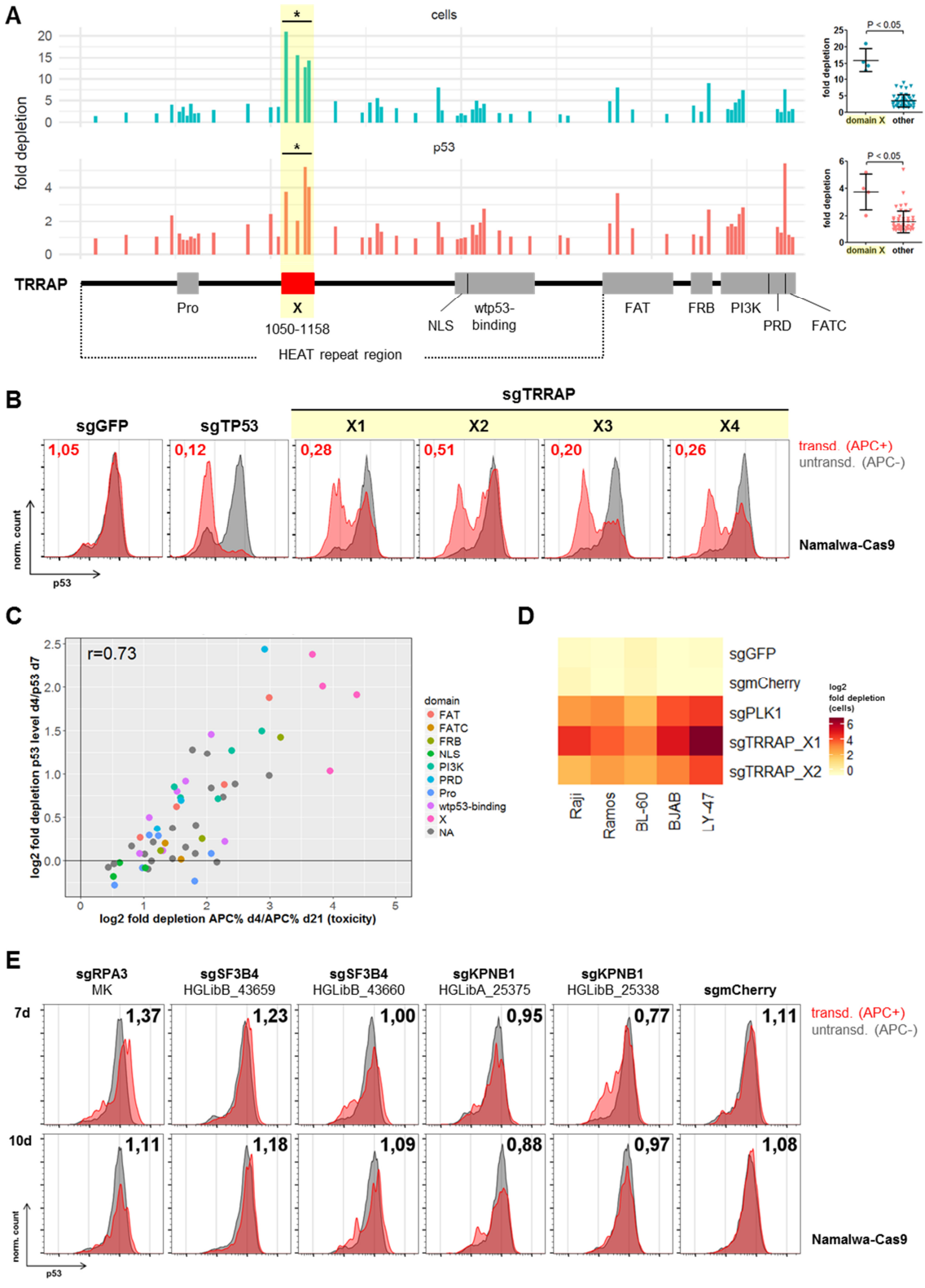

Figure 22: CRISPR scanning to identify TRRAP's domain mediating mutant p53 stabilization and cell survival.

(**A**) Namalwa-Cas9 cells were transduced with sgRNAs targeting different regions of TRRAP protein, including all annotated domains. The proportion of transduced cells (APC+) and p53 levels were quantified by flow cytometry over time. Negative cell selection (top, cyan) and mutp53 depletion (bottom, red) is shown as fold depletion of transduced cells or mutp53 protein after 21 d or 7 d in culture, respectively. Every bar represents an independent sgRNA and the location of each sgRNA relative to TRRAP protein is indicated along the x-axis. P values were determined by Student's t-test (* indicates P < 0.05). Domain "X" is

highlighted in yellow. Pro, Proline-rich region; NLS, nuclear localization signal; wtp53-binding, wtp53-binding region; FAT, focal adhesion targeting domain; FRB, FKBP12-rapamycin binding domain; PI3K, phosphatidylinositol 3-kinase domain; PRD, PIKK regulatory domain; FATC, FRAP, ATM, TRRAP C-terminal domain. Experiment performed by Marius Jentzsch. (**B**) p53 flow cytometry 7 d after TRRAP knock-out in Namalwa-Cas9 cells. TRRAP sgRNAs (X1-4) are highlighted in yellow in panel A. Values denote the ratio of the p53 median fluorescence intensity (MFI) between transduced (red) and untransduced cells (grey). sgGFP, negative control; sgTP53, positive control. Experiment performed by Marius Jentzsch. (**C**) Correlation of toxicity (APC depletion) and mutp53 protein depletion after TRRAP knock-out using sgRNAs targeting different protein domains. Each data point represents a single sgRNA from panel A. Colors indicate the targeted domains. The Pearson correlation coefficient (r) is indicated. (**D**) Heatmap showing negative selection of TRRAP sgRNA-transduced BL cell lines. Values indicate log2 fold depletion of transduced cells after 24 d in culture. sgGFP & sgmCherry, negative controls; sgPLK1, positive control. Experiment performed by Vineet Dalal. (**E**) p53 flow cytometry 7 d and 10 d after knock-out of essential genes in Namalwa-Cas9 cells. Values denote the ratio of the p53 median fluorescence intensity (MFI) between transduced (red) and untransduced cells (grey). sgmCherry, negative control. Experiment performed by Marius Jentzsch.

To address whether mutp53 depletion upon TRRAP knock-out would be an unspecific side effect caused by cellular stress or toxicity, three essential genes (*RPA3*, *SF3B4*, *KPNB1*) were targeted by CRISPR/Cas9 and mutp53 levels were quantified by flow cytometry (Figure 22E). None of the knock-outs caused a consistent reduction of mutp53 levels, suggesting that the degradation of mutp53 upon TRRAP ablation is not due to general toxicity.

In summary, these results indicate that TRRAP's amino acids 1050-1158 represent a novel functional domain crucial for promoting both cell survival and mutp53 stabilization.

3.10 TRRAP silencing attenuates stabilization and activity of wild-type p53 upon genotoxic stress

Proteins stabilizing mutp53 have been reported to also chaperone wtp53, as for example Hsp90[83,247]. To explore a potential role of TRRAP in stabilization of wtp53, TRRAP was silenced with two independent shRNAs in two wtp53 BL cell lines, wtp53 was induced using the MDM2 inhibitor Nutlin-3a, and wtp53 levels were quantified by flow cytometry (Figure 23A). As expected, wtp53 levels were low in basal conditions and increased ~6-8-fold upon Nutlin-3a treatment. In context of TRRAP knock-down, wtp53 induction was attenuated to ~3-6-fold in both cell lines upon Nutlin-3a exposure. To confirm these results, the experiment was repeated with the DNA damaging agent Etoposide (Figure 23B). In support of the previous results, Etoposide treatment resulted in 4.34-fold wtp53 stabilization, which was decreased to 2.55-2.84-fold in context of TRRAP silencing.

To examine whether the reduced wtp53 accumulation translated into attenuated wtp53 pathway activity, expression of the wtp53 target gene p21 and apoptosis induction via cleavage of PARP was monitored in TRRAP-silenced wtp53 cells after Etoposide treatment (Figure 23C). In line with the previous results, Etoposide treatment resulted in induction of the wtp53 pathway in control cells as indicated by increased wtp53 and p21 protein expression and PARP cleavage. As expected, induction of wtp53 and p21 upon Etoposide treatment was suppressed in wtp53-silenced cells. In line with the flow cytometry results (Figure 23B), wtp53 induction was attenuated in TRRAP-silenced cells for two independent shRNAs. For one of the shRNAs, p21 was less induced compared to control cells. More importantly, both TRRAP shRNAs resulted in a strong suppression of PARP cleavage, indicating that wtp53's function to induce apoptosis was markedly reduced.

In summary, this suggests that TRRAP regulates the stability and activity of wtp53 upon exposure to genotoxic stress.

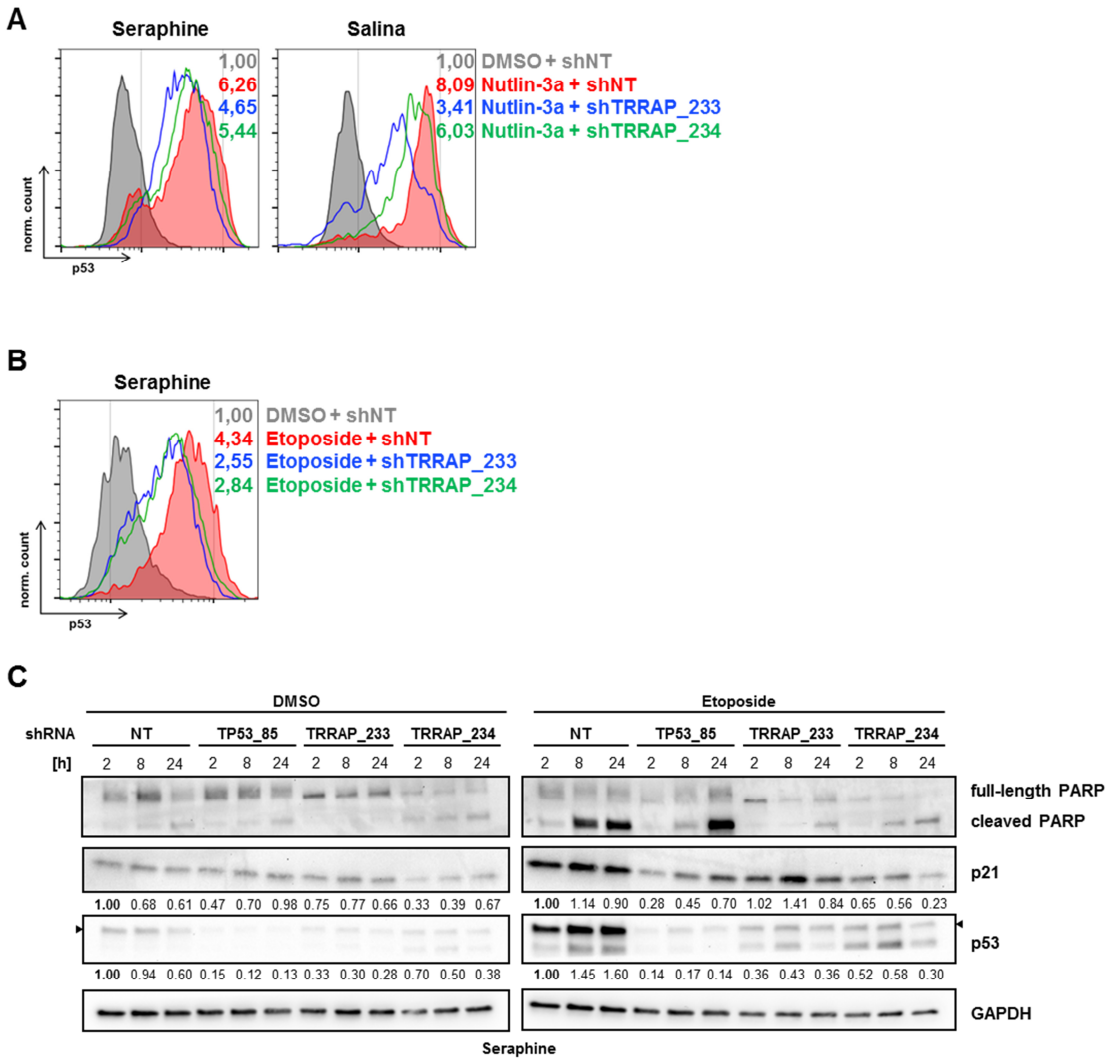

Figure 23: TRRAP silencing attenuates stabilization and activity of wild-type p53 upon genotoxic stress.
(**A**) Seraphine and Salina wtp53 BL cells were transduced with shRNAs against TRRAP or a non-targeting control (NT). 4 d after transduction, cells were treated with DMSO (0.1%) or the MDM2 inhibitor Nutlin-3a (10 µM) for 24 h before they were subjected to p53 flow cytometry. Values denote p53 median fluorescence intensities (MFI) normalized to DMSO-treated cells transduced with the NT. (**B**) Seraphine wtp53 cells were transduced with shRNAs against TRRAP or a non-targeting control (NT). 5 d after transduction, cells were treated with DMSO (0.1%) or Etoposide (25 µM) for 5 h before they were subjected to p53 flow cytometry. Values denote p53 median fluorescence intensities (MFI) normalized to DMSO-treated cells transduced with the NT. (**C**) Protein level of p53, p21, and PARP in Seraphine wtp53 cells transduced with shRNAs against TRRAP, p53, or a non-targeting control (NT). Cells were selected with puromycin for 72 h. 6 d after transduction, cells were treated with DMSO (0.1%) or Etoposide (25 µM) before they were harvested at the indicated time points. Expression was determined by Western Blot and normalized to GAPDH and to cells transduced with the NT (2 h sample). ◄, specific band.

3.11 Histone deacetylase inhibition decreases mutant p53 levels and phenocopies TRRAP silencing

To identify small molecule inhibitors able to modulate mutp53 levels similarly to TRRAP silencing, p53 levels were quantified in mutp53 lymphoma cell lines after exposure to a panel of inhibitors targeting various proteins/cellular pathways (Figure 24A): MDM2 (Nutlin-3a), Hsp90 (17-AAG), histone deacetylases (Vorinostat), autophagy (Chloroquine), and the proteasome (MG-132). The pan-histone deacetylase inhibitor (HDACi) Vorinostat was the only inhibitor resulting in strong and consistent depletion of mutp53 levels across all cell lines (Figure 24B).

To address whether Vorinostat would also cause specific mutp53 degradation via the MDM2-proteasome axis (Figure 20), cells were treated with either Vorinostat alone or in combination with Nutlin-3a and p53 protein and mRNA expression was quantified (Figure 24C,D). The Vorinostat phenotype was salvaged to nearly full extent by co-treatment with Nutlin-3a. Notably, Vorinostat caused strong downregulation of *TP53* and *MDM2* mRNA, which was not rescued by combination treatment with Nutlin-3a, while no change in *TRRAP* mRNA expression was observed. These findings indicate that Vorinostat regulates mutp53 expression on both the transcriptional level and the translational or post-translational level.

Since Vorinostat is a broad range HDAC inhibitor[248], it was aimed to identify HDAC subgroups crucial for regulating mutp53 accumulation. To this end, a panel of subgroup-specific HDAC inhibitors was tested for their effect on mutp53 levels by flow cytometry (Figure 24E). Inhibition of HDAC6 with Tubacin and Tubastatin A[249] and HDAC8 with PCI-34051[250] resulted in only mild reduction of mutp53 accumulation (53-91% of the basal level), suggesting that these HDACs do not contribute to mutp53 stabilization in a major way. In contrast, treatment with the HDAC1/2/3-specific inhibitors Entinostat and Mocetinostat[248,251] caused strong depletion of mutp53 (12-42% of the basal level), indicating that these HDACs are main drivers of mutp53 stabilization.

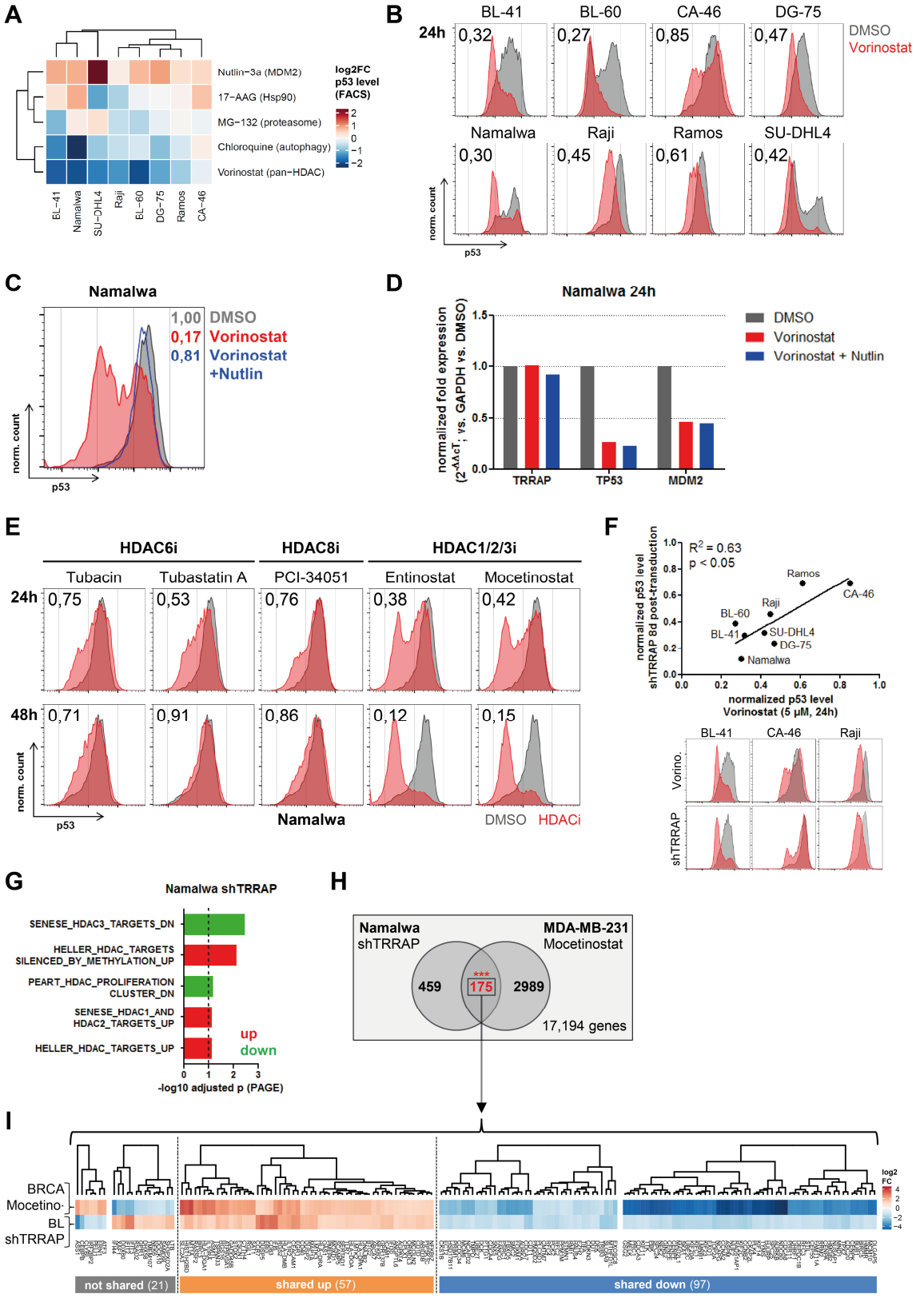

Figure 24: Histone deacetylase inhibition decreases mutant p53 levels and phenocopies TRRAP silencing.

(**A**) Impact of different small molecule inhibitors on mutp53 levels. Cells were treated with 0.1% DMSO or the indicated inhibitors. 24 h after treatment, cells were subjected to p53 flow cytometry. Values denote log2 fold changes (FC) of p53 median fluorescence intensities (MFI) normalized to DMSO-treated cells. Nutlin-3a (10 µM), MDM2 inhibitor; 17-AAG (5 µM), Hsp90 inhibitor; Vorinostat (5 µM), histone deacetylase inhibitor; Chloroquine (10 µM), autophagy inhibitor; MG-132 (5 µM), proteasome inhibitor. Experiment performed

jointly with Sophie Rabe. (**B**) p53 flow cytometry of mutp53 lymphoma cell lines after treatment with 0.1% DMSO (grey) or 5 µM of the histone deacetylase inhibitor Vorinostat (red) for 24 h. Values denote the ratio of the p53 median fluorescence intensity (MFI) between treated and control cells. Experiment performed jointly with Sophie Rabe. (**C**) Rescue of the Vorinostat-mediated mutp53 degradation by combination treatment with the MDM2 inhibitor Nutlin-3a. Namalwa cells were treated with DMSO (0.1%), Vorinostat (5 µM), or a combination of Vorinostat and Nutlin-3a (10 µM) for 24 h before they were subjected to p53 flow cytometry. Values denote p53 median fluorescence intensities (MFI) normalized to DMSO-treated cells. (**D**) mRNA level of *TRRAP, TP53,* and *MDM2* in Namalwa cells treated with DMSO (0.1%), Vorinostat (5 µM), or a combination of Vorinostat and Nutlin-3a (10 µM). Cells were harvested 24 h post-treatment. Expression values were determined by qRT-PCR and normalized to GAPDH and to DMSO-treated cells. (**E**) p53 flow cytometry of Namalwa cells after treatment with 0.1% DMSO (grey) or different histone deacetylase inhibitors (HDACi, red) for 24 h and 48 h. The targets of the different inhibitors are indicated. Values denote the ratio of the p53 median fluorescence intensity (MFI) between treated and control cells. Concentrations used: Tubacin, 7.5 µM; Tubastatin A, 7.5 µM; PCI34051, 10 µM; Entinostat, 500 nM; Mocetinostat, 500 nM. (**F**) Correlation of the impact of TRRAP silencing (8 d post-transduction) and Vorinostat treatment (5 µM, 24 h) on mutp53 levels. p53 protein levels were determined by flow cytometry. Values denote normalized p53 median fluorescence intensities (MFI) normalized to either untransduced cells (shTRRAP) or DMSO-treated cells (Vorinostat), respectively. The Pearson correlation coefficient (R^2) and the corresponding P value are indicated. (**G**) Gene set enrichment analysis of significantly differentially expressed genes (adj. P < 0.05 & |log2FC| > 1) upon TRRAP knock-down in mutp53 Namalwa cells. Upregulated gene sets are denoted in red, downregulated in green. Analysis was performed using Parametric Analysis of Gene Set Enrichment (PAGE)[213] with the MSigDB[214] gene set collection "c2cgp" filtered for the term "HDAC". Only significantly altered gene sets are shown (adj. P < 0.1). (**H**) Venn diagram showing the overlap of significantly differentially expressed genes after TRRAP knock-down in the mutp53 BL cell line Namalwa and after Mocetinostat treatment in the mutp53 breast cancer cell line MDA-MB-231. Mocetinostat data were downloaded from NCBI GEO, accession number GSE65495[218]. ***, P value = 2.6e-9 (hypergeometric test). (**I**) Heatmap of all 175 significantly differentially expressed genes shared between TRRAP knock-down and Mocetinostat treatment from panel H. log2 fold changes were subjected to hierarchical clustering. Numbers below the clusters indicate the number of genes. BRCA, breast cancer cell line (MDA-MB-231); BL, Burkitt's lymphoma cell line (Namalwa).

Upon comparison of the mutp53 phenotypes after pan-HDAC inhibition and after TRRAP silencing, a highly similar response pattern was observed (Pearson correlation R^2=0.63, p<0.05), i.e. cell lines responded either strongly (e.g. BL-41) or weakly (e.g. CA-46) to both perturbations (Figure 24F). To evaluate whether TRRAP silencing and HDAC inhibition altered transcription of similar genes, gene expression data after TRRAP knock-down in a mutp53 model (Figure 21A) was reanalyzed with a specific focus on gene sets known to be altered by HDAC inhibition (Figure 24G). In fact, five HDAC-related gene sets were found to be differentially expressed upon TRRAP silencing (2 down, 3 up). Interestingly, the most significant gene set consisted of genes downregulated upon HDAC3 knock-down (*SENESE_HDAC3_TARGETS_DN*, adj. p = 0.0035)[252], which is in support of the finding that HDAC1/2/3 inhibition using Entinostat or Mocetinostat had the strongest impact on mutp53 levels (Figure 24E). To investigate this further, published gene expression data of mutp53 breast cancer cells treated with Mocetinostat[218] were analyzed and compared to expression data after TRRAP silencing in mutp53 BL cells. To find similarities, the focus was set on the subset of 175 genes significantly differentially expressed in both data sets (Figure 24H). Strikingly, expression of the vast majority of genes (154/175, 88%) was changed in a similar fashion in both data sets (Figure 24I, 97/175 shared down, 57/175 shared up, 21/175 not shared) and the overlap was highly significant (p=6.6e-5, hypergeometric test). This indicates that TRRAP silencing and HDAC1/2/3 inhibition regulate mutp53

levels potentially by sharing a subset of target genes. Alternatively, there may be additional functional convergence for both perturbations beyond mutp53 regulation.

Finally, it was investigated whether TRRAP silencing or HDAC inhibition (using Vorinostat, Mocetinostat, or Entinostat) directly regulated acetylation of mutp53 in BL cells (Figure 25). Since p53 can potentially be acetylated on ten different lysine residues[50,52] (Figure 4), mutp53 was immunoprecipitated and acetylation was quantified by Western Blot using a pan-anti-acetylated lysine antibody. In basal conditions, mutp53 acetylation was not detectable. Strikingly, mutp53 acetylation remained undetectable upon HDAC inhibition and TRRAP silencing. Merely treatment of cells with high doses of the pan-HDAC inhibitors sodium butyrate and nicotinamide resulted in a detectable mutp53 acetylation. This indicates that TRRAP and HDACs are unlikely to regulate mutp53 stabilization via direct acetylation.

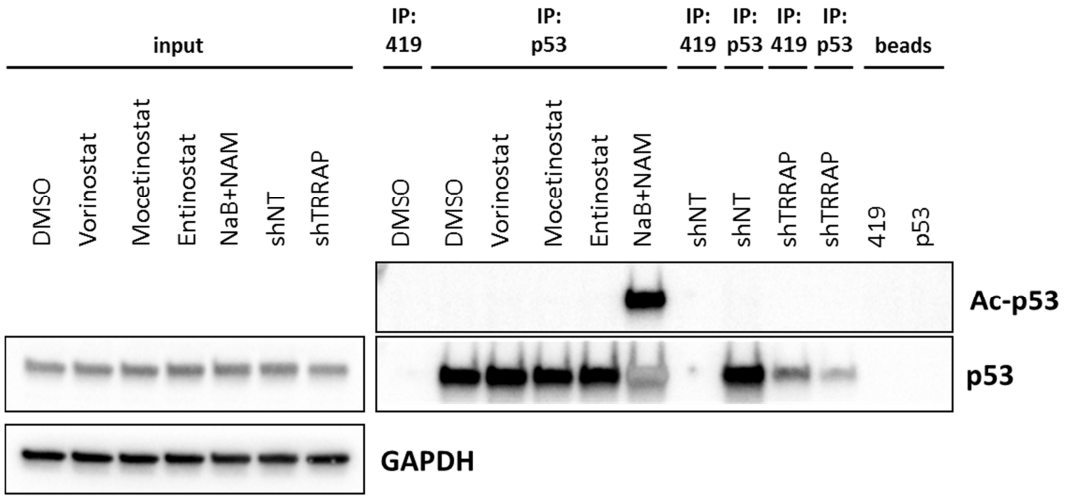

Figure 25: Impact of HDAC inhibition and TRRAP silencing on mutant p53 acetylation.
Namalwa cells were treated with DMSO (0.05%) or different HDAC inhibitors before they were subjected to p53 or control (419) immunoprecipitation (IP). Silencing experiments were performed using Namalwa cells with IPTG-inducible shRNAs against TRRAP or a non-targeting control (NT). Cells were harvested 5 h after drug exposure or 48 h after shRNA induction. Protein expression was determined by Western Blot. Acetylation (Ac) was detected by using an anti-acetylated lysine antibody. Concentrations used: Vorinostat, 1 µM; Entinostat, 500 nM; Mocetinostat, 500 nM; Sodium butyrate (NaB), 5 mM; Nicotinamide (NAM), 10 mM. 419, anti-SV40 T-antigen mouse (negative control for IP p53); GAPDH, loading control.

In summary, these results suggest that histone-modifying complexes, including TRRAP-containing HAT complexes and HDAC1/2/3, participate in regulation of mutp53 levels.

4 Discussion

4.1 p53 mutations and levels in Burkitt's lymphoma

In the beginning of this study, the frequency of p53 mutation was investigated in a panel of 67 BL patients, which identified mutations in 43% of cases. Most previous BL studies reported a slightly lower frequency of p53 mutations (mean: 34.7%, Table 1, p. 21), but frequencies were highly variable between studies (16.7-63.0%). In general, BL is among the B-NHLs with the highest frequency of p53 mutation[170], while mutations are for example rare in FL (8%)[170] and DLBCL (ABC subtype: 3.5%, GCB subtype: 11.5%)[163]. The high frequency of p53 mutation in BL may be explained by the fact that BL is a MYC-driven lymphoma[157]. Since MYC overexpression results in p53-dependent apoptosis induction[165], p53 mutation and thus inactivation could be a way to circumvent this. In BL patients retaining wtp53, alternative mechanisms of p53 inactivation include overexpression of the negative regulators MDM2 and MDM4[171,172]. The pattern of p53 mutations that was found in this study, i.e. a high frequency of missense mutations that clustered in the DNA-binding domain, has been reported previously in BL[163]. In fact, this pattern is typical for p53 in cancer in general and is assumed to be a proof for the oncogenic GOF of mutp53[253]. Although Bhatia *et al.*[166] reported differences in the pattern of p53 mutations between BL and solid tumors (i.e. most mutations in codons 213-248, codon 273 mutations very rare), this study and a meta-analysis of more recent studies[254] could not confirm this.

This study found a massive accumulation of mutp53 protein in BL patients and cell lines, which is a hallmark of mutp53 in most cancers[73-75] but has not been specifically reported for BL so far. While a significant correlation between presence of p53 mutation and accumulation was observed here in B-NHL and BL patients, contradictory results are reported in the literature[171,255-258]. In this study, evidence was found for a translational or post-translational mechanism of mutp53 stabilization in BL since p53 protein expression was not correlated with *TP53* mRNA expression. This is in support of the ubiquitin-proteasome pathway being the major node of p53 regulation[31]. In contrast, Balint and Reisman[259] reported elevated levels of *TP53* mRNA in a panel of mutp53 BL cell lines (BL-41, DG-75, Raji, Namalwa) caused by an increased rate of transcription. This conflict may be explained by the fact that the investigators used immortalized B lymphoblastoid cell lines with unknown p53 status as a reference, while this study specifically compared mutp53 to wtp53 BL cells.

The use of flow cytometry allowed identification of heterogeneous p53 accumulation in a subset of mutp53 BL cell lines in spite of homogeneous p53 mutation. Similar observations have already been made with p53 immunohistochemistry in B-NHL patients[256] and various cancer cell lines, even after generation of single cell clones[77]. The extent of mutp53 stabilization was found to neither correlate with protein conformation nor with mutation severity[77]. It has been suggested that the heterogeneity is a result of variable stabilization of mutp53 in response to local stress factors provided by the cellular tumor environment[77,260]. In line with this, it has been shown that mutp53 can be stabilized by stress signals such as irradiation[261]. However, this was unlikely to occur under *in vitro* conditions that were used in this study. Instead, it was hypothesized that part of mutp53 was actively degraded by MDM2. In support of this, all tested mutp53 BL cell lines retained basal MDM2 expression and further stabilized mutp53 upon MDM2 inhibition by Nutlin-3a treatment, which both has been also demonstrated in several cancer cell lines[77,82,83]. Importantly, this strongly argues against a usage of Nutlin-3a (or wtp53-stabilizing therapy in general) in patients with tumors harboring p53 mutations since this may actually promote tumorigenesis[262].

4.2 shRNA screen for regulators of mutant p53 protein accumulation

To get an unbiased view on the regulation of mutp53 accumulation, an shRNA screen was performed which used flow cytometry to readout p53 levels. This allowed direct quantification of endogenous p53 levels and thereby avoided the usage of an exogenous reporter system (e.g. p53-GFP), which not only is often challenging to establish but also merely provides an indirect quantification of the protein of interest. The approach presented here is instead highly flexible and may be adapted for investigating the regulation of any protein for which quantification by flow cytometry is possible[228]. In support of this, screens with a similar experimental approach have been successfully used in the past to, for example, identify regulators of cell surface AC133 expression[263], CD20 expression[228], and tumor necrosis factor (TNF) in response to lipopolysaccharide (LPS)[264]. The study presented here is the first one investigating the regulation of mutp53 accumulation in lymphoma on a comprehensive level.

With the shRNA library used in this study, the ~5,000 best characterized coding genes were probed for their potential to regulate mutp53 levels. The fact that the human genome comprises ~20,000 genes[265] calls therefore for additional screenings in the

future. For example, it is believed that non-coding RNAs such as microRNAs play a major role in directly and indirectly regulating mutp53 levels[266].

The high performance of the screening was not only supported by the high reproducibility of technical replicates but also by the drop-out of core essential and BL-specific viability genes (CDK6). This indicates that the presented approach may additionally be used for the identification of cancer-specific vulnerabilities. Since the culturing time of cells after library transduction before harvesting was rather short (8 days), the degree of drop-out and thus the detection power are expected to increase with prolonged culturing time (typically >14 days).

For identification of candidate genes potentially regulating mutp53 levels, the weighted z-score method was employed to reduce the chance of false positive hits. Further confidence in hit selection was gained by separate analysis of the p53-low and p53-high population and by making use of their “opposing behavior”. Strong support for the analysis method was provided by the shRNAs targeting *TP53*, which were strongly enriched in the p53-low population and highly depleted in the p53-high population. Attention was focused on the p53-low population, i.e. proteins driving aberrant mutp53 stabilization, due to their potential use as therapeutic targets[103]. Nevertheless, the identification and characterization of proteins with the potential to keep mutp53 levels low, i.e. hits from the p53-high population, will be crucial to gain a comprehensive picture of mutp53 regulation.

The molecular chaperone Hsp90 has been reported to stabilize mutp53 in breast, prostate, and colorectal cancer[83,103]. However, Hsp90 was not enriched in the p53-low population in the shRNA screen performed in BL. In line with this, Hsp90 inhibition using 17-AAG did not result in mutp53 destabilization in the tested B-NHL cell lines and Hsp90 was also not detected in the basal mutp53 interactome in BL using mass spectrometry. This suggests that Hsp90 is unlikely to contribute to mutp53 accumulation in BL.

4.3 Identification of TRRAP as a regulator of mutant p53 levels

Using stringent hit selection criteria, the focus was set on characterization of the top hit TRRAP. TRRAP silencing had no impact on *TP53* mRNA expression, thus hinting towards a translational or post-translational regulation of p53 levels, which is in line with the finding that mutp53 is stabilized on the protein level in BL. To confirm TRRAP as a regulator of mutp53 accumulation, a set of comprehensive validation experiments was

performed. While TRRAP silencing consistently downregulated mutp53 levels in multiple cancer cell lines (BL, DLBCL, CRC) across p53 mutations, TRRAP overexpression increased mutp53 levels. In addition, mutp53 depletion upon TRRAP silencing could successfully be reversed by TRRAP overexpression, thus providing important evidence for the shRNA on-target effect[188]. The RNAi phenotype was further validated with an independent technique[184,188] via CRISPR/Cas9-mediated TRRAP knock-out, which phenocopied shRNA-mediated TRRAP silencing.

The finding that TRRAP impacts mutp53 accumulation independent of p53 mutation residue and cancer entity suggests that TRRAP is key positive regulator of p53 levels in physiological conditions. This is supported by the finding that TRRAP was found to also positively regulate wtp53 levels and function. Thus, this indicates that stabilization of mutp53 in BL is not achieved by proteins that specifically gain a p53-stabilizing function in tumors but rather by hijacking the physiological machinery of wtp53 regulation. A striking example supporting this idea and acting in a similar fashion as TRRAP is Hsp90, which functions as a chaperone to stabilize wtp53 in response to stress in non-transformed human fibroblasts[247] but also contributes to mutp53 stabilization in tumors[83,103].

Despite the fact that TRRAP knock-down caused mutp53 depletion across different p53 mutations, the extent of depletion was variable. Since this study and others found that MDM2 at least in part retains its ability to degrade mutp53[35,84], it was hypothesized that the degree of mutp53 depletion upon TRRAP silencing was most likely a function of residual MDM2 activity. Accordingly, cell lines which strongly stabilized mutp53 upon MDM2 inhibition with Nutlin-3a (= high MDM2 activity; e.g. BL-41, Namalwa) also strongly downregulated mutp53 upon TRRAP knock-down and *vice versa* (e.g. CA-46, Raji).

Both TRRAP knock-down and knock-out were found to impair cell growth independent of p53 mutation status. This is in line with a study by Herceg *et al.*[267] that characterized TRRAP knock-out mice and found that TRRAP is mandatory for early embryonic development and cell proliferation. In addition, TRRAP was also shown to be essential for proper B-cell development *in vivo*[268] and was found to be a “common essential gene” across entities on the basis of previous RNAi and CRISPR/Cas9 screens[233,269]. Therefore, this suggests that therapeutic targeting of TRRAP may be challenging.

4.4 Physical interaction of mutant p53 and TRRAP

To investigate whether TRRAP mediated its stabilizing effect towards mutp53 via physical interaction, co-IP was performed. This experiment showed binding of mutp53 to TRRAP in an exogenous, p53-deficient model in which a FLAG-tagged version of TRRAP and mutp53 were artificially introduced. Furthermore, evidence was found for a preferred binding of TRRAP to mutp53 over wtp53. However, no evidence was found for a binding of mutp53 and TRRAP in an endogenous, mutp53 BL model. This is in contrast to Ard *et al.*[238] who showed binding of TRRAP to wtp53 in basal conditions in 293 (human embryonic kidney, HEK) cells. There are several reasons which may explain the difference between the results from the exogenous and endogenous model system. First, the observed interaction may have been an artifact caused by introduction of mutp53 and TRRAP in a p53-null model. For example, overexpression may result in protein expression in a wrong cellular compartment or protein aggregation, especially in the case of massive overexpression[270]. Second, different mutp53 proteins were studied in both systems, which may vary in their ability to bind to mutp53. While the endogenous model system harbored p53 with a R248Q mutation, experiments in the exogenous system were performed with a R175H mutation. However, both mutp53 proteins are conformational mutants prone to aggregation[129] and, more importantly, TRRAP's capability to regulate mutp53 level was found to be independent of the kind of p53 mutation. Third, the binding of TRRAP to mutp53 may be of catalytic nature and therefore only transient, which may be difficult to reliably detect via classical IP without crosslinking[271]. Fourth, co-IP may not be sensitive enough in an endogenous setting, which may be caused by for example lower IP efficiency of endogenous proteins as compared to overexpressed exogenous proteins.

In conclusion, it is suggested that mutp53 and TRRAP do not interact in BL, thereby ruling out the possibility that TRRAP chaperones mutp53.

4.5 TRRAP silencing exports mutant p53 from the nucleus to the cytosol

Total proteome profiling by mass spectrometry after TRRAP silencing showed that expression of only 44 proteins was significantly altered, including mutp53. This suggests that TRRAP-mediated p53 degradation is highly specific and unlikely to be a secondary effect, for example caused by cellular stress. Against the background that TRRAP is a

constituent of many HAT complexes[237], this indicates that TRRAP may not regulate histone acetylation on a global scale but rather sequence-specifically, i.e. on a small scale for a very limited set of specific target genes. Accordingly, Wurdak *et al.*[272] showed specific downregulation of H3K9 promoter acetylation for the TRRAP target gene *CCNA2* after TRRAP knock-down, while global H3K9 acetylation levels were unchanged. Jin *et al.*[273] reported that loss of KAT2A and KAT2B, the catalytic subunits of two TRRAP-containing HAT complexes, caused differential expression of only 6% of active genes in fibroblasts, providing further support for a gene-specific instead of a global function. Among the 44 proteins, no candidates or cellular pathways became apparent that could have been linked to regulation of mutp53 levels with the exception of the interferon signaling, which will be discussed later (see 4.6, p. 92).

Mass spectrometry of p53 immunoprecipitates in mutp53 BL cells showed that TRRAP silencing induced major changes in the mutp53 interactome. Proteins lost upon TRRAP knock-down, i.e. proteins binding in basal conditions to mutp53, mainly participated in mRNA splicing. Against the background of mutp53 GOF, this suggests that mutp53 may play a role in mRNA processing. Accordingly, it has been reported that p53 can physically interact with and regulate the protein stability of SF3B2 (SAP145)[274], one of the core components of the spliceosome. More importantly, two studies showed that silencing of several members of the mRNA splicing machinery (including SF3B1 and HNRNPL) can activate wtp53 via decreased MDM4 expression and increased MDM2 degradation[275] or via alternative splicing of *MDM4*[276]. Based on this, it is tempting to hypothesize that mutp53 maintains its own stabilization by exploiting the splicing machinery to regulate MDM2 or MDM4 expression. However, this study found no evidence for differential MDM2 expression between mutp53 and wtp53 BL cell lines. Alternatively, mutp53 may alter mRNA splicing to improve conditions for tumorigenesis, tumor growth, and survival. In fact, alternative splicing is exploited by many tumors for their own benefit, for example by specifically altering splicing of oncogenes and tumor suppressors[277]. Therefore, the findings of this study warrant testing the impact of mutp53 on mRNA splicing in the future, which may help in delineating mutp53 GOF in lymphoma.

TRRAP silencing caused translocation of mutp53 from the nucleus to the cytosol, indicating that TRRAP usually retains mutp53 in the nucleus. Along with this, mutp53 was then found to physically interact with the eukaryotic translation initiation factor 3 (eIF3), a multiprotein complex important for promoting translation initiation[278]. Since this interaction was not found in basal conditions, it is unlikely that mutp53 has an impact on protein translation. However, numerous studies have shown that eIF3 interacts with the

26S proteasome[279-281]. Given that mutp53 is degraded via the proteasome upon TRRAP knock-down, mutp53 may first bind to eIF3 before being funneled into the proteasome. However, mass spectrometry did not identify binding of proteasomal proteins to mutp53 upon TRRAP knock-down.

Mass spectrometry showed that nuclear export of mutp53 after TRRAP silencing was a prerequisite for its destabilization. Since p53 can in general be degraded in both the cytosol[31,44,45] and the nucleus[46,47], this indicates that mutp53 is protected from nuclear degradation but sensitive to cytosolic destruction. Importantly, this study and others[113] found that nuclear export inhibition results in augmented mutp53 stabilization, suggesting that part of mutp53 is constantly exported and degraded in the cytosol. From a clinical point of view, this finding may argue against a usage of nuclear export inhibitors (CRM1 inhibitors) in patients with mutp53. Accordingly, acute myeloid leukemia, hepatocellular carcinoma, and mantle cell lymphoma cells harboring p53 mutation are less sensitive towards CRM1 inhibition than their wtp53 counterparts[282-284].

mutp53 has been reported to localize to the cytosol upon ubiquitination[84,285]. In line with this, the usage of small-molecule inhibitors and knock-out models showed that TRRAP-driven mutp53 degradation was strictly dependent on the ubiquitin ligase MDM2 and the proteasome. This indicates that TRRAP silencing unleashes the classical wtp53 degradation machinery on mutp53, which is again in support of the idea that MDM2 in general retains the capacity to degrade mutp53[84]. However, the specific role of MDM2 in mutp53 degradation is still under debate and not limited to ubiquitination[37] but may also include facilitating access to the proteasome[48] and nuclear export[31,42,286]. Notably, several other ubiquitin ligases are assumed to play a role in mutp53 ubiquitination[84]. For example, mutp53 degradation upon Hsp90 inhibition was shown to additionally depend on CHIP[83], suggesting distinct mechanisms of TRRAP and Hsp90 for mutp53 stabilization.

Ard *et al.*[238] reported that TRRAP is crucial for maintaining p53-dependent MDM2 transcription in wtp53 cells. In addition, massive MDM2 overexpression has been shown to degrade mutp53[35]. Given the strict MDM2 dependence of TRRAP-mediated mutp53 regulation, MDM2 levels were investigated after TRRAP silencing, which showed no major alterations in mutp53 BL cells. This indicates that TRRAP does not regulate MDM2 expression in a mutp53 context, which may be explained by disruption of the p53-MDM2 feedback loop[65,81]. Therefore, it is hypothesized that TRRAP silencing exposes mutp53 to MDM2 without altering MDM2 expression.

4.6 TRRAP silencing induces interferon signaling and suppresses cell cycle-related genes

To investigate the role of TRRAP in regulation of global transcription, gene expression profiling of mutp53, wtp53, and $p53^{KO}$ BL cell lines was performed after TRRAP knock-down. In each cell line, TRRAP silencing altered the expression of only a small number of genes, which again provides evidence for the idea that TRRAP specifically regulates expression of a small subset of target genes[272]. In all cell lines, TRRAP silencing caused downregulation of genes related to cell cycle and chromosome segregation, which is in line with previous studies which showed that TRRAP knock-down in fact causes chromosomal missegregation and defects in the mitotic checkpoint[267,272,287].

Both gene expression profiling and mass spectrometric analysis indicated that TRRAP silencing resulted in a strong type I interferon (IFN) response across cell lines. IFNs are cytokines which trigger a potent antiviral response in cells[242]. Since IFN responses are typically only induced by double-stranded RNA present after viral infections[288], the finding that TRRAP knock-down caused activation of IFN signaling is at first surprising. TRRAP is a common component of many HAT complexes, including the STAGA and the PCAF complex[237]. Importantly, knock-out of the catalytic subunits of these two HAT complexes (*KAT2A*, *KAT2B*) has been shown to induce IFN-β signaling without the need of viral infection[273]. In fact, both proteins were found to be negative regulators of IFN-β production since they inhibit activity of TBK1, the key kinase needed for activation of the IFN pathway[273]. Against the background that TRRAP is assumed to play a "nonredundant role"[237] in HAT complexes, TRRAP ablation may thus trigger IFN signaling via disruption of the IFN-inhibitory complexes STAGA and PCAF. Worthy of note is that the observed IFN response after TRRAP knock-down may also be an unspecific side-effect caused by lentiviral transduction, which has been reported to occasionally trigger IFN activation[289]. However, since the transcriptome data after TRRAP knock-down was normalized to cells transduced with a non-targeting shRNA, lentiviral shRNA expression is unlikely to be the sole cause of the IFN response. Importantly, IFN signaling did not contribute to mutp53 downregulation upon TRRAP silencing in BL, which is in contrast to a study performed by Madar *et al.*[203].

4.7 Identification of TRRAP's domain crucial for mutant p53 stabilization and cell survival

For a systematic assessment of the role of TRRAP's different protein domains in promoting both cell survival and mutp53 accumulation, the recently described "CRISPR scanning" technique was employed[223]. The traditional way of testing protein domains for a specific function includes the characterization of truncation/deletion mutants specifically lacking the domain of interest. The generation of these mutants is typically done via site-directed mutagenesis[290], which is not only technically challenging but also depends on availability or generation of an overexpression construct. Moreover, characterization of these mutants is done by artificially introducing them into cells, which often does not reflect physiological conditions[270]. This is especially the case for massive overexpression, which can for example cause protein aggregation and result in a false positive loss-of-function[270]. CRISPR scanning overcomes all of these limitations since it acts directly on the endogenously expressed protein and only depends on the proper design of sgRNAs targeting the domain of interest. It has been successfully used in the past to identify protein domains essential for cell survival in for example chromatin regulatory proteins in MLL-AF9 leukemia[223] or in MLL1 in NPM1-mutant leukemia[291]. This study describes the first usage of CRISPR scanning for studying a phenotype beyond cell survival, namely mutp53 levels.

TRRAP belongs to the phosphatidylinositol 3-kinase-related kinase (PIKK) family, which in humans consists of six members (Figure 26A): ATM, ATR, DNA-PKcs, SMG1, mTOR, and TRRAP[235]. PIKKs play a role in diverse biological processes[235], including DNA repair[292], cell growth[293], and RNA surveillance[294]. They are very large proteins with molecular weights in the range of ~280-470 kDa and the structural architecture is shared between all family members[236]. Typically up to 90% of the protein length of PIKKs is made up of a very long stretch of HEAT repeats[235]. This is followed by a short conserved C-terminus, which contains three domains (FAT, PI3K, and FATC)[235]. Some PIKK members, including TRRAP, contain an additional small domain between the FAT and PI3K domain termed FRB[236]. Electron microscopy and X-ray crystallography experiments identified the three-dimensional organization of PIKKs to be divided into a compact "head" formed by the C-terminus and into "arms" formed by the HEAT repeats that assemble as helical scaffolds (Figure 26B)[236]. The "arms" are suggested to play a crucial role in regulating PIKK function as they promote interaction with other proteins and DNA[236].

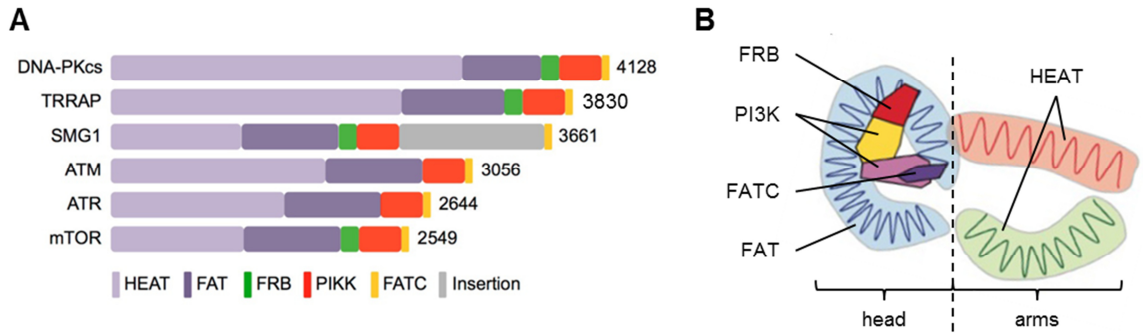

Figure 26: Phosphatidylinositol 3-kinase-related kinase (PIKK) family.
(**A**) Schematic representation of the domain organization and total number of amino acids of all human PIKK family proteins. Domain annotation according to Figure 22A. Adapted by permission from AIMS Press: *AIMS Biophysics*, Rivera-Calzada *et al.*[236], copyright 2015. (**B**) Schematic model of the three-dimensional structure of PIKK family proteins. The overall structure can be divided into "head" and "arms". Domain annotation according to Figure 22A. Adapted by permission from AIMS Press: *AIMS Biophysics*, Rivera-Calzada *et al.*[236], copyright 2015.

Due to the fact that high-resolution structural information is rare[236], the molecular function of the different PIKK domains is especially in the case of TRRAP not well understood and based on only a very limited number of studies. Knutson and Hahn[246] performed a large scale deletion mutant study in yeast and identified regions in Tra1 (TRRAP homolog in yeast) essential for cell viability, which were all defective for interacting with HAT complexes. Ard *et al.*[238] identified a small region (residues 1992-2370) capable of binding to wtp53. While all PIKKs possess kinase activity, TRRAP lacks the conserved kinase motifs responsible for ATP binding and is therefore kinase-dead[234].

CRISPR scanning confirmed TRRAP's crucial function for cell survival[267] since cells transduced with sgRNAs targeting TRRAP were depleted over time. None of the annotated domains of TRRAP protruded in terms of toxicity upon targeting, indicating that they are equally important for maintaining TRRAP's essential function. The lack of severe toxicity upon targeting of the wtp53-binding region may be explained by the fact that this study did not find evidence for a physical interaction of mutp53 and TRRAP in BL. Interestingly, a 109 aa stretch mapping to HEAT repeats 21 and 22 in the N-terminus of TRRAP[246] could be identified, whose targeting was highly fatal. Accordingly, deletion of this region was also identified to be detrimental in yeast (HEAT repeats 20 and 21)[246]. Single HEAT repeats (or motifs) are 30-40 amino acids in length and consist of two α-helices which are connected by a linker region[295]. It is challenging to speculate on the function of the identified region due to the fact that HEAT repeat domains can play a plethora of different roles[295]. Importantly, also single repeats within long HEAT repeat regions can be essential for proper functioning of the whole protein[296]. Based on observations made in other PIKKs[236], it is suggested that HEAT repeats 21 and 22 in

TRRAP either facilitate protein-protein interaction or are modulated by post-translational modification.

Using flow cytometry for the phenotypic readout of the CRISPR scanning allowed a simultaneous monitoring of cell and mutp53 depletion upon TRRAP targeting. Both phenotypes were highly correlative, indicating that TRRAP's survival-promoting and mutp53-stabilizing function are tightly linked and mediated by similar domains. In other words, no evidence could be found for a specific mutp53-regulatory domain in TRRAP. This suggests that therapeutic targeting of TRRAP to specifically downregulate mutp53 levels may be challenging and compromised by general toxicity.

4.8 TRRAP silencing attenuates stabilization and activity of wild-type p53 upon genotoxic stress

In a TRRAP-deficient context, wtp53 accumulation after exposure to genotoxic stress was impaired which may be caused by three distinct mechanisms. First, TRRAP may directly bind to wtp53 and assist in its stabilization for example by recruiting chaperones. This is partially supported by a study by Ard *et al.*[238] that showed binding of TRRAP to wtp53 in basal conditions in 293 (human embryonic kidney, HEK) cells. However, this study was unable to find evidence for a direct interaction of TRRAP and (mut)p53 in BL. Second, this may be explained by the increased MDM2 protein expression that was observed upon TRRAP knock-down in basal conditions in wtp53 BL cells. This is in contrast to the finding that TRRAP is essential for maintaining MDM2 transcription[238]. Again, this controversy may be explained by the usage of different experimental models (HEK vs. BL). Third, similar to mutp53, TRRAP may retain wtp53 in the nucleus in stressed conditions and may thereby protect it from cytosolic proteasomal degradation.

TRRAP deficiency also resulted in reduced wtp53 pathway activity upon DNA damage induction as indicated by reduced p21 induction. In support of this, Barlev *et al.*[53] showed that TRRAP is recruited to the p21 promoter upon irradiation. This suggests that TRRAP may be important for facilitating p21 expression, potentially by modification of histone acetylation. In fact, binding of wtp53 to many of its target gene promoters was shown to result in an increased histone H3 and H4 acetylation with differences in the acetylation patterns between different promoters[297,298]. This indicates that promoter acetylation is not only crucial for driving wtp53 target gene expression but also important for differential

target gene expression in response to different stress signals[297], i.e. expression of the correct genes in response to a certain stress.

The fact that TRRAP silencing protected wtp53 cells from apoptosis after exposure to Etoposide may be best explained by the impaired p53 protein accumulation. Multiple independent studies showed that a certain threshold of p53 protein level has to be reached in the cell in order to induce p53-dependent apoptosis[299-302]. Low p53 levels, however, can still be sufficient to induce cell cycle arrest.

Cell's TRRAP dependence for full activation of wtp53 has important consequences for potential therapeutic targeting of TRRAP. Irrespective of TRRAP's essential role for cell survival discussed previously, TRRAP inhibition is hence expected to not only destabilize mutp53 in tumor cells but to also impair wtp53 function in healthy cells. Although wtp53 knock-out mice and humans with wtp53 germline mutations (Li-Fraumeni syndrome) are viable and fertile, they suffer from a tremendously increased cancer risk[303-305]. Therefore, TRRAP inhibition in patients will either have to be targeted specifically to mutp53 cancer cells or will have to be administered only short-term, potentially with treatment breaks, in order for wtp53 cells to recover.

One may ask why TRRAP does not constantly stabilize wtp53, i.e. also in non-stressed conditions, since TRRAP appears to stabilize mutp53 in basal conditions. This can probably be best explained by the fact that tumors often experience chronic DNA damage and are hence under constant stress[65]. In line with this, mutp53 has been shown to be intrinsically instable and to require additional oncogenic events such as genotoxic stress to be stabilized[78-80]. Therefore, TRRAP is likely to exert its stabilizing effect on p53 only under stressed conditions, potentially by preventing the nuclear export of p53.

4.9 Histone deacetylase inhibition decreases mutant p53 levels and phenocopies TRRAP silencing

Small-scale drug screening identified that pan-HDAC inhibition using Vorinostat resulted in MDM2-dependent mutp53 downregulation in BL on both the RNA and protein level. Several studies have previously described a link between HDACs and the regulation of p53 expression. In line with this study, pan-HDAC inhibition in multiple mutp53 cancer cells was shown to deplete p53 protein in a MDM2-dependent manner[82,105,107]. While Blagosklonny *et al.*[105] found no impact on mutp53 RNA expression upon Vorinostat treatment, this could not be confirmed by more recent studies in which strong mutp53

mRNA depletion was observed upon HDAC inhibition[107,163]. The results presented here are in agreement with the latter studies and hint towards an HDAC-mediated p53 regulation on both the transcriptional and translational or post-translational level, probably by independent mechanisms. Interestingly, impaired wtp53 mRNA expression upon HDAC inhibition has been reported repeatedly[306-309], indicating that the transcriptional regulation of wtp53 and mutp53 may be similar.

To assess the contribution of individual HDACs to mutp53 regulation, HDAC inhibitors with a high specificity towards single HDACs were used. The HDAC6-specific inhibitors Tubacin and Tubastatin A resulted in only mild depletion of mutp53 in BL. Since HDAC6 was shown to stabilize mutp53 via positive regulation of Hsp90[82,83], this indicates again that Hsp90 does not contribute to mutp53 stabilization in BL. This is supported by the findings presented here that Hsp90 inhibition did not cause mutp53 degradation in B-NHL cell lines and that Hsp90 was not detected in the mutp53 interactome in BL. Similar to HDAC6 inhibition, also HDAC8 inhibition with PCI-34051 caused only mild depletion of mutp53 in BL. Due to the fact that previous studies showed that HDAC8 regulates mutp53 on the transcriptional level via HOXA5[163] and YY1[107], this provides further evidence that mutp53 is mainly regulated on the protein level in BL. Importantly, an almost complete depletion of mutp53 protein was observed in BL in this study upon inhibition of HDACs 1, 2, and 3 using Entinostat and Mocetinostat. This is in agreement with a recent study performed by Stojanovic *et al.*[106] which showed that HDAC1 and HDAC2 act in concert to positively regulate mutp53 on the transcriptional level in pancreatic cancer. Worthy of note is that both HDACs were also reported to play a crucial role in B-cell lymphomagenesis *in vivo*[310].

Surprisingly, HDAC inhibition and TRRAP silencing caused mutp53 protein depletion to a very comparable degree. In general, both proteins share their role in regulating protein acetylation. However, while HDAC inhibition should globally increase both histone and non-histone acetylation[104,311], silencing of the HAT complex member TRRAP is expected to cause reduced histone H3 and H4 target gene promoter acetylation[272,287,312]. TRRAP's role beyond histone acetylation, for example in acetylation of non-histones or a potential acetylation-independent function, has been suggested but not proven so far[237]. Interestingly, HDAC inhibition and TRRAP silencing appear to share more functions beyond mutp53 regulation since gene expression profiling showed that TRRAP knock-down altered expression of a subset of HDAC target genes. This suggests that HDAC and HAT inhibition impinge on expression (or regulation) of similar genes by unknown but potentially diverse mechanisms, which may in turn regulate mutp53 levels.

Strikingly, mutp53 acetylation was not detectable in basal conditions and also not upon HDAC inhibition or TRRAP knock-down. This suggests that mutp53 acetylation may not contribute to its stabilization in BL, which is in support of a study performed by Li *et al.*[83] in different cancer cell lines. In line with this, Ard *et al.*[238] found no evidence for TRRAP-mediated acetylation of wtp53. Given the MDM2 dependence of TRRAP- and HDAC-dependent mutp53 regulation, it is tempting to speculate that they alter MDM2 acetylation, which may in turn regulate its ability to promote p53 degradation. In fact, MDM2 has been shown to be acetylated by CBP but not PCAF (on residues K466/467) which blocks its ability to degrade p53[313]. In addition, Nihira *et al.*[314] showed recently that p300-mediated acetylation (on residues K182/185) stabilizes MDM2. In combination with the findings of this study, this warrants testing the impact of histone-modifying complexes on MDM2 acetylation and activity in the future.

Based on the GOF properties of mutp53[2,65], the finding that HDAC inhibition causes mutp53 depletion may provide a basis for therapeutic targeting of mutp53 in lymphoma and other cancers. In fact, a plethora of HDAC inhibitors is currently under clinical development since HDACs are known to contribute to tumorigenesis via aberrant acetylation of both histones and non-histones[104]. Notably, two studies found evidence for preferential toxicity of pan-HDAC inhibition in mutp53 cancer cells compared to wtp53 cells[82,105]. Importantly, and similar to TRRAP inhibition, HDAC inhibitors may inhibit wtp53 function[15], suggesting that long-term treatment of patients may have undesirable side effects.

4.10 Known links between p53 and TRRAP

This study identified TRRAP as a key regulator of mutp53 and wtp53 levels. In fact, there are several lines of evidence for a specific link between TRRAP and p53 regulation and function, which are briefly summarized below:

1. All the other five members of the PIKK family (Figure 26A), the protein family to which TRRAP belongs[235], are either direct regulators of p53 or are under the control of p53:
    a. *Ataxia telangiectasia mutated* (ATM) is a central regulator of the cellular response to DNA double-strand breaks[292,315]. It mediates not only the activating phosphorylation of p53 both directly[7] and indirectly (via CHK2)[316,317] but also the inactivating phosphorylation of MDM2[39].

   b. *Ataxia telangiectasia and Rad3-related protein* (ATR) is activated mainly in response to replication stress and phosphorylates CHK1[318], which mediates the appropriate cellular response for example by phosphorylating p53[317].
   c. *DNA-dependent protein kinase catalytic subunit* (DNA-PKcs) plays a crucial role in the non-homologous end joining (NHEJ) pathway of DNA repair[319]. It is required for p53 phosphorylation at S18 and p53-mediated apoptosis induction[320,321].
   d. *Suppressor with morphogenetic effect on genitalia 1* (SMG1) regulates the mRNA surveillance pathway but also upregulates p53 upon genotoxic stress by phosphorylation[322,323].
   e. *Mammalian target of rapamycin* (mTOR) is the key regulator of nutrient and growth factor signaling and its activation upregulates cell proliferation[324]. While wtp53 typically inhibits the mTOR pathway[325], mutp53 can stimulate mTOR signaling[326,327].
2. TRRAP has been repeatedly reported to take part in the p53 downstream effector machinery:
   a. TRRAP is essential for p53-dependent MDM2 expression[238].
   b. TRRAP is recruited to the p21 promoter upon irradiation[53].
   c. TRRAP is recruited to and necessary for the proper repair of DNA double-strand breaks, most likely because histone acetylation facilitates access of repair proteins to chromatin[237,328]. Notably, upstream signaling to ATM and ATR is not affected by TRRAP depletion[328].
3. Three of the four human HAT complexes of which TRRAP is a member of[329] have a reported role in regulating p53:
   a. The *p300/CBP-associated factor* (PCAF) complex controls p53 expression via its intrinsic ubiquitination activity towards MDM2[330]. Accordingly, overexpression of the PCAF complex member ADA3 stabilizes p53 protein[331].
   b. The TIP60 complex is required for p53-mediated expression of p21, binds to both p53 and MDM2, and interferes with MDM2-mediated p53 degradation, potentially by affecting its nuclear export[332]. In addition, TIP60 is stabilized upon irradiation and is also a substrate of MDM2[333].
   c. The STAGA complex physically interacts with p53 and is required for p53-dependent activation of p21, PUMA, and GADD45[334]. Notably, this study could not detect a physical interaction between (mut)p53 and TRRAP.
4. TRRAP and p53 levels show a strong positive correlation in breast cancer patient samples[335].

5 Conclusions & Perspectives

Tumors often accumulate high levels of mutp53, which contribute to mutp53 GOF properties and thereby to tumorigenesis. The mechanisms that control this excessive accumulation are not completely understood. By using subgenome-wide RNAi, this study identified a crucial role of the PIKK family member TRRAP in regulating both mutp53 and wtp53 levels, potentially by preventing the MDM2-dependent nuclear export and proteasomal degradation of p53.

Since TRRAP is a constituent of many HAT complexes, future studies will have to elucidate its specific function in these complexes. In line with this, it will be tempting to probe each complex (member) for its potential to regulate p53 levels. Against the background that tumors often become addicted to constitutively high levels of mutp53, therapeutic targeting of TRRAP in cancer may be appealing but challenging given that TRRAP is an essential protein. However, since inhibition of HDACs was found to phenocopy TRRAP silencing, HDAC inhibitors may be used as surrogates – especially because many HDAC inhibitors are currently under clinical development. Additional investigations are needed to test whether HDAC inhibition is suitable to preferentially target mutp53 over wtp53 cells. In general, the finding that inhibition of a HAT complex member resulted in a similar phenotype as inhibition of HDACs is striking and should be investigated more deeply in the future. For example, investigating the impact of TRRAP and HDAC inhibition on non-histone protein acetylation, especially MDM2, may yield novel insights into the functional mechanism underlying p53 regulation.

Despite the fact that this study focused on the characterization of TRRAP, the performed RNAi screen identified a number of hits with a potential role in regulating mutp53 levels, which may be investigated in the future. Given the advance of the CRISPR/Cas9 technology and its potential superiority compared to RNAi (e.g. less off-target effects), a CRISPR/Cas9 screen may shed additional light on the regulation of mutp53 accumulation.

In summary, this study provides a link between histone-modifying complexes and regulation of p53 levels, which may be exploitable in cancer therapy.

6 Appendix

6.1 CRISPR scanning – TRRAP sgRNA sequences

The order of the sgRNA sequences in Table 11 below is according to the x-axis in Figure 22A ascending from left to right, i.e. from TRRAP's N-terminus to C-terminus.

Table 11: sgRNA sequences used for CRISPR scanning.

#	Name	Sequence [5'→3']	#	Name	Sequence [5'→3']
1	sgTRRAP _98878173	AGTGGTCTGGTCAACCACCG	**29**	sgTRRAP _98884240	CCTGGGCAGAATCCACGGAC
2	sgTRRAP _98878703	ATCATACCAACCATTTCTGG	**30**	sgTRRAP _98884251	CCTGTCCGTGGATTCTGCCC
3	sgTRRAP _98879290	GCTGGCGGACATGGTGCACG	**31**	sgTRRAP _98884374	CAAGCAGCACACAGACACTG
4	sgTRRAP _98879515	GCTGGTACCGAGCAATTGTG	**32**	sgTRRAP _98884395	GGTGAACTTCCTTATCCGCG
5	sgTRRAP _98879609	CCAGGAGCTGCAGGGGCAGT	**33**	sgTRRAP _98884428	TAATGACAACACCAACACAG
6	sgTRRAP _98879617	GAGCAGGGCCAGGAGCTGCA	**34**	sgTRRAP _98884487	ACCTTCTGAAGACTGCGTTG
7	sgTRRAP _98879656	GCGGGGGTGGAGGTGGGGCA	**35**	sgTRRAP _98884704	CATGACATGTGGAAACACCA
8	sgTRRAP _98879697	CACGGGGGCCGGGGTCACAG	**36**	sgTRRAP _98884860	AGGGCTCACCAACTACGAGA
9	sgTRRAP _98879700	ACCTGCCACCCCTGTGACCC	**37**	sgTRRAP _98885226	GGTCAAGAATAACTCCCCAA
10	sgTRRAP _98879712	CTTCTCGAAGGGAGGCACGG	**38**	sgTRRAP _98885751	GGAGAACAGCGAGTCCAAAG
11	sgTRRAP _98879988	TGGACAGACATACATCCGTG	**39**	sgTRRAP _98885895	GTTTCTGGACACTCTCCGAG
12	sgTRRAP _98880635	CCATTGAGTGCAGACACCAA	**40**	sgTRRAP _98886656	TCGTCCTGGAGTGCGCCTGG
13	sgTRRAP _98881019	ACACTGAGCCCTACTACCGG	**41**	sgTRRAP _98886748	TGGAAGGTGAACATGTACCG
14	sgTRRAP _98881141	GATGTGAGATGATAACATTG	**42**	sgTRRAP _98887007	AGACGGTGGTGAAGACCTGG
15	**sgTRRAP _Bru8295_3 (X1)**	**CTTGATCCGCCACTATACGA**	**43**	sgTRRAP _98887637	ATCAGAACGAGAGCAAATCG
16	**sgTRRAP _98881473 (X2)**	**GGAGCTTTGCAAAATCGGGG**	**44**	sgTRRAP _98888100	CCTGGCGAAATGTTACTCCG
17	**sgTRRAP _98881579 (X3)**	**GTTCATAACAACATGCACAC**	**45**	sgTRRAP _98888217	GGAGAACATGGTCGAGACGT
18	**sgTRRAP _98881615 (X4)**	**GCGTGGTATGCAAAGCTGGG**	**46**	sgTRRAP _98888316	GCTGAAAGGCCAGTTCACGA
19	sgTRRAP _98882094	GAAGAGCCTGGGCTGCAACG	**47**	sgTRRAP _98888669	ACGCCTGCCTCACAGAGTCA
20	sgTRRAP _98882571	GCGCAAGTGGATGGAAGTGG	**48**	sgTRRAP _98888719	CCTTTCTCTTCTCCAAACAG
21	sgTRRAP _98882714	AGGTTGTCATGAAAACGGAG	**49**	sgTRRAP _98888745	GAAAAACAAGTGCCTCTTGG
22	sgTRRAP _Bru8295_2	CCACTGGGGATCGTTCAGTG	**50**	sgTRRAP _98888806	AAGAGGGGTTGTCCTCCACG
23	sgTRRAP _98882837	ATAAACATTCTGCTCCACTG	**51**	sgTRRAP _98888836	GCTGCTTGTAGATCTCCACA
24	sgTRRAP _98883119	TGAGTGAGAACTTCCAAGAG	**52**	sgTRRAP _98889444	CATGTTCTCTGGCTGCCCGG

25	sgTRRAP_98883484	TTGGGACCTCCCAATCCAGA	**53**	sgTRRAP_98889486	GGTGACGGCTTTCTGAACCA
26	sgTRRAP_98883873	GATGGCCATTCTGACCCCGG	**54**	sgTRRAP_98889507	GTGCAGGCGGGTCATGATGG
27	sgTRRAP_98883936	CTGGACCCGGAAGATCATTG	**55**	sgTRRAP_98889567	AAGCAAGGTGAACACCCTGG
28	sgTRRAP_98884189	GATATGGACCCAAATTCCAG	**56**	sgTRRAP_98889579	ATTGTCCAGGCTGTTTGCCG

Median TRRAP sgRNA on-target score[207]: 70.0.

7 References

1 Levine, A. J. & Oren, M. The first 30 years of p53: growing ever more complex. *Nat Rev Cancer* **9**, 749-758 (2009).
2 Brosh, R. & Rotter, V. When mutants gain new powers: news from the mutant p53 field. *Nat Rev Cancer* **9**, 701-713 (2009).
3 Lane, D. P. p53, guardian of the genome. *Nature* **358**, 15-16 (1992).
4 Vousden, K. H. & Lane, D. P. p53 in health and disease. *Nat Rev Mol Cell Biol* **8**, 275-283 (2007).
5 Riley, T., Sontag, E., Chen, P. & Levine, A. Transcriptional control of human p53-regulated genes. *Nat Rev Mol Cell Biol* **9**, 402-412 (2008).
6 Kamijo, T. *et al.* Loss of the ARF tumor suppressor reverses premature replicative arrest but not radiation hypersensitivity arising from disabled atm function. *Cancer Res* **59**, 2464-2469 (1999).
7 Banin, S. *et al.* Enhanced phosphorylation of p53 by ATM in response to DNA damage. *Science* **281**, 1674-1677 (1998).
8 Canman, C. E. *et al.* Activation of the ATM kinase by ionizing radiation and phosphorylation of p53. *Science* **281**, 1677-1679 (1998).
9 Bieging, K. T., Mello, S. S. & Attardi, L. D. Unravelling mechanisms of p53-mediated tumour suppression. *Nat Rev Cancer* **14**, 359-370 (2014).
10 Brady, C. A. *et al.* Distinct p53 transcriptional programs dictate acute DNA-damage responses and tumor suppression. *Cell* **145**, 571-583 (2011).
11 Yates, A. *et al.* Ensembl 2016. *Nucleic Acids Res* **44**, D710-716 (2016).
12 Walker, D. R. *et al.* Evolutionary conservation and somatic mutation hotspot maps of p53: correlation with p53 protein structural and functional features. *Oncogene* **18**, 211-218 (1999).
13 Marcel, V. *et al.* Biological functions of p53 isoforms through evolution: lessons from animal and cellular models. *Cell Death Differ* **18**, 1815-1824 (2011).
14 May, P. & May, E. Twenty years of p53 research: structural and functional aspects of the p53 protein. *Oncogene* **18**, 7621-7636 (1999).
15 Bode, A. M. & Dong, Z. Post-translational modification of p53 in tumorigenesis. *Nat Rev Cancer* **4**, 793-805 (2004).
16 Somasundaram, K. Tumor suppressor p53: regulation and function. *Front Biosci* **5**, D424-437 (2000).
17 Fields, S. & Jang, S. K. Presence of a potent transcription activating sequence in the p53 protein. *Science* **249**, 1046-1049 (1990).
18 Unger, T., Nau, M. M., Segal, S. & Minna, J. D. p53: a transdominant regulator of transcription whose function is ablated by mutations occurring in human cancer. *EMBO J* **11**, 1383-1390 (1992).
19 Lu, H. & Levine, A. J. Human TAFII31 protein is a transcriptional coactivator of the p53 protein. *Proc Natl Acad Sci U S A* **92**, 5154-5158 (1995).
20 Oliner, J. D. *et al.* Oncoprotein MDM2 conceals the activation domain of tumour suppressor p53. *Nature* **362**, 857-860 (1993).
21 Sakamuro, D., Sabbatini, P., White, E. & Prendergast, G. C. The polyproline region of p53 is required to activate apoptosis but not growth arrest. *Oncogene* **15**, 887-898 (1997).
22 Venot, C. *et al.* The requirement for the p53 proline-rich functional domain for mediation of apoptosis is correlated with specific PIG3 gene transactivation and with transcriptional repression. *EMBO J* **17**, 4668-4679 (1998).
23 Bargonetti, J., Manfredi, J. J., Chen, X., Marshak, D. R. & Prives, C. A proteolytic fragment from the central region of p53 has marked sequence-specific DNA-binding activity when generated from wild-type but not from oncogenic mutant p53 protein. *Genes Dev* **7**, 2565-2574 (1993).
24 Halazonetis, T. D., Davis, L. J. & Kandil, A. N. Wild-type p53 adopts a 'mutant'-like conformation when bound to DNA. *EMBO J* **12**, 1021-1028 (1993).
25 Pavletich, N. P., Chambers, K. A. & Pabo, C. O. The DNA-binding domain of p53 contains the four conserved regions and the major mutation hot spots. *Genes Dev* **7**, 2556-2564 (1993).
26 Wang, Y. *et al.* p53 domains: identification and characterization of two autonomous DNA-binding regions. *Genes Dev* **7**, 2575-2586 (1993).
27 Stenger, J. E. *et al.* p53 oligomerization and DNA looping are linked with transcriptional activation. *EMBO J* **13**, 6011-6020 (1994).
28 Pietenpol, J. A. *et al.* Sequence-specific transcriptional activation is essential for growth suppression by p53. *Proc Natl Acad Sci U S A* **91**, 1998-2002 (1994).
29 Vousden, K. H. & Prives, C. Blinded by the Light: The Growing Complexity of p53. *Cell* **137**, 413-431 (2009).
30 Lee, S., Elenbaas, B., Levine, A. & Griffith, J. p53 and its 14 kDa C-terminal domain recognize primary DNA damage in the form of insertion/deletion mismatches. *Cell* **81**, 1013-1020 (1995).
31 Michael, D. & Oren, M. The p53-Mdm2 module and the ubiquitin system. *Semin Cancer Biol* **13**, 49-58 (2003).
32 Barak, Y., Juven, T., Haffner, R. & Oren, M. mdm2 expression is induced by wild type p53 activity. *EMBO J* **12**, 461-468 (1993).

33 Wu, X., Bayle, J. H., Olson, D. & Levine, A. J. The p53-mdm-2 autoregulatory feedback loop. *Genes Dev* **7**, 1126-1132 (1993).
34 Kubbutat, M. H., Jones, S. N. & Vousden, K. H. Regulation of p53 stability by Mdm2. *Nature* **387**, 299-303 (1997).
35 Haupt, Y., Maya, R., Kazaz, A. & Oren, M. Mdm2 promotes the rapid degradation of p53. *Nature* **387**, 296-299 (1997).
36 Metzger, M. B., Hristova, V. A. & Weissman, A. M. HECT and RING finger families of E3 ubiquitin ligases at a glance. *J Cell Sci* **125**, 531-537 (2012).
37 Lai, Z. *et al.* Human mdm2 mediates multiple mono-ubiquitination of p53 by a mechanism requiring enzyme isomerization. *J Biol Chem* **276**, 31357-31367 (2001).
38 Maki, C. G., Huibregtse, J. M. & Howley, P. M. In vivo ubiquitination and proteasome-mediated degradation of p53. *Cancer Res* **56**, 2649-2654 (1996).
39 Maya, R. *et al.* ATM-dependent phosphorylation of Mdm2 on serine 395: role in p53 activation by DNA damage. *Genes Dev* **15**, 1067-1077 (2001).
40 Fang, S., Jensen, J. P., Ludwig, R. L., Vousden, K. H. & Weissman, A. M. Mdm2 is a RING finger-dependent ubiquitin protein ligase for itself and p53. *J Biol Chem* **275**, 8945-8951 (2000).
41 Honda, R. & Yasuda, H. Activity of MDM2, a ubiquitin ligase, toward p53 or itself is dependent on the RING finger domain of the ligase. *Oncogene* **19**, 1473-1476 (2000).
42 Roth, J., Dobbelstein, M., Freedman, D. A., Shenk, T. & Levine, A. J. Nucleo-cytoplasmic shuttling of the hdm2 oncoprotein regulates the levels of the p53 protein via a pathway used by the human immunodeficiency virus rev protein. *EMBO J* **17**, 554-564 (1998).
43 Stommel, J. M. *et al.* A leucine-rich nuclear export signal in the p53 tetramerization domain: regulation of subcellular localization and p53 activity by NES masking. *EMBO J* **18**, 1660-1672 (1999).
44 Boyd, S. D., Tsai, K. Y. & Jacks, T. An intact HDM2 RING-finger domain is required for nuclear exclusion of p53. *Nat Cell Biol* **2**, 563-568 (2000).
45 Geyer, R. K., Yu, Z. K. & Maki, C. G. The MDM2 RING-finger domain is required to promote p53 nuclear export. *Nat Cell Biol* **2**, 569-573 (2000).
46 Yu, Z. K., Geyer, R. K. & Maki, C. G. MDM2-dependent ubiquitination of nuclear and cytoplasmic P53. *Oncogene* **19**, 5892-5897 (2000).
47 Xirodimas, D. P., Stephen, C. W. & Lane, D. P. Cocompartmentalization of p53 and Mdm2 is a major determinant for Mdm2-mediated degradation of p53. *Exp Cell Res* **270**, 66-77 (2001).
48 Kulikov, R. *et al.* Mdm2 facilitates the association of p53 with the proteasome. *Proc Natl Acad Sci U S A* **107**, 10038-10043 (2010).
49 Hupp, T. R. & Lane, D. P. Allosteric activation of latent p53 tetramers. *Curr Biol* **4**, 865-875 (1994).
50 Meek, D. W. & Anderson, C. W. Posttranslational modification of p53: cooperative integrators of function. *Cold Spring Harb Perspect Biol* **1**, a000950 (2009).
51 Ito, A. *et al.* p300/CBP-mediated p53 acetylation is commonly induced by p53-activating agents and inhibited by MDM2. *EMBO J* **20**, 1331-1340 (2001).
52 Dai, C. & Gu, W. p53 post-translational modification: deregulated in tumorigenesis. *Trends Mol Med* **16**, 528-536 (2010).
53 Barlev, N. A. *et al.* Acetylation of p53 activates transcription through recruitment of coactivators/histone acetyltransferases. *Mol Cell* **8**, 1243-1254 (2001).
54 Brown, C. J., Lain, S., Verma, C. S., Fersht, A. R. & Lane, D. P. Awakening guardian angels: drugging the p53 pathway. *Nat Rev Cancer* **9**, 862-873 (2009).
55 Momand, J., Zambetti, G. P., Olson, D. C., George, D. & Levine, A. J. The mdm-2 oncogene product forms a complex with the p53 protein and inhibits p53-mediated transactivation. *Cell* **69**, 1237-1245 (1992).
56 Shangary, S. & Wang, S. Targeting the MDM2-p53 interaction for cancer therapy. *Clin Cancer Res* **14**, 5318-5324 (2008).
57 Esteller, M. *et al.* p14ARF silencing by promoter hypermethylation mediates abnormal intracellular localization of MDM2. *Cancer Res* **61**, 2816-2821 (2001).
58 Eischen, C. M., Weber, J. D., Roussel, M. F., Sherr, C. J. & Cleveland, J. L. Disruption of the ARF-Mdm2-p53 tumor suppressor pathway in Myc-induced lymphomagenesis. *Genes Dev* **13**, 2658-2669 (1999).
59 Kandoth, C. *et al.* Mutational landscape and significance across 12 major cancer types. *Nature* **502**, 333-339 (2013).
60 Hollstein, M., Sidransky, D., Vogelstein, B. & Harris, C. C. p53 mutations in human cancers. *Science* **253**, 49-53 (1991).
61 Petitjean, A. *et al.* Impact of mutant p53 functional properties on TP53 mutation patterns and tumor phenotype: lessons from recent developments in the IARC TP53 database. *Hum Mutat* **28**, 622-629 (2007).
62 Olivier, M., Hollstein, M. & Hainaut, P. TP53 mutations in human cancers: origins, consequences, and clinical use. *Cold Spring Harb Perspect Biol* **2**, a001008 (2010).
63 Bullock, A. N. & Fersht, A. R. Rescuing the function of mutant p53. *Nat Rev Cancer* **1**, 68-76 (2001).
64 Kato, S. *et al.* Understanding the function-structure and function-mutation relationships of p53 tumor suppressor protein by high-resolution missense mutation analysis. *Proc Natl Acad Sci U S A* **100**, 8424-8429 (2003).

65 Oren, M. & Rotter, V. Mutant p53 gain-of-function in cancer. *Cold Spring Harb Perspect Biol* **2**, 1-15 (2010).
66 Gualberto, A., Aldape, K., Kozakiewicz, K. & Tlsty, T. D. An oncogenic form of p53 confers a dominant, gain-of-function phenotype that disrupts spindle checkpoint control. *Proc Natl Acad Sci U S A* **95**, 5166-5171 (1998).
67 Lotem, J. & Sachs, L. A mutant p53 antagonizes the deregulated c-myc-mediated enhancement of apoptosis and decrease in leukemogenicity. *Proc Natl Acad Sci U S A* **92**, 9672-9676 (1995).
68 Blandino, G., Levine, A. J. & Oren, M. Mutant p53 gain of function: differential effects of different p53 mutants on resistance of cultured cells to chemotherapy. *Oncogene* **18**, 477-485 (1999).
69 Adorno, M. *et al.* A Mutant-p53/Smad complex opposes p63 to empower TGFbeta-induced metastasis. *Cell* **137**, 87-98 (2009).
70 Zhu, J. *et al.* Gain-of-function p53 mutants co-opt chromatin pathways to drive cancer growth. *Nature* **525**, 206-211 (2015).
71 Walerych, D. *et al.* Proteasome machinery is instrumental in a common gain-of-function program of the p53 missense mutants in cancer. *Nat Cell Biol* **18**, 897-909 (2016).
72 Mantovani, F., Walerych, D. & Sal, G. D. Targeting mutant p53 in cancer: a long road to precision therapy. *FEBS J* **284**, 837-850 (2017).
73 Rotter, V. p53, a transformation-related cellular-encoded protein, can be used as a biochemical marker for the detection of primary mouse tumor cells. *Proc Natl Acad Sci U S A* **80**, 2613-2617 (1983).
74 Iggo, R., Gatter, K., Bartek, J., Lane, D. & Harris, A. L. Increased expression of mutant forms of p53 oncogene in primary lung cancer. *Lancet* **335**, 675-679 (1990).
75 Bartek, J. *et al.* Aberrant expression of the p53 oncoprotein is a common feature of a wide spectrum of human malignancies. *Oncogene* **6**, 1699-1703 (1991).
76 Soussi, T. & Beroud, C. Assessing TP53 status in human tumours to evaluate clinical outcome. *Nat Rev Cancer* **1**, 233-240 (2001).
77 Bouchalova, P. *et al.* Mutant p53 accumulation in human breast cancer is not an intrinsic property or dependent on structural or functional disruption but is regulated by exogenous stress and receptor status. *J Pathol* **233**, 238-246 (2014).
78 Lang, G. A. *et al.* Gain of function of a p53 hot spot mutation in a mouse model of Li-Fraumeni syndrome. *Cell* **119**, 861-872 (2004).
79 Terzian, T. *et al.* The inherent instability of mutant p53 is alleviated by Mdm2 or p16INK4a loss. *Genes Dev* **22**, 1337-1344 (2008).
80 Olive, K. P. *et al.* Mutant p53 gain of function in two mouse models of Li-Fraumeni syndrome. *Cell* **119**, 847-860 (2004).
81 Midgley, C. A. & Lane, D. P. p53 protein stability in tumour cells is not determined by mutation but is dependent on Mdm2 binding. *Oncogene* **15**, 1179-1189 (1997).
82 Li, D., Marchenko, N. D. & Moll, U. M. SAHA shows preferential cytotoxicity in mutant p53 cancer cells by destabilizing mutant p53 through inhibition of the HDAC6-Hsp90 chaperone axis. *Cell Death Differ* **18**, 1904-1913 (2011).
83 Li, D. *et al.* Functional inactivation of endogenous MDM2 and CHIP by HSP90 causes aberrant stabilization of mutant p53 in human cancer cells. *Mol Cancer Res* **9**, 577-588 (2011).
84 Lukashchuk, N. & Vousden, K. H. Ubiquitination and degradation of mutant p53. *Mol Cell Biol* **27**, 8284-8295 (2007).
85 Bartel, F., Taubert, H. & Harris, L. C. Alternative and aberrant splicing of MDM2 mRNA in human cancer. *Cancer Cell* **2**, 9-15 (2002).
86 Zheng, T. *et al.* Spliced MDM2 isoforms promote mutant p53 accumulation and gain-of-function in tumorigenesis. *Nat Commun* **4**, 2996 (2013).
87 Schopf, F. H., Biebl, M. M. & Buchner, J. The HSP90 chaperone machinery. *Nat Rev Mol Cell Biol* **18**, 345-360 (2017).
88 Proia, D. A. & Bates, R. C. Ganetespib and HSP90: translating preclinical hypotheses into clinical promise. *Cancer Res* **74**, 1294-1300 (2014).
89 Yue, X. *et al.* A novel mutant p53 binding partner BAG5 stabilizes mutant p53 and promotes mutant p53 GOFs in tumorigenesis. *Cell Discov* **2**, 16039 (2016).
90 Yue, X. *et al.* BAG2 promotes tumorigenesis through enhancing mutant p53 protein levels and function. *Elife* **4** (2015).
91 Nguyen, T. A., Menendez, D., Resnick, M. A. & Anderson, C. W. Mutant TP53 posttranslational modifications: Challenges and opportunities. *Hum Mutat* **35**, 738-755 (2014).
92 Suh, Y. A. *et al.* Multiple stress signals activate mutant p53 in vivo. *Cancer Res* **71**, 7168-7175 (2011).
93 Guo, L. *et al.* Ionizing radiation induces a dramatic persistence of p53 protein accumulation and DNA damage signaling in mutant p53 zebrafish. *Oncogene* **32**, 4009-4016 (2013).
94 Gillotin, S., Yap, D. & Lu, X. Mutation at Ser392 specifically sensitizes mutant p53H175 to mdm2-mediated degradation. *Cell Cycle* **9**, 1390-1398 (2010).
95 Yap, D. B. *et al.* Ser392 phosphorylation regulates the oncogenic function of mutant p53. *Cancer Res* **64**, 4749-4754 (2004).

96 Melnikova, V. O., Santamaria, A. B., Bolshakov, S. V. & Ananthaswamy, H. N. Mutant p53 is constitutively phosphorylated at Serine 15 in UV-induced mouse skin tumors: involvement of ERK1/2 MAP kinase. *Oncogene* **22**, 5958-5966 (2003).
97 Matsumoto, M., Furihata, M., Kurabayashi, A. & Ohtsuki, Y. Phosphorylation state of tumor-suppressor gene p53 product overexpressed in skin tumors. *Oncol Rep* **12**, 1039-1043 (2004).
98 Minamoto, T. *et al.* Distinct pattern of p53 phosphorylation in human tumors. *Oncogene* **20**, 3341-3347 (2001).
99 Yi, Y. W. *et al.* Targeting mutant p53 by a SIRT1 activator YK-3-237 inhibits the proliferation of triple-negative breast cancer cells. *Oncotarget* **4**, 984-994 (2013).
100 Perez, R. E. *et al.* Restoration of DNA-binding and growth-suppressive activity of mutant forms of p53 via a PCAF-mediated acetylation pathway. *J Cell Phys* **225**, 394-405 (2010).
101 Muller, P. A. & Vousden, K. H. Mutant p53 in cancer: new functions and therapeutic opportunities. *Cancer Cell* **25**, 304-317 (2014).
102 Muller, P. A. & Vousden, K. H. p53 mutations in cancer. *Nat Cell Biol* **15**, 2-8 (2013).
103 Alexandrova, E. M. *et al.* Improving survival by exploiting tumour dependence on stabilized mutant p53 for treatment. *Nature* **523**, 352-356 (2015).
104 Li, Y. & Seto, E. HDACs and HDAC Inhibitors in Cancer Development and Therapy. *Cold Spring Harb Perspect Med* **6** (2016).
105 Blagosklonny, M. V. *et al.* Depletion of mutant p53 and cytotoxicity of histone deacetylase inhibitors. *Cancer Res* **65**, 7386-7392 (2005).
106 Stojanovic, N. *et al.* HDAC1 and HDAC2 integrate the expression of p53 mutants in pancreatic cancer. *Oncogene* **36**, 1804-1815 (2017).
107 Wang, Z. T. *et al.* Histone deacetylase inhibitors suppress mutant p53 transcription via HDAC8/YY1 signals in triple negative breast cancer cells. *Cell Signal* **28**, 506-515 (2016).
108 An, W. G., Hwang, S. G., Trepel, J. B. & Blagosklonny, M. V. Protease inhibitor-induced apoptosis: accumulation of wt p53, p21WAF1/CIP1, and induction of apoptosis are independent markers of proteasome inhibition. *Leukemia* **14**, 1276-1283 (2000).
109 Halasi, M., Pandit, B. & Gartel, A. L. Proteasome inhibitors suppress the protein expression of mutant p53. *Cell Cycle* **13**, 3202-3206 (2014).
110 Choudhury, S., Kolukula, V. K., Preet, A., Albanese, C. & Avantaggiati, M. L. Dissecting the pathways that destabilize mutant p53: the proteasome or autophagy? *Cell Cycle* **12**, 1022-1029 (2013).
111 Yin, Z., Pascual, C. & Klionsky, D. J. Autophagy: machinery and regulation. *Microb Cell* **3**, 588-596 (2016).
112 Rodriguez, O. C. *et al.* Dietary downregulation of mutant p53 levels via glucose restriction: mechanisms and implications for tumor therapy. *Cell Cycle* **11**, 4436-4446 (2012).
113 Vakifahmetoglu-Norberg, H. *et al.* Chaperone-mediated autophagy degrades mutant p53. *Genes Dev* **27**, 1718-1730 (2013).
114 Zhao, Y., Yu, H. & Hu, W. The regulation of MDM2 oncogene and its impact on human cancers. *Acta Biochim Biophys Sin (Shanghai)* **46**, 180-189 (2014).
115 Li, Y. *et al.* PTEN has tumor-promoting properties in the setting of gain-of-function p53 mutations. *Cancer Res* **68**, 1723-1731 (2008).
116 Rosivatz, E. *et al.* A small molecule inhibitor for phosphatase and tensin homologue deleted on chromosome 10 (PTEN). *ACS Chem Biol* **1**, 780-790 (2006).
117 Selivanova, G. & Wiman, K. G. Reactivation of mutant p53: molecular mechanisms and therapeutic potential. *Oncogene* **26**, 2243-2254 (2007).
118 Zhang, W. *et al.* A temperature-sensitive mutant of human p53. *EMBO J* **13**, 2535-2544 (1994).
119 Bullock, A. N., Henckel, J. & Fersht, A. R. Quantitative analysis of residual folding and DNA binding in mutant p53 core domain: definition of mutant states for rescue in cancer therapy. *Oncogene* **19**, 1245-1256 (2000).
120 Oren, M., Tal, P. & Rotter, V. Targeting mutant p53 for cancer therapy. *Aging (Albany NY)* **8**, 1159-1160 (2016).
121 Tal, P. *et al.* Cancer therapeutic approach based on conformational stabilization of mutant p53 protein by small peptides. *Oncotarget* **7**, 11817-11837 (2016).
122 Zawacka-Pankau, J. & Selivanova, G. Pharmacological reactivation of p53 as a strategy to treat cancer. *J Intern Med* **277**, 248-259 (2015).
123 Deneberg, S. *et al.* An open-label phase I dose-finding study of APR-246 in hematological malignancies. *Blood Cancer J* **6**, e447 (2016).
124 Lehmann, S. *et al.* Targeting p53 in vivo: a first-in-human study with p53-targeting compound APR-246 in refractory hematologic malignancies and prostate cancer. *J Clin Oncol* **30**, 3633-3639 (2012).
125 Loh, S. N. The missing zinc: p53 misfolding and cancer. *Metallomics* **2**, 442-449 (2010).
126 Puca, R. *et al.* Restoring p53 active conformation by zinc increases the response of mutant p53 tumor cells to anticancer drugs. *Cell Cycle* **10**, 1679-1689 (2011).
127 Yu, X., Vazquez, A., Levine, A. J. & Carpizo, D. R. Allele-specific p53 mutant reactivation. *Cancer Cell* **21**, 614-625 (2012).
128 Xu, J. *et al.* Gain of function of mutant p53 by coaggregation with multiple tumor suppressors. *Nat Chem Biol* **7**, 285-295 (2011).

129 Soragni, A. *et al.* A Designed Inhibitor of p53 Aggregation Rescues p53 Tumor Suppression in Ovarian Carcinomas. *Cancer Cell* **29**, 90-103 (2016).
130 Wang, G. & Fersht, A. R. Multisite aggregation of p53 and implications for drug rescue. *Proc Natl Acad Sci U S A* **114**, E2634-E2643 (2017).
131 Kravchenko, J. E. *et al.* Small-molecule RETRA suppresses mutant p53-bearing cancer cells through a p73-dependent salvage pathway. *Proc Natl Acad Sci U S A* **105**, 6302-6307 (2008).
132 Freed-Pastor, W. A. *et al.* Mutant p53 disrupts mammary tissue architecture via the mevalonate pathway. *Cell* **148**, 244-258 (2012).
133 Kuppers, R. Mechanisms of B-cell lymphoma pathogenesis. *Nat Rev Cancer* **5**, 251-262 (2005).
134 Armitage, J. O., Gascoyne, R. D., Lunning, M. A. & Cavalli, F. Non-Hodgkin lymphoma. *Lancet* **390**, 298-310 (2017).
135 Hochberg, J., El-Mallawany, N. K. & Abla, O. Adolescent and young adult non-Hodgkin lymphoma. *Br J Haematol* **173**, 637-650 (2016).
136 MacLennan, I. C. Germinal centers. *Annu Rev Immunol* **12**, 117-139 (1994).
137 Victora, G. D. & Nussenzweig, M. C. Germinal centers. *Annu Rev Immunol* **30**, 429-457 (2012).
138 De Silva, N. S. & Klein, U. Dynamics of B cells in germinal centres. *Nat Rev Immunol* **15**, 137-148 (2015).
139 Klein, U. & Dalla-Favera, R. Germinal centres: role in B-cell physiology and malignancy. *Nat Rev Immunol* **8**, 22-33 (2008).
140 Stavnezer, J., Guikema, J. E. & Schrader, C. E. Mechanism and regulation of class switch recombination. *Annu Rev Immunol* **26**, 261-292 (2008).
141 Basso, K. & Dalla-Favera, R. Germinal centres and B cell lymphomagenesis. *Nat Rev Immunol* **15**, 172-184 (2015).
142 Kuppers, R., Klein, U., Hansmann, M. L. & Rajewsky, K. Cellular origin of human B-cell lymphomas. *N Engl J Med* **341**, 1520-1529 (1999).
143 Stevenson, F. K. *et al.* The occurrence and significance of V gene mutations in B cell-derived human malignancy. *Adv Cancer Res* **83**, 81-116 (2001).
144 Victora, G. D. *et al.* Identification of human germinal center light and dark zone cells and their relationship to human B-cell lymphomas. *Blood* **120**, 2240-2248 (2012).
145 Pasqualucci, L. *et al.* Hypermutation of multiple proto-oncogenes in B-cell diffuse large-cell lymphomas. *Nature* **412**, 341-346 (2001).
146 Kuppers, R. & Dalla-Favera, R. Mechanisms of chromosomal translocations in B cell lymphomas. *Oncogene* **20**, 5580-5594 (2001).
147 de-The, G. The Epstein-Barr virus (EBV): a Rosetta Stone for understanding the role of viruses in immunopathological disorders and in human carcinogenesis. *Biomed Pharmacother* **39**, 49-51 (1985).
148 Molyneux, E. M. *et al.* Burkitt's lymphoma. *Lancet* **379**, 1234-1244 (2012).
149 Burkitt, D. P. Etiology of Burkitt's lymphoma--an alternative hypothesis to a vectored virus. *J Natl Cancer Inst* **42**, 19-28 (1969).
150 Epstein, M. A., Achong, B. G. & Barr, Y. M. Virus Particles in Cultured Lymphoblasts from Burkitt's Lymphoma. *Lancet* **1**, 702-703 (1964).
151 Schulz, T. F., Boshoff, C. H. & Weiss, R. A. HIV infection and neoplasia. *Lancet* **348**, 587-591 (1996).
152 Manolov, G. & Manolova, Y. Marker band in one chromosome 14 from Burkitt lymphomas. *Nature* **237**, 33-34 (1972).
153 Zech, L., Haglund, U., Nilsson, K. & Klein, G. Characteristic chromosomal abnormalities in biopsies and lymphoid-cell lines from patients with Burkitt and non-Burkitt lymphomas. *Int J Cancer* **17**, 47-56 (1976).
154 Dozzo, M. *et al.* Burkitt lymphoma in adolescents and young adults: management challenges. *Adolesc Health Med Ther* **8**, 11-29 (2017).
155 Burkitt, D. A sarcoma involving the jaws in African children. *Br J Surg* **46**, 218-223 (1958).
156 Jaffe, E. S. The 2008 WHO classification of lymphomas: implications for clinical practice and translational research. *Hematology Am Soc Hematol Educ Program*, 523-531 (2009).
157 Schmitz, R., Ceribelli, M., Pittaluga, S., Wright, G. & Staudt, L. M. Oncogenic mechanisms in Burkitt lymphoma. *Cold Spring Harb Perspect Med* **4** (2014).
158 Fujita, S. *et al.* Early stage of Epstein-Barr virus lytic infection leading to the "starry sky" pattern formation in endemic Burkitt lymphoma. *Arch Pathol Lab Med* **128**, 549-552 (2004).
159 Jacobson, C. & LaCasce, A. How I treat Burkitt lymphoma in adults. *Blood* **124**, 2913-2920 (2014).
160 Wildes, T. M. *et al.* Rituximab is associated with improved survival in Burkitt lymphoma: a retrospective analysis from two US academic medical centers. *Ther Adv Hematol* **5**, 3-12 (2014).
161 Adams, J. M. *et al.* The c-myc oncogene driven by immunoglobulin enhancers induces lymphoid malignancy in transgenic mice. *Nature* **318**, 533-538 (1985).
162 Sander, S. *et al.* Synergy between PI3K signaling and MYC in Burkitt lymphomagenesis. *Cancer Cell* **22**, 167-179 (2012).
163 Schmitz, R. *et al.* Burkitt lymphoma pathogenesis and therapeutic targets from structural and functional genomics. *Nature* **490**, 116-120 (2012).
164 Hemann, M. T. *et al.* Evasion of the p53 tumour surveillance network by tumour-derived MYC mutants. *Nature* **436**, 807-811 (2005).

165 Meyer, N., Kim, S. S. & Penn, L. Z. The Oscar-worthy role of Myc in apoptosis. *Semin Cancer Biol* **16**, 275-287 (2006).
166 Bhatia, K. G., Gutierrez, M. I., Huppi, K., Siwarski, D. & Magrath, I. T. The pattern of p53 mutations in Burkitt's lymphoma differs from that of solid tumors. *Cancer Res* **52**, 4273-4276 (1992).
167 Wiman, K. G., Magnusson, K. P., Ramqvist, T. & Klein, G. Mutant p53 detected in a majority of Burkitt lymphoma cell lines by monoclonal antibody PAb240. *Oncogene* **6**, 1633-1639 (1991).
168 Farrell, P. J., Allan, G. J., Shanahan, F., Vousden, K. H. & Crook, T. p53 is frequently mutated in Burkitt's lymphoma cell lines. *EMBO J* **10**, 2879-2887 (1991).
169 Preudhomme, C. *et al.* Clinical significance of p53 mutations in newly diagnosed Burkitt's lymphoma and acute lymphoblastic leukemia: a report of 48 cases. *J Clin Oncol* **13**, 812-820 (1995).
170 Tessoulin, B. *et al.* p53 dysregulation in B-cell malignancies: More than a single gene in the pathway to hell. *Blood Rev* **31**, 251-259 (2017).
171 Leventaki, V. *et al.* TP53 pathway analysis in paediatric Burkitt lymphoma reveals increased MDM4 expression as the only TP53 pathway abnormality detected in a subset of cases. *Br J Haematol* **158**, 763-771 (2012).
172 Wilda, M. *et al.* Inactivation of the ARF-MDM-2-p53 pathway in sporadic Burkitt's lymphoma in children. *Leukemia* **18**, 584-588 (2004).
173 Sachs, L. & Lotem, J. Control of programmed cell death in normal and leukemic cells: new implications for therapy. *Blood* **82**, 15-21 (1993).
174 Gaidano, G. *et al.* p53 mutations in human lymphoid malignancies: association with Burkitt lymphoma and chronic lymphocytic leukemia. *Proc Natl Acad Sci U S A* **88**, 5413-5417 (1991).
175 Haberl, S. *et al.* MYC rearranged B-cell neoplasms: Impact of genetics on classification. *Cancer Genet* **209**, 431-439 (2016).
176 Kretzmer, H. *et al.* DNA methylome analysis in Burkitt and follicular lymphomas identifies differentially methylated regions linked to somatic mutation and transcriptional control. *Nat Genet* **47**, 1316-1325 (2015).
177 Love, C. *et al.* The genetic landscape of mutations in Burkitt lymphoma. *Nat Genet* **44**, 1321-1325 (2012).
178 Richter, J. *et al.* Recurrent mutation of the ID3 gene in Burkitt lymphoma identified by integrated genome, exome and transcriptome sequencing. *Nat Genet* **44**, 1316-1320 (2012).
179 Sanchez-Beato, M. *et al.* Overall survival in aggressive B-cell lymphomas is dependent on the accumulation of alterations in p53, p16, and p27. *Am J Pathol* **159**, 205-213 (2001).
180 Iorns, E., Lord, C. J., Turner, N. & Ashworth, A. Utilizing RNA interference to enhance cancer drug discovery. *Nat Rev Drug Discov* **6**, 556-568 (2007).
181 Fire, A. *et al.* Potent and specific genetic interference by double-stranded RNA in Caenorhabditis elegans. *Nature* **391**, 806-811 (1998).
182 Elbashir, S. M. *et al.* Duplexes of 21-nucleotide RNAs mediate RNA interference in cultured mammalian cells. *Nature* **411**, 494-498 (2001).
183 de Fougerolles, A., Vornlocher, H. P., Maraganore, J. & Lieberman, J. Interfering with disease: a progress report on siRNA-based therapeutics. *Nat Rev Drug Discov* **6**, 443-453 (2007).
184 Mohr, S. E., Smith, J. A., Shamu, C. E., Neumuller, R. A. & Perrimon, N. RNAi screening comes of age: improved techniques and complementary approaches. *Nat Rev Mol Cell Biol* **15**, 591-600 (2014).
185 Rao, D. D., Vorhies, J. S., Senzer, N. & Nemunaitis, J. siRNA vs. shRNA: similarities and differences. *Adv Drug Deliv Rev* **61**, 746-759 (2009).
186 Stewart, S. A. *et al.* Lentivirus-delivered stable gene silencing by RNAi in primary cells. *RNA* **9**, 493-501 (2003).
187 Brummelkamp, T. R., Bernards, R. & Agami, R. A system for stable expression of short interfering RNAs in mammalian cells. *Science* **296**, 550-553 (2002).
188 Echeverri, C. J. *et al.* Minimizing the risk of reporting false positives in large-scale RNAi screens. *Nat Methods* **3**, 777-779 (2006).
189 Sigoillot, F. D. & King, R. W. Vigilance and validation: Keys to success in RNAi screening. *ACS Chem Biol* **6**, 47-60 (2011).
190 Grimm, D. *et al.* Fatality in mice due to oversaturation of cellular microRNA/short hairpin RNA pathways. *Nature* **441**, 537-541 (2006).
191 Bridge, A. J., Pebernard, S., Ducraux, A., Nicoulaz, A. L. & Iggo, R. Induction of an interferon response by RNAi vectors in mammalian cells. *Nat Genet* **34**, 263-264 (2003).
192 Persengiev, S. P., Zhu, X. & Green, M. R. Nonspecific, concentration-dependent stimulation and repression of mammalian gene expression by small interfering RNAs (siRNAs). *RNA* **10**, 12-18 (2004).
193 Lin, A., Giuliano, C. J., Sayles, N. M. & Sheltzer, J. M. CRISPR/Cas9 mutagenesis invalidates a putative cancer dependency targeted in on-going clinical trials. *Elife* **6** (2017).
194 Boutros, M. & Ahringer, J. The art and design of genetic screens: RNA interference. *Nat Rev Genet* **9**, 554-566 (2008).
195 Shalem, O., Sanjana, N. E. & Zhang, F. High-throughput functional genomics using CRISPR-Cas9. *Nat Rev Genet* **16**, 299-311 (2015).

196 Mohr, S., Bakal, C. & Perrimon, N. Genomic screening with RNAi: results and challenges. *Annu Rev Biochem* **79**, 37-64 (2010).
197 Toyoshima, M. *et al.* Functional genomics identifies therapeutic targets for MYC-driven cancer. *Proc Natl Acad Sci U S A* **109**, 9545-9550 (2012).
198 Cowley, G. S. *et al.* Parallel genome-scale loss of function screens in 216 cancer cell lines for the identification of context-specific genetic dependencies. *Sci Data* **1**, 140035 (2014).
199 Hullein, J. *et al.* Next-generation sequencing of cancer consensus genes in lymphoma. *Leuk Lymphoma* **54**, 1831-1835 (2013).
200 Jethwa, A. *et al.* Targeted resequencing for analysis of clonal composition of recurrent gene mutations in chronic lymphocytic leukaemia. *Br J Haematol* **163**, 496-500 (2013).
201 Hüllein, J. *Identification of Burkitt lymphoma vulnerabilities using RNAi.* PhD thesis, Heidelberg University, (2016).
202 Bouaoun, L. *et al.* TP53 Variations in Human Cancers: New Lessons from the IARC TP53 Database and Genomics Data. *Hum Mutat* **37**, 865-876 (2016).
203 Madar, S. *et al.* Mutant p53 attenuates the anti-tumorigenic activity of fibroblasts-secreted interferon beta. *PLoS One* **8**, e61353 (2013).
204 Roulois, D. *et al.* DNA-Demethylating Agents Target Colorectal Cancer Cells by Inducing Viral Mimicry by Endogenous Transcripts. *Cell* **162**, 961-973 (2015).
205 Wang, X., Spandidos, A., Wang, H. & Seed, B. PrimerBank: a PCR primer database for quantitative gene expression analysis, 2012 update. *Nucleic Acids Res* **40**, D1144-1149 (2012).
206 Sanjana, N. E., Shalem, O. & Zhang, F. Improved vectors and genome-wide libraries for CRISPR screening. *Nat Methods* **11**, 783-784 (2014).
207 Doench, J. G. *et al.* Optimized sgRNA design to maximize activity and minimize off-target effects of CRISPR-Cas9. *Nat Biotechnol* **34**, 184-191 (2016).
208 Castro, F. *et al.* High-throughput SNP-based authentication of human cell lines. *Int J Cancer* **132**, 308-314 (2013).
209 Schmitt, M. & Pawlita, M. High-throughput detection and multiplex identification of cell contaminations. *Nucleic Acids Res* **37**, e119 (2009).
210 Shalem, O. *et al.* Genome-scale CRISPR-Cas9 knockout screening in human cells. *Science* **343**, 84-87 (2014).
211 Heckl, D. *et al.* Generation of mouse models of myeloid malignancy with combinatorial genetic lesions using CRISPR-Cas9 genome editing. *Nat Biotechnol* **32**, 941-946 (2014).
212 Varemo, L., Nielsen, J. & Nookaew, I. Enriching the gene set analysis of genome-wide data by incorporating directionality of gene expression and combining statistical hypotheses and methods. *Nucleic Acids Res* **41**, 4378-4391 (2013).
213 Kim, S. Y. & Volsky, D. J. PAGE: parametric analysis of gene set enrichment. *BMC Bioinformatics* **6**, 144 (2005).
214 Subramanian, A. *et al.* Gene set enrichment analysis: a knowledge-based approach for interpreting genome-wide expression profiles. *Proc Natl Acad Sci U S A* **102**, 15545-15550 (2005).
215 Liberzon, A. *et al.* The Molecular Signatures Database (MSigDB) hallmark gene set collection. *Cell Syst* **1**, 417-425 (2015).
216 Chen, E. Y. *et al.* Enrichr: interactive and collaborative HTML5 gene list enrichment analysis tool. *BMC Bioinformatics* **14**, 128 (2013).
217 Kuleshov, M. V. *et al.* Enrichr: a comprehensive gene set enrichment analysis web server 2016 update. *Nucleic Acids Res* **44**, W90-97 (2016).
218 Borbely, G., Haldosen, L. A., Dahlman-Wright, K. & Zhao, C. Induction of USP17 by combining BET and HDAC inhibitors in breast cancer cells. *Oncotarget* **6**, 33623-33635 (2015).
219 Hughes, C. S. *et al.* Ultrasensitive proteome analysis using paramagnetic bead technology. *Mol Syst Biol* **10**, 757 (2014).
220 Franken, H. *et al.* Thermal proteome profiling for unbiased identification of direct and indirect drug targets using multiplexed quantitative mass spectrometry. *Nat Protoc* **10**, 1567-1593 (2015).
221 Ritchie, M. E. *et al.* limma powers differential expression analyses for RNA-sequencing and microarray studies. *Nucleic Acids Res* **43**, e47 (2015).
222 Huber, W., von Heydebreck, A., Sultmann, H., Poustka, A. & Vingron, M. Variance stabilization applied to microarray data calibration and to the quantification of differential expression. *Bioinformatics* **18 Suppl 1**, S96-104 (2002).
223 Shi, J. *et al.* Discovery of cancer drug targets by CRISPR-Cas9 screening of protein domains. *Nat Biotechnol* **33**, 661-667 (2015).
224 Hummel, M. *et al.* A biologic definition of Burkitt's lymphoma from transcriptional and genomic profiling. *N Engl J Med* **354**, 2419-2430 (2006).
225 Rosolowski, M. *et al.* Massive transcriptional perturbation in subgroups of diffuse large B-cell lymphomas. *PLoS One* **8**, e76287 (2013).
226 Scholtysik, R. *et al.* Detection of genomic aberrations in molecularly defined Burkitt's lymphoma by array-based, high resolution, single nucleotide polymorphism analysis. *Haematologica* **95**, 2047-2055 (2010).
227 Boettcher, M. *et al.* High throughput synthetic lethality screen reveals a tumorigenic role of adenylate cyclase in fumarate hydratase-deficient cancer cells. *BMC Genomics* **15**, 158 (2014).

228 Slabicki, M. *et al.* Dissection of CD20 regulation in lymphoma using RNAi. *Leukemia* **30**, 2409-2412 (2016).
229 Li, H. *et al.* Integrated high-throughput analysis identifies Sp1 as a crucial determinant of p53-mediated apoptosis. *Cell Death Differ* **21**, 1493-1502 (2014).
230 Dai, Z. *et al.* edgeR: a versatile tool for the analysis of shRNA-seq and CRISPR-Cas9 genetic screens. *F1000Res* **3**, 95 (2014).
231 Robinson, M. D., McCarthy, D. J. & Smyth, G. K. edgeR: a Bioconductor package for differential expression analysis of digital gene expression data. *Bioinformatics* **26**, 139-140 (2010).
232 Kim, J. & Tan, A. C. BiNGS!SL-seq: a bioinformatics pipeline for the analysis and interpretation of deep sequencing genome-wide synthetic lethal screen. *Methods Mol Biol* **802**, 389-398 (2012).
233 Hart, T., Brown, K. R., Sircoulomb, F., Rottapel, R. & Moffat, J. Measuring error rates in genomic perturbation screens: gold standards for human functional genomics. *Mol Syst Biol* **10**, 733 (2014).
234 McMahon, S. B., Van Buskirk, H. a., Dugan, K. a., Copeland, T. D. & Cole, M. D. The novel ATM-related protein TRRAP is an essential cofactor for the c- Myc and E2F oncoproteins. *Cell* **94**, 363-374 (1998).
235 Lempiainen, H. & Halazonetis, T. D. Emerging common themes in regulation of PIKKs and PI3Ks. *EMBO J* **28**, 3067-3073 (2009).
236 Rivera-Calzada, A. *et al.* Structure and Assembly of the PI3K-like Protein Kinases (PIKKs) Revealed by Electron Microscopy. *AIMS Biophysics* **2**, 36-57 (2015).
237 Murr, R., Vaissière, T., Sawan, C., Shukla, V. & Herceg, Z. Orchestration of chromatin-based processes: mind the TRRAP. *Oncogene* **26**, 5358-5372 (2007).
238 Ard, P. G. *et al.* Transcriptional regulation of the mdm2 oncogene by p53 requires TRRAP acetyltransferase complexes. *Mol Cell Biol* **22**, 5650-5661 (2002).
239 Stark, C. *et al.* BioGRID: a general repository for interaction datasets. *Nucleic Acids Res* **34**, D535-539 (2006).
240 An, W., Kim, J. & Roeder, R. G. Ordered cooperative functions of PRMT1, p300, and CARM1 in transcriptional activation by p53. *Cell* **117**, 735-748 (2004).
241 Binder, J. X. *et al.* COMPARTMENTS: unification and visualization of protein subcellular localization evidence. *Database (Oxford)* **2014**, bau012 (2014).
242 Platanias, L. C. Mechanisms of type-I- and type-II-interferon-mediated signalling. *Nat Rev Immunol* **5**, 375-386 (2005).
243 Fabregat, A. *et al.* The Reactome pathway Knowledgebase. *Nucleic Acids Res* **44**, D481-487 (2016).
244 Jinek, M. *et al.* A programmable dual-RNA-guided DNA endonuclease in adaptive bacterial immunity. *Science* **337**, 816-821 (2012).
245 Rouet, P., Smih, F. & Jasin, M. Introduction of double-strand breaks into the genome of mouse cells by expression of a rare-cutting endonuclease. *Mol Cell Biol* **14**, 8096-8106 (1994).
246 Knutson, B. A. & Hahn, S. Domains of Tra1 important for activator recruitment and transcription coactivator functions of SAGA and NuA4 complexes. *Mol Cell Biol* **31**, 818-831 (2011).
247 Walerych, D. *et al.* Hsp90 Chaperones Wild-type p53 Tumor Suppressor Protein. *J Biol Chem* **279**, 48836-48845 (2004).
248 Lauffer, B. E. *et al.* Histone deacetylase (HDAC) inhibitor kinetic rate constants correlate with cellular histone acetylation but not transcription and cell viability. *J Biol Chem* **288**, 26926-26943 (2013).
249 Butler, K. V. *et al.* Rational design and simple chemistry yield a superior, neuroprotective HDAC6 inhibitor, tubastatin A. *J Am Chem Soc* **132**, 10842-10846 (2010).
250 Balasubramanian, S. *et al.* A novel histone deacetylase 8 (HDAC8)-specific inhibitor PCI-34051 induces apoptosis in T-cell lymphomas. *Leukemia* **22**, 1026-1034 (2008).
251 Fournel, M. *et al.* MGCD0103, a novel isotype-selective histone deacetylase inhibitor, has broad spectrum antitumor activity in vitro and in vivo. *Mol Cancer Ther* **7**, 759-768 (2008).
252 Senese, S. *et al.* Role for histone deacetylase 1 in human tumor cell proliferation. *Mol Cell Biol* **27**, 4784-4795 (2007).
253 Soussi, T. p53 alterations in human cancer: more questions than answers. *Oncogene* **26**, 2145-2156 (2007).
254 Hjortsberg, L. *et al. The p53 Mutation handbook 2.0*, <http://p53.free.fr> (October 2008).
255 Adamson, D. J., Thompson, W. D., Dawson, A. A., Bennett, B. & Haites, N. E. p53 mutation and expression in lymphoma. *Br J Cancer* **72**, 150-154 (1995).
256 Koduru, P. R. *et al.* Correlation between mutation in P53, p53 expression, cytogenetics, histologic type, and survival in patients with B-cell non-Hodgkin's lymphoma. *Blood* **90**, 4078-4091 (1997).
257 Oka, T., Sarker, A. B., Teramoto, N., Yoshino, T. & Akagi, T. p53 protein expression in non-Hodgkin's lymphomas is infrequently related to p53 gene mutations. *Pathol Int* **48**, 15-21 (1998).
258 Tzardi, M. *et al.* p53 protein expression in non-Hodgkin's lymphoma. Comparative study with the wild type p53 induced proteins mdm2 and p21/waf1. *Clin Mol Pathol* **49**, M278-282 (1996).
259 Balint, E. & Reisman, D. Increased rate of transcription contributes to elevated expression of the mutant p53 gene in Burkitt's lymphoma cells. *Cancer Res* **56**, 1648-1653 (1996).
260 Hall, P. A. & Lane, D. P. p53 in tumour pathology: can we trust immunohistochemistry?--Revisited! *J Pathol* **172**, 1-4 (1994).
261 Yue, X. *et al.* Mutant p53 in Cancer: Accumulation, Gain-of-Function, and Therapy. *J Mol Biol* **429**, 1595-1606 (2017).

262 Prives, C. & White, E. Does control of mutant p53 by Mdm2 complicate cancer therapy? *Genes Dev* **22**, 1259-1264 (2008).
263 Mak, A. B. *et al.* CD133 protein N-glycosylation processing contributes to cell surface recognition of the primitive cell marker AC133 epitope. *J Biol Chem* **286**, 41046-41056 (2011).
264 Parnas, O. *et al.* A Genome-wide CRISPR Screen in Primary Immune Cells to Dissect Regulatory Networks. *Cell* **162**, 675-686 (2015).
265 Ezkurdia, I. *et al.* Multiple evidence strands suggest that there may be as few as 19,000 human protein-coding genes. *Hum Mol Genet* **23**, 5866-5878 (2014).
266 Vijayakumaran, R., Tan, K. H., Miranda, P. J., Haupt, S. & Haupt, Y. Regulation of Mutant p53 Protein Expression. *Front Oncol* **5**, 284 (2015).
267 Herceg, Z. *et al.* Disruption of Trrap causes early embryonic lethality and defects in cell cycle progression. *Nat Genet* **29**, 206-211 (2001).
268 Leduc, C. *et al.* Tissue-specific inactivation of HAT cofactor TRRAP reveals its essential role in B cells. *Cell Cycle* **13**, 1583-1589 (2014).
269 Hart, T. *et al.* High-Resolution CRISPR Screens Reveal Fitness Genes and Genotype-Specific Cancer Liabilities. *Cell* **163**, 1515-1526 (2015).
270 Gibson, T. J., Seiler, M. & Veitia, R. A. The transience of transient overexpression. *Nat Methods* **10**, 715-721 (2013).
271 Zhang, L., Rayner, S., Katoku-Kikyo, N., Romanova, L. & Kikyo, N. Successful co-immunoprecipitation of Oct4 and Nanog using cross-linking. *Biochem Biophys Res Commun* **361**, 611-614 (2007).
272 Wurdak, H. *et al.* An RNAi Screen Identifies TRRAP as a Regulator of Brain Tumor-Initiating Cell Differentiation. *Cell Stem Cell* **6**, 37-47 (2010).
273 Jin, Q. *et al.* Gcn5 and PCAF negatively regulate interferon-beta production through HAT-independent inhibition of TBK1. *EMBO Rep* **15**, 1192-1201 (2014).
274 Truong, L. N., Hertel, K. J. & Brachmann, R. K. p53 interacts with the spliceosomal protein SAP145 and affects pre-mRNA processing. *Cancer Res* **65**, 1086-1086 (2014).
275 Allende-Vega, N. *et al.* p53 is activated in response to disruption of the pre-mRNA splicing machinery. *Oncogene* **32**, 1-14 (2013).
276 Siebring-van Olst, E. *et al.* A genome-wide siRNA screen for regulators of tumor suppressor p53 activity in human non-small cell lung cancer cells identifies components of the RNA splicing machinery as targets for anticancer treatment. *Mol Oncol* **11**, 534-551 (2017).
277 David, C. J. & Manley, J. L. Alternative pre-mRNA splicing regulation in cancer: pathways and programs unhinged. *Genes Dev* **24**, 2343-2364 (2010).
278 Hinnebusch, A. G. eIF3: a versatile scaffold for translation initiation complexes. *Trends Biochem Sci* **31**, 553-562 (2006).
279 Dunand-Sauthier, I. *et al.* Sum1, a component of the fission yeast eIF3 translation initiation complex, is rapidly relocalized during environmental stress and interacts with components of the 26S proteasome. *Mol Biol Cell* **13**, 1626-1640 (2002).
280 Hoareau Alves, K., Bochard, V., Rety, S. & Jalinot, P. Association of the mammalian proto-oncoprotein Int-6 with the three protein complexes eIF3, COP9 signalosome and 26S proteasome. *FEBS Lett* **527**, 15-21 (2002).
281 Sha, Z. *et al.* The eIF3 interactome reveals the translasome, a supercomplex linking protein synthesis and degradation machineries. *Mol Cell* **36**, 141-152 (2009).
282 Kojima, K. *et al.* Prognostic impact and targeting of CRM1 in acute myeloid leukemia. *Blood* **121**, 4166-4174 (2013).
283 Zheng, Y. *et al.* KPT-330 inhibitor of XPO1-mediated nuclear export has anti-proliferative activity in hepatocellular carcinoma. *Cancer Chemother Pharmacol* **74**, 487-495 (2014).
284 Yoshimura, M. *et al.* Induction of p53-mediated transcription and apoptosis by exportin-1 (XPO1) inhibition in mantle cell lymphoma. *Cancer Sci* **105**, 795-801 (2014).
285 Nie, L., Sasaki, M. & Maki, C. G. Regulation of p53 nuclear export through sequential changes in conformation and ubiquitination. *J Biol Chem* **282**, 14616-14625 (2007).
286 Li, M. *et al.* Mono- versus polyubiquitination: differential control of p53 fate by Mdm2. *Science* **302**, 1972-1975 (2003).
287 Herceg, Z. *et al.* Genome-wide analysis of gene expression regulated by the HAT cofactor Trrap in conditional knockout cells. *Nucleic Acids Res* **31**, 7011-7023 (2003).
288 Haller, O., Kochs, G. & Weber, F. The interferon response circuit: induction and suppression by pathogenic viruses. *Virology* **344**, 119-130 (2006).
289 Kenworthy, R. *et al.* Short-hairpin RNAs delivered by lentiviral vector transduction trigger RIG-I-mediated IFN activation. *Nucleic Acids Res* **37**, 6587-6599 (2009).
290 Wu, D. *et al.* A rapid and efficient one-step site-directed deletion, insertion, and substitution mutagenesis protocol. *Anal Biochem* **434**, 254-258 (2013).
291 Kuhn, M. W. *et al.* Targeting Chromatin Regulators Inhibits Leukemogenic Gene Expression in NPM1 Mutant Leukemia. *Cancer Discov* **6**, 1166-1181 (2016).
292 Shiloh, Y. ATM and related protein kinases: safeguarding genome integrity. *Nat Rev Cancer* **3**, 155-168 (2003).

293 Wullschleger, S., Loewith, R. & Hall, M. N. TOR signaling in growth and metabolism. *Cell* **124**, 471-484 (2006).
294 Yamashita, A., Kashima, I. & Ohno, S. The role of SMG-1 in nonsense-mediated mRNA decay. *Biochim Biophys Acta* **1754**, 305-315 (2005).
295 Yoshimura, S. H. & Hirano, T. HEAT repeats - versatile arrays of amphiphilic helices working in crowded environments? *J Cell Sci* **129**, 3963-3970 (2016).
296 Nobumori, Y., Shouse, G. P., Fan, L. & Liu, X. HEAT repeat 1 motif is required for B56gamma-containing protein phosphatase 2A (B56gamma-PP2A) holoenzyme assembly and tumor-suppressive function. *J Biol Chem* **287**, 11030-11036 (2012).
297 Kaeser, M. D. & Iggo, R. D. Promoter-specific p53-dependent histone acetylation following DNA damage. *Oncogene* **23**, 4007-4013 (2004).
298 Vrba, L., Junk, D. J., Novak, P. & Futscher, B. W. p53 induces distinct epigenetic states at its direct target promoters. *BMC Genomics* **9**, 486 (2008).
299 Chen, X., Ko, L. J., Jayaraman, L. & Prives, C. p53 levels, functional domains, and DNA damage determine the extent of the apoptotic response of tumor cells. *Genes Dev* **10**, 2438-2451 (1996).
300 Nakano, H., Yonekawa, H. & Shinohara, K. Threshold level of p53 required for the induction of apoptosis in X-irradiated MOLT-4 cells. *Int J Radiat Oncol Biol Phys* **68**, 883-891 (2007).
301 Kracikova, M., Akiri, G., George, A., Sachidanandam, R. & Aaronson, S. A. A threshold mechanism mediates p53 cell fate decision between growth arrest and apoptosis. *Cell Death Differ* **20**, 576-588 (2013).
302 Paek, A. L., Liu, J. C., Loewer, A., Forrester, W. C. & Lahav, G. Cell-to-Cell Variation in p53 Dynamics Leads to Fractional Killing. *Cell* **165**, 631-642 (2016).
303 Donehower, L. A. *et al.* Mice deficient for p53 are developmentally normal but susceptible to spontaneous tumours. *Nature* **356**, 215-221 (1992).
304 Malkin, D. Li-fraumeni syndrome. *Genes Cancer* **2**, 475-484 (2011).
305 McBride, K. A. *et al.* Li-Fraumeni syndrome: cancer risk assessment and clinical management. *Nat Rev Clin Oncol* **11**, 260-271 (2014).
306 Sonnemann, J. *et al.* p53-dependent and p53-independent anticancer effects of different histone deacetylase inhibitors. *Br J Cancer* **110**, 656-667 (2014).
307 Peltonen, K., Kiviharju, T. M., Jarvinen, P. M., Ra, R. & Laiho, M. Melanoma cell lines are susceptible to histone deacetylase inhibitor TSA provoked cell cycle arrest and apoptosis. *Pigment Cell Res* **18**, 196-202 (2005).
308 Sachweh, M. C., Drummond, C. J., Higgins, M., Campbell, J. & Lain, S. Incompatible effects of p53 and HDAC inhibition on p21 expression and cell cycle progression. *Cell Death Dis* **4**, e533 (2013).
309 Wang, Z. *et al.* Genome-wide mapping of HATs and HDACs reveals distinct functions in active and inactive genes. *Cell* **138**, 1019-1031 (2009).
310 Pillonel, V. *et al.* Histone deacetylase 1 plays a predominant pro-oncogenic role in Emu-myc driven B cell lymphoma. *Sci Rep* **6**, 37772 (2016).
311 Scholz, C. *et al.* Acetylation site specificities of lysine deacetylase inhibitors in human cells. *Nat Biotechnol* **33**, 415-423 (2015).
312 Tapias, A. *et al.* Trrap-dependent histone acetylation specifically regulates cell-cycle gene transcription to control neural progenitor fate decisions. *Cell Stem Cell* **14**, 632-643 (2014).
313 Wang, X., Taplick, J., Geva, N. & Oren, M. Inhibition of p53 degradation by Mdm2 acetylation. *FEBS Lett* **561**, 195-201 (2004).
314 Nihira, N. T. *et al.* Acetylation-dependent regulation of MDM2 E3 ligase activity dictates its oncogenic function. *Sci Signal* **10** (2017).
315 Shiloh, Y. & Ziv, Y. The ATM protein kinase: regulating the cellular response to genotoxic stress, and more. *Nat Rev Mol Cell Biol* **14**, 197-210 (2013).
316 Chehab, N. H., Malikzay, A., Appel, M. & Halazonetis, T. D. Chk2/hCds1 functions as a DNA damage checkpoint in G(1) by stabilizing p53. *Genes Dev* **14**, 278-288 (2000).
317 Shieh, S. Y., Ahn, J., Tamai, K., Taya, Y. & Prives, C. The human homologs of checkpoint kinases Chk1 and Cds1 (Chk2) phosphorylate p53 at multiple DNA damage-inducible sites. *Genes Dev* **14**, 289-300 (2000).
318 Rundle, S., Bradbury, A., Drew, Y. & Curtin, N. J. Targeting the ATR-CHK1 Axis in Cancer Therapy. *Cancers (Basel)* **9** (2017).
319 Dungl, D. A., Maginn, E. N. & Stronach, E. A. Preventing Damage Limitation: Targeting DNA-PKcs and DNA Double-Strand Break Repair Pathways for Ovarian Cancer Therapy. *Front Oncol* **5**, 240 (2015).
320 Woo, R. A. *et al.* DNA damage-induced apoptosis requires the DNA-dependent protein kinase, and is mediated by the latent population of p53. *EMBO J* **21**, 3000-3008 (2002).
321 Woo, R. A., McLure, K. G., Lees-Miller, S. P., Rancourt, D. E. & Lee, P. W. DNA-dependent protein kinase acts upstream of p53 in response to DNA damage. *Nature* **394**, 700-704 (1998).
322 Brumbaugh, K. M. *et al.* The mRNA surveillance protein hSMG-1 functions in genotoxic stress response pathways in mammalian cells. *Mol Cell* **14**, 585-598 (2004).
323 Gewandter, J. S., Bambara, R. A. & O'Reilly, M. A. The RNA surveillance protein SMG1 activates p53 in response to DNA double-strand breaks but not exogenously oxidized mRNA. *Cell Cycle* **10**, 2561-2567 (2011).

324 Dancey, J. mTOR signaling and drug development in cancer. *Nat Rev Clin Oncol* **7**, 209-219 (2010).
325 Feng, Z., Zhang, H., Levine, A. J. & Jin, S. The coordinate regulation of the p53 and mTOR pathways in cells. *Proc Natl Acad Sci U S A* **102**, 8204-8209 (2005).
326 Cordani, M. *et al.* Mutant p53 proteins counteract autophagic mechanism sensitizing cancer cells to mTOR inhibition. *Mol Oncol* **10**, 1008-1029 (2016).
327 Dando, I., Cordani, M. & Donadelli, M. Mutant p53 and mTOR/PKM2 regulation in cancer cells. *IUBMB Life* **68**, 722-726 (2016).
328 Murr, R. *et al.* Histone acetylation by Trrap-Tip60 modulates loading of repair proteins and repair of DNA double-strand breaks. *Nat Cell Biol* **8**, 91-99 (2006).
329 Lee, K. K. & Workman, J. L. Histone acetyltransferase complexes: one size doesn't fit all. *Nat Rev Mol Cell Biol* **8**, 284-295 (2007).
330 Linares, L. K. *et al.* Intrinsic ubiquitination activity of PCAF controls the stability of the oncoprotein Hdm2. *Nat Cell Biol* **9**, 331-338 (2007).
331 Kumar, A. *et al.* Human papillomavirus oncoprotein E6 inactivates the transcriptional coactivator human ADA3. *Mol Cell Biol* **22**, 5801-5812 (2002).
332 Legube, G. *et al.* Role of the histone acetyl transferase Tip60 in the p53 pathway. *J Biol Chem* **279**, 44825-44833 (2004).
333 Legube, G. *et al.* Tip60 is targeted to proteasome-mediated degradation by Mdm2 and accumulates after UV irradiation. *EMBO J* **21**, 1704-1712 (2002).
334 Gamper, A. M. & Roeder, R. G. Multivalent binding of p53 to the STAGA complex mediates coactivator recruitment after UV damage. *Mol Cell Biol* **28**, 2517-2527 (2008).
335 Wang, J. *et al.* Analysis of TRRAP as a Potential Molecular Marker and Therapeutic Target for Breast Cancer. *J Breast Cancer* **19**, 61-67 (2016).

8 Abbreviations

AACR	American Association for Cancer Research
ABC DLBCL	Activated B-cell like diffuse large B-cell lymphoma
AIDS	Acquired immunodeficiency syndrome
APC	Allophycocyanin
ASHM	Aberrant somatic hypermutation
ATCC	American Type Culture Collection
ATP	Adenosine triphosphate
BCA	Bicinchoninic acid
BCR	B-cell receptor
BL	Burkitt's lymphoma
B-NHL	B-cell non-Hodgkin lymphoma
BRCA	Breast cancer
BSA	Bovine serum albumine
CCE	Constitutive core essential
cDNA	Complementary deoxyribonucleic acid
CRC	Colorectal cancer
CRISPR	Clustered regularly interspaced short palindromic repeats
CSR	Class-switch recombination
ddH_2O	Double-distilled water
DKFZ	Deutsches Krebsforschungszentrum (German Cancer Research Center), Heidelberg, Germany
DLBCL	Diffuse large B-cell lymphoma
DMEM	Dulbecco's Modified Eagle Medium
DMSO	Dimethyl sulfoxide
DNA	Deoxyribonucleic acid
dNTP	Deoxynucleotide
DSMZ	Deutsche Sammlung von Mikroorganismen und Zellkulturen, Braunschweig, Germany
dsRNA	Double stranded ribonucleic acid
DZ	Dark zone (germinal center)
eBL	Endemic Burkitt's lymphoma
EBV	Epstein-Barr virus
ECL	Enhanced chemiluminescence
EDTA	Ethylenediaminetetraacetic acid
EMBL	European Molecular Biology Laboratory, Heidelberg, Germany
EtOH	Ethanol
FACS	Fluorescence activated cell sorting (flow cytometry)
FAT	Focal adhesion targeting domain
FATC	FRAP, ATM, TRRAP C-terminal domain
FBS	Fetal bovine serum
FC	Fold change
FITC	Fluorescein isothiocyanate
FL	Follicular lymphoma
FRB	FKBP12-rapamycin binding domain
FSC	Forward scatter

GC	Germinal center
GCB DLBCL	Germinal center B-cell like diffuse large B-cell lymphoma
GFP	Green fluorescent protein
GOF	Gain-of-function
HAT	Histone acetyltransferase
HDAC	Histone deacetylase
HDACi	Histone deacetylase inhibitor
HEAT	Huntingtin, elongation factor 3 (EF3), protein phosphatase 2A (PP2A), yeast kinase TOR1
HEPES	4-(2-hydroxyethyl)-1-piperazineethanesulfonic acid
HIV	Human immunodeficiency virus
HPLC	High-performance liquid chromatography
HRP	Horseradish peroxidase
HT	High-throughput
IARC	International Agency for Research on Cancer, Lyon, France
ICGC	International Cancer Genome Consortium
IFN	Interferon
Ig	Immunoglobulin
IgG	Immunoglobulin G
IgV	Immunoglobulin variable gene
IHC	Immunohistochemistry
IP	Immunoprecipitation
IPTG	Isopropyl β-D-1-thiogalactopyranoside
KO	Knock-out
LB	Lysogeny broth
LC	Liquid chromatography
LZ	Light zone (germinal center)
MeOH	Methanol
MFI	Median fluorescence intensity
MMML	Molecular mechanisms of malignant lymphoma
mRNA	Messenger ribonucleic acid
MS	Mass spectrometry
mutp53	Mutant cellular tumor antigen p53
NaOAc	Sodium acetate
NCT	National Center for Tumor Diseases, Heidelberg, Germany
NE	Non-essential
NES	Nuclear export sequence
NHL	Non-Hodgkin lymphoma
NLS	Nuclear localization sequence
NT	Non-targeting
OTEs	Off-target effects
p53	Cellular tumor antigen p53
PBS	Phosphate-buffered saline
PCR	Polymerase chain reaction
PEI	Polyethylenimine
PFA	Paraformaldehyde
PI3K	Phosphatidylinositol 3-kinase domain

PIKK	Phosphatidylinositol 3-kinase-related kinase
PNK	Polynucleotide kinase
PRD	PIKK regulatory domain
PTM	Post-translational modification
PVDF	Polyvinylidene fluoride
RFP	Red fluorescent protein
RING	Really interesting new gene
RIPA	Radioimmunoprecipitation assay
RNA	Ribonucleic acid
RNAi	Ribonucleic acid interference
rnx	Reaction
ROS	Reactive oxygen species
RPMI	Roswell Park Memorial Institute
rRNA	Ribosomal ribonucleic acid
RT-qPCR	Real-time quantitative polymerase chain reaction
Rux	Ruxolitinib
sBL	Sporadic Burkitt's lymphoma
S.O.C.	Super optimal broth with catabolite repression
SDS-PAGE	Sodium dodecyl sulfate polyacrylamide gel electrophoresis
sgRNA	Small guide ribonucleic acid
SHM	Somatic hypermutation
shRNA	Small hairpin ribonucleic acid
siRNA	Small interfering ribonucleic acid
SNP	Single nucleotide polymorphism
SSC	Sideward scatter
T7E1	T7 endonuclease I
TBST	Tris-buffered saline with TWEEN 20
TMA	Tissue microarray
tRNA	Transfer ribonucleic acid
TRRAP	Transformation/transcription domain-associated protein
WHO	World Health Organization
WIS	Weizmann Institute of Science
wtp53	Wild-type cellular tumor antigen p53
wZ	Weighted z-score

9 Publications & Conferences

9.1 Publications

1. Slabicki, M., Lee, K. S., **Jethwa, A.**, Sellner, L., Sacco, F., Walther, T., Hullein, J., Dietrich, S., Wu, B., Lipka, D. B., Oakes, C. C., Mamidi, S., Pyrzynska, B., Winiarska, M., Oles, M., Seifert, M., Plass, C., Kirschfink, M., Boettcher, M., Golab, J., Huber, W., Frohling, S. & Zenz, T. Dissection of CD20 regulation in lymphoma using RNAi. *Leukemia* **30**, 2409-2412 (2016).

2. Dietrich, S., Pircher, A., Endris, V., Peyrade, F., Wendtner, C. M., Follows, G. A., Hullein, J., **Jethwa, A.**, Ellert, E., Walther, T., Liu, X., Dyer, M. J., Elter, T., Brummer, T., Zeiser, R., Hermann, M., Herold, M., Weichert, W., Dearden, C., Haferlach, T., Seiffert, M., Hallek, M., von Kalle, C., Ho, A. D., Gaehler, A., Andrulis, M., Steurer, M. & Zenz, T. BRAF inhibition in hairy cell leukemia with low-dose vemurafenib. *Blood* **127**, 2847-2855 (2016).

3. Te Raa, G. D., Derks, I. A., Navrkalova, V., Skowronska, A., Moerland, P. D., van Laar, J., Oldreive, C., Monsuur, H., Trbusek, M., Malcikova, J., Loden, M., Geisler, C. H., Hullein, J., **Jethwa, A.**, Zenz, T., Pospisilova, S., Stankovic, T., van Oers, M. H., Kater, A. P. & Eldering, E. The impact of SF3B1 mutations in CLL on the DNA-damage response. *Leukemia* **29**, 1133-1142 (2015).

4. Blume, C. J., Hotz-Wagenblatt, A., Hullein, J., Sellner, L., **Jethwa, A.**, Stolz, T., Slabicki, M., Lee, K., Sharathchandra, A., Benner, A., Dietrich, S., Oakes, C. C., Dreger, P., te Raa, D., Kater, A. P., Jauch, A., Merkel, O., Oren, M., Hielscher, T. & Zenz, T. p53-dependent non-coding RNA networks in chronic lymphocytic leukemia. *Leukemia* **29**, 2015-2023 (2015).

5. **Jethwa, A.***, Hullein, J.*, Stolz, T., Blume, C., Sellner, L., Jauch, A., Sill, M., Kater, A. P., te Raa, G. D., Geisler, C., van Oers, M., Dietrich, S., Dreger, P., Ho, A. D., Paruzynski, A., Schmidt, M., von Kalle, C., Glimm, H. & Zenz, T. Targeted resequencing for analysis of clonal composition of recurrent gene mutations in chronic lymphocytic leukaemia. *Br J Haematol* **163**, 496-500 (2013).

6. Hullein, J.*, **Jethwa, A.***, Stolz, T., Blume, C., Sellner, L., Sill, M., Langer, C., Jauch, A., Paruzynski, A., von Kalle, C., Schmidt, M., Glimm, H. & Zenz, T. Next-generation sequencing of cancer consensus genes in lymphoma. *Leuk Lymphoma* **54**, 1831-1835 (2013).

7. Dietrich, S., Hullein, J., Hundemer, M., Lehners, N., **Jethwa, A.**, Capper, D., Acker, T., Garvalov, B. K., Andrulis, M., Blume, C., Schulte, C., Mandel, T., Meissner, J., Frohling, S., von Kalle, C., Glimm, H., Ho, A. D. & Zenz, T. Continued response off treatment after BRAF inhibition in refractory hairy cell leukemia. *J Clin Oncol* **31**, e300-303 (2013).

8. Seiffert, M., Dietrich, S., **Jethwa, A.**, Glimm, H., Lichter, P. & Zenz, T. Exploiting biological diversity and genomic aberrations in chronic lymphocytic leukemia. *Leuk Lymphoma* **53**, 1023-1031 (2012).

*co-first author

9.2 Conferences

Aug 2014 Meeting of the German-Israeli Helmholtz Research School in Cancer Biology, Heidelberg, Germany

Understanding the rewired p53 regulation network in lymphoma
Alexander Jethwa, Mikołaj Słabicki, Jennifer Hüllein, Tatjana Stolz, Christof von Kalle, Moshe Oren, Thorsten Zenz

Oral & poster presentation

Nov 2015 DKFZ PhD retreat, November 2015, Weil der Stadt, Germany

Understanding the rewired p53 regulation network in lymphoma
Alexander Jethwa, Mikołaj Słabicki, Jennifer Hüllein, Tatjana Walther, Christof von Kalle, Moshe Oren, Thorsten Zenz

Oral presentation

May 2016 DKFZ Cancer Systems Genetics Conference, Heidelberg, Germany

Understanding the regulation of mutant p53 expression in lymphoma
Alexander Jethwa, Mikołaj Słabicki, Jennifer Hüllein, Tatjana Walther, Moshe Oren, Thorsten Zenz

Poster presentation

Jun 2016 EMBL Partnership Conference Perspectives in Translational Medicine, Heidelberg, Germany

Understanding the regulation of mutant p53 expression in lymphoma
Alexander Jethwa, Mikołaj Słabicki, Jennifer Hüllein, Tatjana Walther, Moshe Oren, Thorsten Zenz

Poster presentation

Nov 2016 DKFZ PhD Poster Presentation, Heidelberg, Germany

Understanding the regulation of mutant p53 expression in lymphoma

Alexander Jethwa, Mikołaj Słabicki, Jennifer Hüllein, Tatjana Walther, Moshe Oren, Thorsten Zenz

Poster presentation

Jan 2017 Meeting of the German-Israeli Helmholtz Research School in Cancer Biology, Rehovot, Israel

Understanding mutant p53 regulation and gain-of-function in lymphoma

Alexander Jethwa, Mikołaj Słabicki, Jennifer Hüllein, Lena Wagner, Marius Jentzsch, Tatjana Walther, Moshe Oren, Thorsten Zenz

Oral & poster presentation

Jul 2017 The 17th International p53 Workshop, Singapore

Large-scale RNAi screen identifies regulators of mutant p53 expression in lymphoma

Alexander Jethwa, Mikołaj Słabicki, Jennifer Hüllein, Marius Jentzsch, Wolfgang Huber, Yael Aylon, Moshe Oren, Thorsten Zenz

Poster presentation

10 Acknowledgements

First and foremost, I would like to thank my supervisor Prof. Thorsten Zenz for giving me the opportunity to work in his group on such an exciting topic. Thank you for all your support, your trust, and for giving me enough freedom to pursue my own ideas.

I am very grateful to my co-supervisor Prof. Moshe Oren for all the discussions, which were essential for the success of this project. Thank you especially for hosting me in your lab in Israel.

I would like to thank Prof. Philipp Beckhove, Prof. Stefan Wiemann, and Prof. Georg Stoecklin for agreeing to be part of my PhD Defense Committee. Thanks also to Prof. Christoph Plass for being part of my Thesis Advisory Committee.

I am especially grateful to Dr. Mikołaj Słabicki who supervised me throughout my PhD and without whom this project would have never been possible. Thank you for everything that you have taught me, for all the discussions, and for sharing your motivation with me. It was amazing to work with you and I think that it is fair to say that you are an inspiration for all of us.

I would like to thank all members of AG Zenz for their endless support and for the great atmosphere; I really enjoyed every single day working together with you and I will miss you very much! Thank you Tati, Kwang, Lena, Vineet, Jenny, Caro, Sina, Sophie, Sebastian, Michelle, and Kasia! Special thanks to Marius Jentzsch, my first student, for joining forces with me – I hope you enjoyed the time as much as I did.

Furthermore, I would like to thank all members of the Dept. of Translational Oncology of Prof. Christof von Kalle (“G100 family”), especially everybody from AG Glimm, AG Sander, and AG Fröhling/Scholl. I am especially grateful to Elias and Peer for all their help, their valuable feedback, and for always cheering me up. I will miss our lunch breaks and having you around!

I am grateful to all members of the Oren lab at the Weizmann Institute for the warm welcome and for making me feel at home: thank you Debby, Sharath, Eran, Michal, Gali, Ambra, Ohad, and Anat! Special thanks to Dr. Yael Aylon and Noa Furth for supervising me and for patiently answering all of my questions.

I would also like to thank Dr. Sabine Schmidt from the DKFZ Genomics & Proteomics Core Facility for assisting in setting up the Illumina sequencing platform. Moreover,

I thank Prof. Wolfgang Huber, Mandy Rettel, Dr. Frank Stein, and Dr. Arne Smits from the EMBL Heidelberg for performing mass spectrometry experiments and data analysis.

A big thank you goes to my friends in Heidelberg with whom I had the pleasure to share the PhD journey. Thank you especially to Flo, Eva, Franzy, and Julia! Special thanks go of course to Niko & Elias for the most awesome WG ever!

I would like to express my deepest gratitude to my parents and my brother Jay. Thank you for your unconditional support and love. Papa, thank you for sparking my interest in science. Mama, I wish you would have been able to witness this moment. Finally, I would like to thank Caro for always being by my side – you are the best thing that ever happened to me.